2F

PNL-3566
UC-70

Waste/Rock Interactions Technology Program

Spent Fuel Special Studies Progress Report: Probable Mechanisms for Oxidation and Dissolution of Single-Crystal UO_2 Surfaces

R. Wang

March 1981

Prepared for the
Office of Nuclear Waste Isolation
U.S. Department of Energy
under Contract DE-AC06-76RLO 1830

Pacific Northwest Laboratory
Operated for the U.S. Department of Energy
by Battelle Memorial Institute

Battelle

PNL-3566

PACIFIC NORTHWEST LABORATORY
operated by
BATTELLE
for the
UNITED STATES DEPARTMENT OF ENERGY
Under Contract DE-AC06-76RLO 1830

Printed in the United States of America
Available from
National Technical Information Service
United States Department of Commerce
5285 Port Royal Road
Springfield, Virginia 22151

Price: Printed Copy $_____*; Microfiche $3.00

*Pages	NTIS Selling Price
001-025	$4.00
026-050	$4.50
051-075	$5.25
076-100	$6.00
101-125	$6.50
126-150	$7.25
151-175	$8.00
176-200	$9.00
201-225	$9.25
226-250	$9.50
251-275	$10.75
276-300	$11.00

PNL-3566
UC-70

Waste/Rock Interactions Technology Program

SPENT FUEL SPECIAL STUDIES PROGRESS REPORT: PROBABLE MECHANISMS FOR OXIDATION AND DISSOLUTION OF SINGLE-CRYSTAL UO_2 SURFACES

R. Wang

March 1981

Prepared for the
Office of Nuclear Waste Isolation
U.S. Department of Energy
under Contract DE-AC06-76RLO 1830

Pacific Northwest Laboratory
Richland, Washington 99352

ACKNOWLEDGMENTS

The following Pacific Northwest Laboratory staff members have contributed to the experimental program: Oxidation Studies--H. E. Kissinger; Static Autoclave Dissolution Studies--G. E. Zima; Electrochemical Oxidation and Oxidation-Dissolution Studies--H. E. Kjarmo and G. R. Robinson; SEM Analysis--H. E. Kjarmo and D. A. Spanner; and Auger Surface Analysis--H. Tenny.

Y. B. Katayama of the Pacific Northwest Laboratory and Professor H. D. Holland, a consultant to the Program, discussed and reviewed the results.

This research is supported by the Waste/Rock Interactions Technology Program conducted by the Pacific Northwest Laboratory. The Program is sponsored by the Office of Nuclear Waste Isolation, managed by Battelle Memorial Institute for the U.S. Department of Energy under Contract DE-AC06-76RLO 1830.

SUMMARY

This status report describes spent-fuel leaching and dissolution mechanism experiments performed at the Pacific Northwest Laboratory from October 1978 through July 1980. It is important to identify and understand these mechanisms in order to predict, via mathematical models, the long-term stability of spent fuel in geological repository conditions. Due to the complexity of the structural, microstructural and compositional characteristics of spent fuel, basic leaching and dissolution mechanisms were studied with UO_2 matrix material, specifically with single-crystal UO_2, to isolate individual contributory factors.

The effects of oxidation and oxidation-dissolution were investigated in different oxidation conditions, such as in air, oxygenated solutions and deionized water containing H_2O_2. In addition, the effects of temperature on dissolution of UO_2 were studied in autoclaves at 75 and 150°C. Also, oxidation and dissolution measurements were investigated via electrochemical methods to determine if those techniques could be applied to the characterization of leaching and dissolution of spent fuel in a hot cell. Finally, the effects of radiation were explored since the radiolysis of water may create a localized oxidizing condition at or near the spent fuel-solution interface, even in neutral or reducing conditions as commonly found in deep geological environments.

The oxidation and oxidation-dissolution mechanisms for UO_2 are proposed as follows: The UO_2 surface is first oxidized in solution to form a UO_{2+x} surface layer several angstroms thick. This oxidized surface has a high dissolution rate since the UO_{2+x} reacts with the dissolved O_2, or H_2O_2, to form uranyl complex ions in a U(VI) state. As the uranyl ions exceed the solubility limits in solution, they become hydrolyzed to form solid deposits and suspended particles of UO_3 hydrates. The thickness and porosity of the deposited UO_3 hydrate surface-film is dependent on temperature, pH and deposition time. A long-term dissolution rate is then determined by the nature of the surface film, such as porosity, solubility and mechanical properties.

The application of these findings to the study of leaching mechanisms of spent fuel requires further investigation. The techniques discussed here for analyzing the oxidation and oxidation-dissolution mechanisms of UO_2 matrix material will be used to characterize spent-fuel leaching processes and to develop data for modeling safety and stability factors of spent fuel in its geologic environments.

CONTENTS

FIGURES

TABLES

INTRODUCTION

A consideration of waste management studies is the geologic disposal of spent nuclear fuel in the form it is removed from pressurized- and boiling-water reactors. A safety analysis is required to assess the stability of spent fuel and the mechanisms that release radioactive nuclides in the event that the cladding of the spent fuel breaches and the fuel core interacts with water. Researchers in the Waste Rock/Interactions (WRIT) Program at the Pacific Northwest Laboratory (PNL) are currently performing this assessment.

Unlike most alternative waste forms under consideration for long-term storage and disposal, spent fuel has a preset form, composition and geometry. Furthermore, spent fuel has various physical, chemical and thermal characteristics that depend upon each reactor's history of operation. Therefore, the behavior of spent fuels in contact with certain environments is complex and difficult to predict. However, this behavior must be known when locations are evaluated for possible geologic disposal of spent fuel.

At PNL, spent-fuel leaching data have been generated since 1975 from hot-cell experiments. In 1979, spent-fuel leaching mechanism studies began. These initial studies have dealt with UO_2--the spent-fuel matrix--in single-crystal and polycrystalline forms. As shown in Figure 1, experiments are designed to allow positive identification of various leaching and dissolution behaviors based on isolated individual contributory factors.

This report describes our present understanding of oxidation and oxidation-dissolution mechanisms observed for single-crystal UO_2 surfaces. Effects of air oxidation in terms of structural and microstructural aspects have been determined. Effects of oxidation-dissolution of UO_2 surfaces have been identified based on autoclave static-dissolution and electrochemical methods. In addition, the effects of radiation in terms of formation of H_2O_2 via radiolysis of water have been explored. Isolated oxidation and dissolution mechanisms and experimental methods for identifying these mechanisms are being applied currently to the leaching of spent fuel under similar conditions (Wang and Katayama 1980).

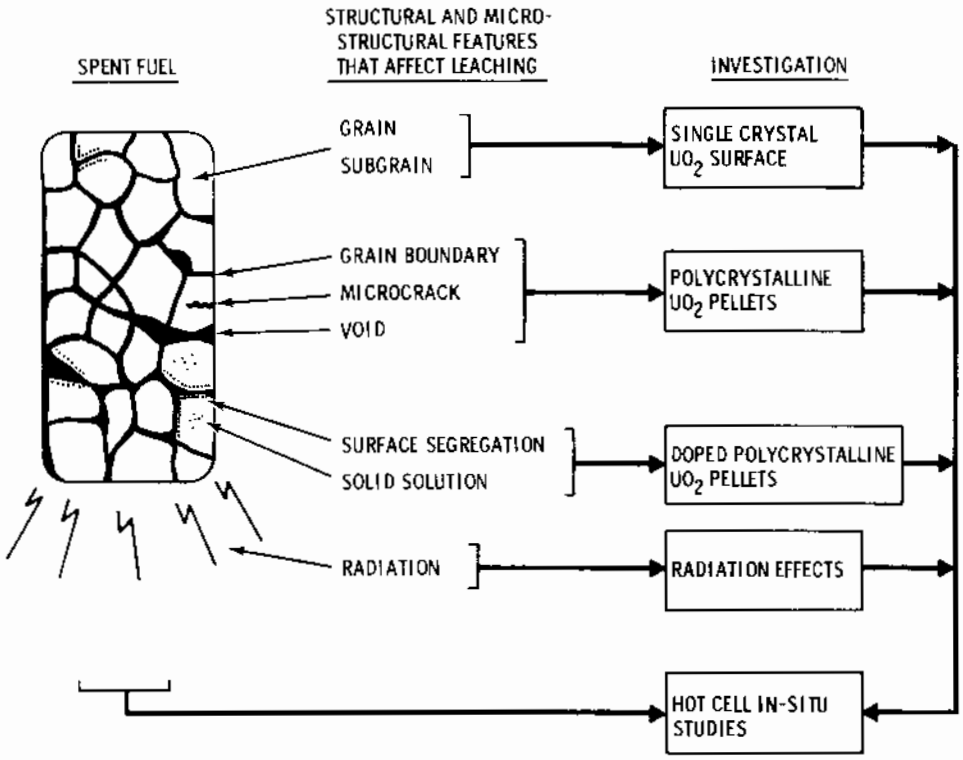

FIGURE 1. Spent-Fuel Oxidation and Leaching Factors Undergoing Study at PNL

OXIDATION OF SINGLE-CRYSTAL UO_2 SURFACES

One objective of these special studies is to identify the oxidation behavior of UO_2 single-crystal surfaces in terms of structural, microstructural and compositional characteristics. The dissolution of UO_2 in aqueous solution is strongly related to the oxidation state of the UO_2 surface. Exposure to thermal and chemical environments can readily produce surfaces having oxidation states markedly different from the bulk UO_2 matrix. Understanding surface oxidation behaviors is required to determine the probable mechanisms for oxidation-dissolution of UO_2 under oxidizing conditions.

EXPERIMENTAL PROCEDURES

Single crystals of UO_2 in 5- to 10-mm sizes were selected from fused UO_2 materials available at PNL in kilogram quantities. The oxidation of the UO_2 was performed in air. X-ray Lang topographs (Lang 1958) were used to observe the microstructural changes on (111) cleavage surfaces. Structural changes were studied through precise lattice-parameter measurements made by the Bond method (Bond 1960), which has an accuracy of ±0.0002 Å. The accuracy of the lattice-parameter measurements (at least an order of magnitude better than the powder diffraction methods) is essential for positive identification of slight structural changes. A modification of the Bond method provides interplanar angle measurements of high precision (±0.01°) for identifying crystal systems.

The composition of the crystal surface was obtained by Auger analysis before and after oxidation. A depth profile of the composition was obtained by sputtering the surface and analyzing the uranium and oxygen content until the matrix UO_2 composition was reached.

RESULTS AND DISCUSSION

Microstructural Aspects

To study the effects of oxidation on the microstructural aspects at 285°C, a single-crystal UO_2 sample was selected. Before oxidation in air, the

single crystal was annealed in a vacuum at 1000°C for several hours to homogenize the microstructure. Then, x-ray topographs were taken of the as-cleaved faces. These topographs show that each cleaved face contains many subgrains (see Figure 2A). Generally, the crystal microstructure contains several subgrains and only a low density of dislocations and inclusions. Judging by the images of the subgrains, which exhibit nearly equal intensities, the subgrains have good alignment parallel to the (111) orientation.

After heating at 285°C for 1 h, topographs show that the subgrains are slightly disoriented--namely, the structure of the subgrain itself is not noticeably changed, but the (111) plane alignment is seriously disturbed (Figure 2B). Oxidation in air may have caused the surface microstructure of the subgrains to change sufficiently so that the sensitive technique of the x-ray topography could resolve the differences.

After 5 h exposure at 285°C, the structures within subgrains appear altered (Figure 2C). Smaller domains have low-angle boundaries different from the previously described subgrain microstructures. Continued heating had little further effect on the sample other than an apparent relief of the subgrain distortion. Whether this is a result of continued oxidation or thermal annealing of earlier distortions is not clear. The predominant changes throughout this and a similar series of micrographs are of subgrain alignment, not within the subgrain; therefore, we may conclude that the subgrain boundaries are the major participants in the oxidation process.

Structural Aspects

Oxidation of UO_2 is accompanied by an increase in density and a decrease in lattice parameters. The lattice constant decreases from 5.470 Å for UO_2 to about 5.44 Å for $UO_{2.25}$ (Rundle et al. 1948). Further oxidation produces a tetragonal distortion of the cubic lattice up to a composition approximating U_3O_7 (Gronvold 1948). Some disagreement exists as to whether these are separate phases or merely end-members of a structural series. In the remainder of this discussion, "UO_2" refers to the cubic form, and "U_3O_7" designates the tetragonal modification. The distinction is structural, not chemical.

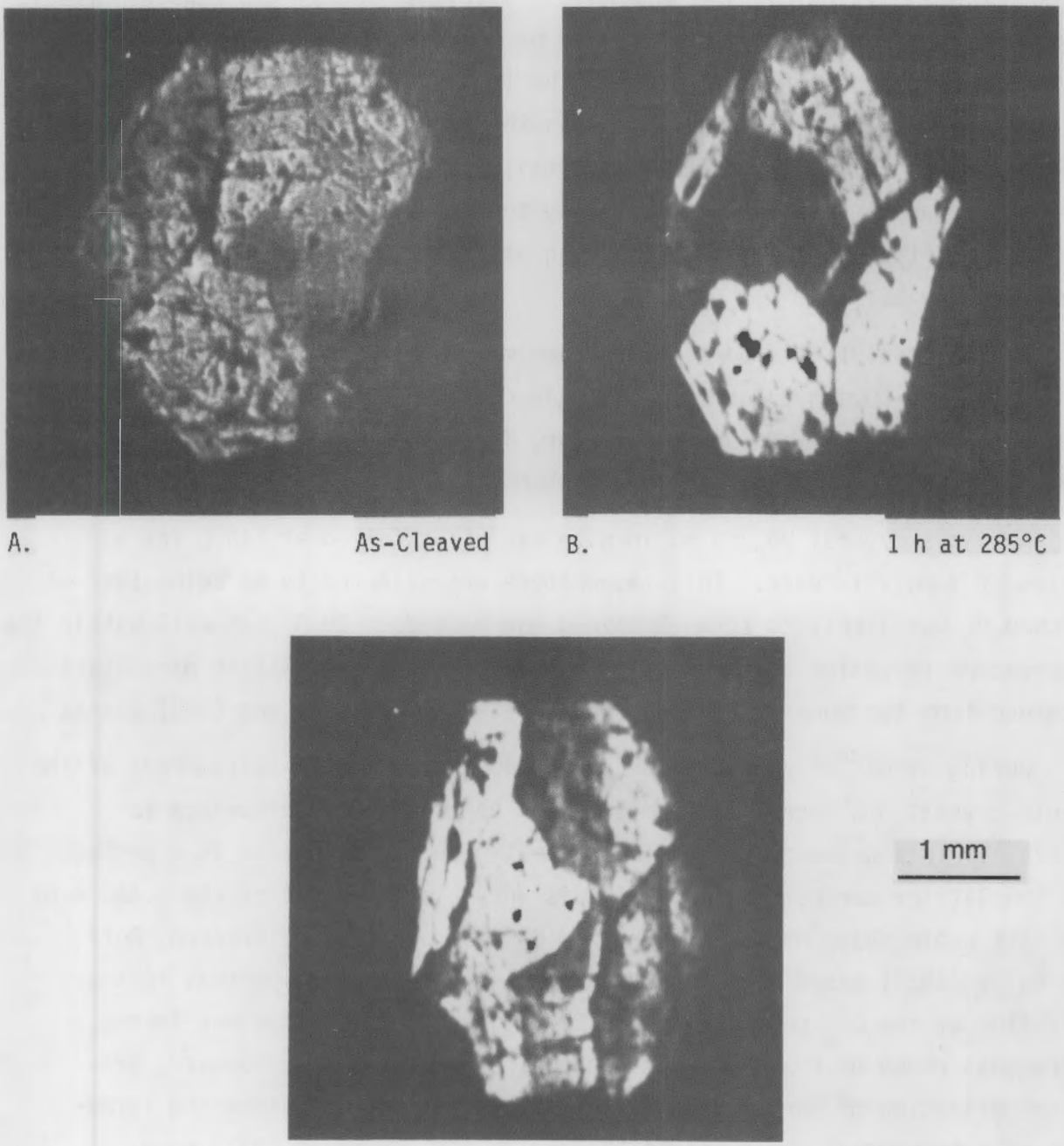

FIGURE 2A,B,C. Microstructure of Single-Crystal UO_2 Surface After Air Oxidation, Lang X-ray Topograph of (111) Surface

In cubic crystal systems, the angles between crystal planes are a property of the crystal system and are otherwise "invariant" (Henry and Lonsdale 1959). Any deviation from cubic symmetry would be immediately evidenced by a change in interplanar angles. In this work, the (111)-(511) angle was used. The third order of (111) is (333), which has the same d-spacing as (511). Once the crystal is aligned on a <110> zone axis, it is an easy matter to measure the desired angle. It is necessary only to turn the crystal from the one diffracting position to the other. So long as the crystal remains cubic, this angle must be 38.942°.

The purpose of this particular experiment was to determine if a thin film of U_3O_7 formed during oxidation of single-crystal UO_2 surfaces as those observed on a UO_2 pellet surface (Taylor, Burgess and Owen 1980), and if so, to determine the crystallographic relationship with the underlying UO_2.

A single-crystal UO_2 ~3 mm in size was air-oxidized at 145°C for a series of time intervals. This temperature was selected to be below that at which U_3O_8 was likely to form (Gronvold and Haraldsen 1948) but well within the temperature range for U_3O_7 formation. Table 1 shows the lattice parameters obtained from the Bond method and angles between the (511) and (333) planes.

During oxidation at 145°C for up to 240 h, the lattice parameters of the single-crystal UO_2 decreased from 5.4703 Å on an as-cleaved surface to 5.4675 Å. This decrease of lattice parameter during oxidation is expected, and the lattice parameter of 5.4675 Å is very close to that of the 5.467 Å of the last cubic phase of UO_{2+x} where x = 0.10 as reported by Aronson, Roff and Belle (1957) based on UO_2 powder samples. Aronson showed that further oxidation of the UO_2 powder between 120 and 280°C at longer times formed a tetragonal phase of UO_{2+x} where x ranged from 0.2 to 0.33. However, prolonged oxidation of our single-crystal UO_2 surface did not show the formation of a tetragonal phase, since the angles between (511)-(333) were unchanged. After 312 h, the lattice parameter began to increase (see Figure 3). This increase of the lattice parameter may be a result of the continued oxidation, but the structure of the oxidized surface remained cubic.

TABLE 1. Lattice Parameter and Angle Between (511) and (333) Planes for UO_2 Crystal Oxidized in Air (145°C)

Time, h	a_o (Å)	Angle Between (511) and (333)
0	5.4703 ± 0.0002	38.94°
24	5.4702	38.94°
96	5.4693	38.94°
168	5.4693	38.94°
240	5.4675	38.94°
312	5.4690	38.94°
408	5.4705	38.94°
480	5.4725	38.94°
570	5.4710	38.94°
570 + 24 (at 270°C)	5.4705	38.94°

After 570 h of oxidation at 145°C failed to produce the tetragonal phase, additional oxidation at 270°C for 24 h was applied. However, the lattice parameter and angle measurement also did not indicate the formation of a tetragonal phase. No U_3O_7 phase was detected for the single-crystal UO_2 oxidized at 270°C for 24 h, as shown in Table 1. Therefore, the oxidation rate for a single-crystal surface must be quite low as compared to that reported for the crystalline UO_2 pellets (Taylor, Burgess and Owen 1980).

Compositional Aspects

Surface analysis by Auger spectroscopy indicated that O diffusion into the single-crystal UO_2 surface was very slow, even at 285°C. The as-cleaved surface (Figure 4) was very clean and only had a few angstroms of O-rich layer. After air oxidation at 285°C for 24 h (Figure 5), diffusion of O only reached to about 20 Å deep. The extremely high O/U ratio near the first 5 Å may be due to absorbed O and formation of a UO_3 hydrated layer. At nearly 7 Å beneath the surface, the composition was close to UO_3 and rapidly decreased to UO_2 composition at a depth of nearly 20 Å. Depth determination was based

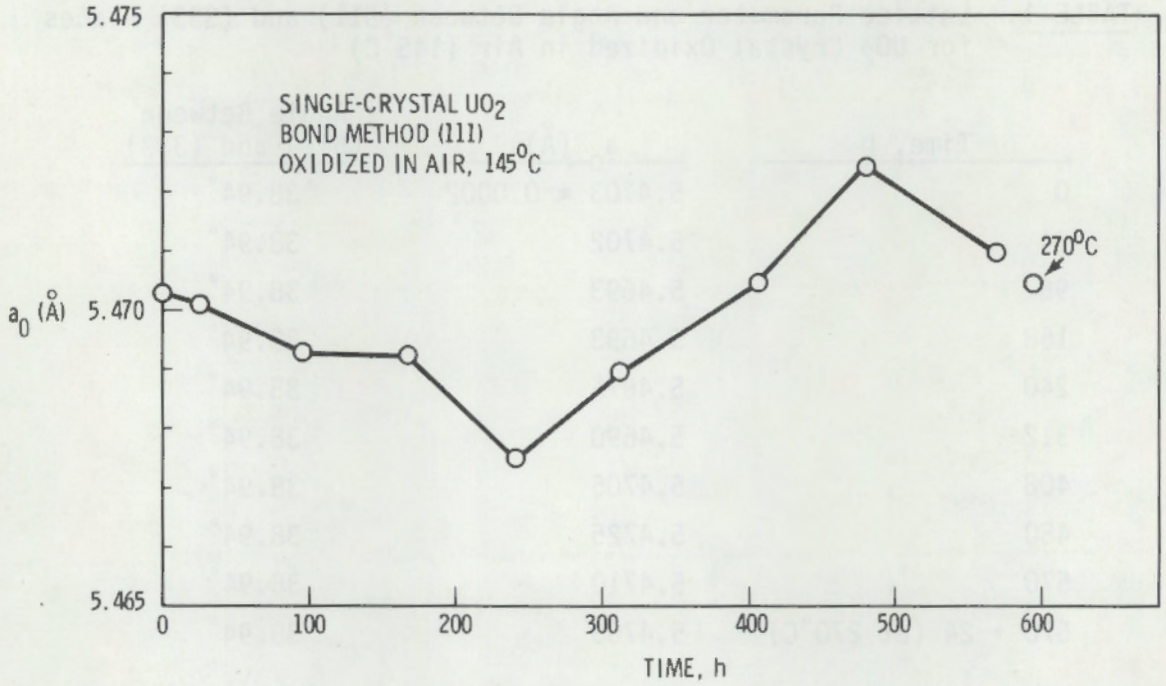

FIGURE 3. Lattice Parameter of UO_2 Surface as a Function of Time for Oxidation in Air at 145°C

on sputtering profiles of the surface and had a 50% error. The profiles demonstrated that the bulk diffusion rate of O was indeed very low as compared to the grain-boundary diffusion rate observed for the UO_2 pellets, which caused a several-micron-deep oxidation.

As a concurrent experiment, some of the fused UO_2 was crushed and sieved as powders of -400, -325, and -200 mesh sizes. These powders were oxidized in air and oxide phases determined by x-ray diffraction as shown in Table 2. Lattice parameters are given for cubic UO_2 and tetragonal U_3O_7. No attempt was made to determine lattice parameters for orthorhombic U_2O_5 or for hexagonal U_3O_8.

After oxidation at 250°C, all three crushed UO_2 powders showed that the changes of lattice parameter for a cubic UO_2 phase were small, reducing only from 5.470 Å to 5.466 Å. Further reduction in UO_2 lattice parameter by oxidation led to the transformation into a tetragonal U_3O_7 phase. This detailed

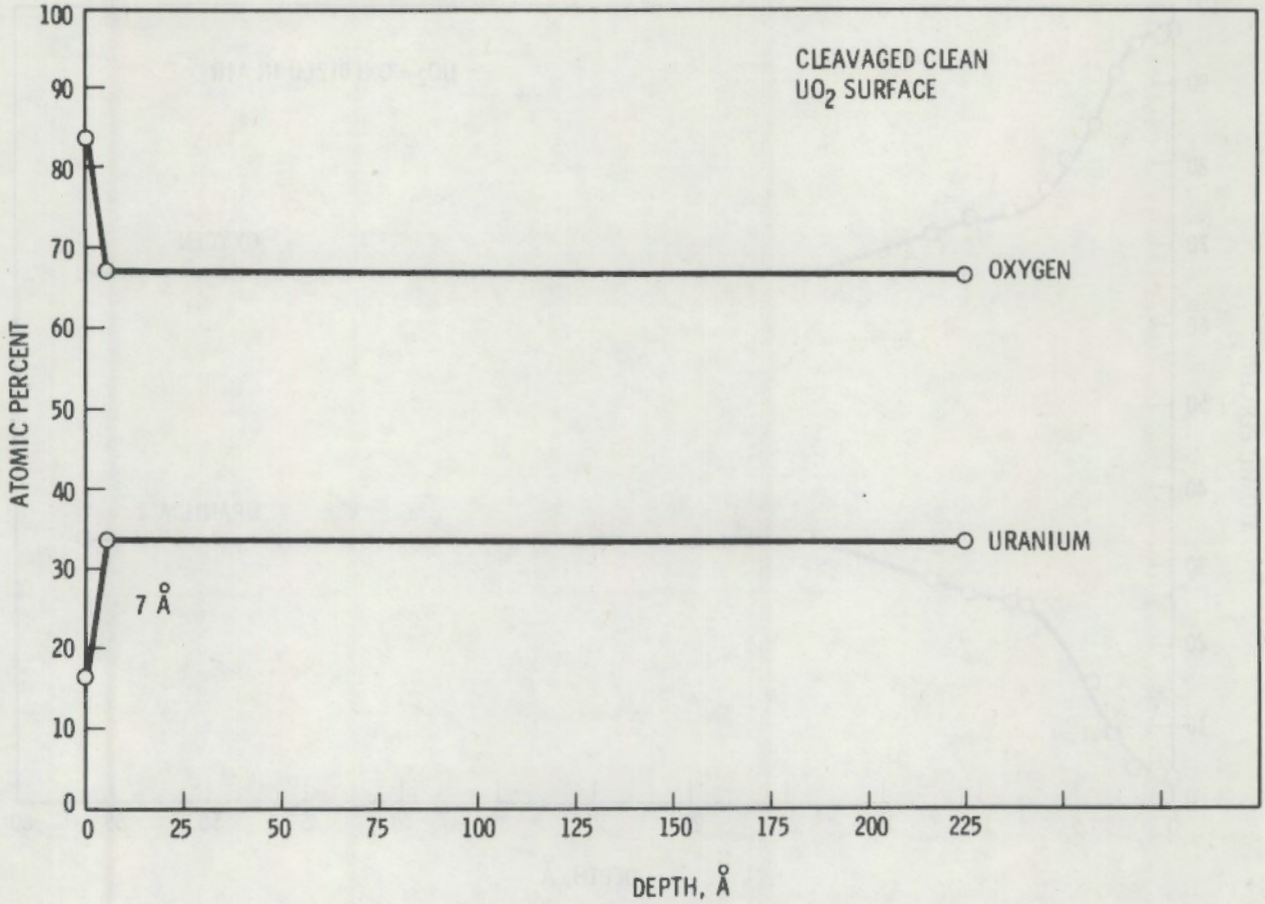

FIGURE 4. Surface of Single-Crystal UO_2 Studied by Auger Analysis

structural investigation, based on both single-crystal UO_2 and crushed powders, indicates that the effects of oxidation on UO_2 may have different results for UO_2 of different particle sizes.

CONCLUSIONS

The results of oxidizing single-crystal UO_2 surfaces in air were quite different compared to the crushed-powder experiments and other data obtained from powder and pellet studies. We believe that oxidation of single-crystal UO_2 with a crystal size of several millimeters was mostly due to O diffusion through subgrain boundaries and microcracks. On the surface of the single crystal, the oxidation forms a thin, O-rich region of several-angstrom thickness, which inhibits further oxidation. This thin, oxidized region tends to

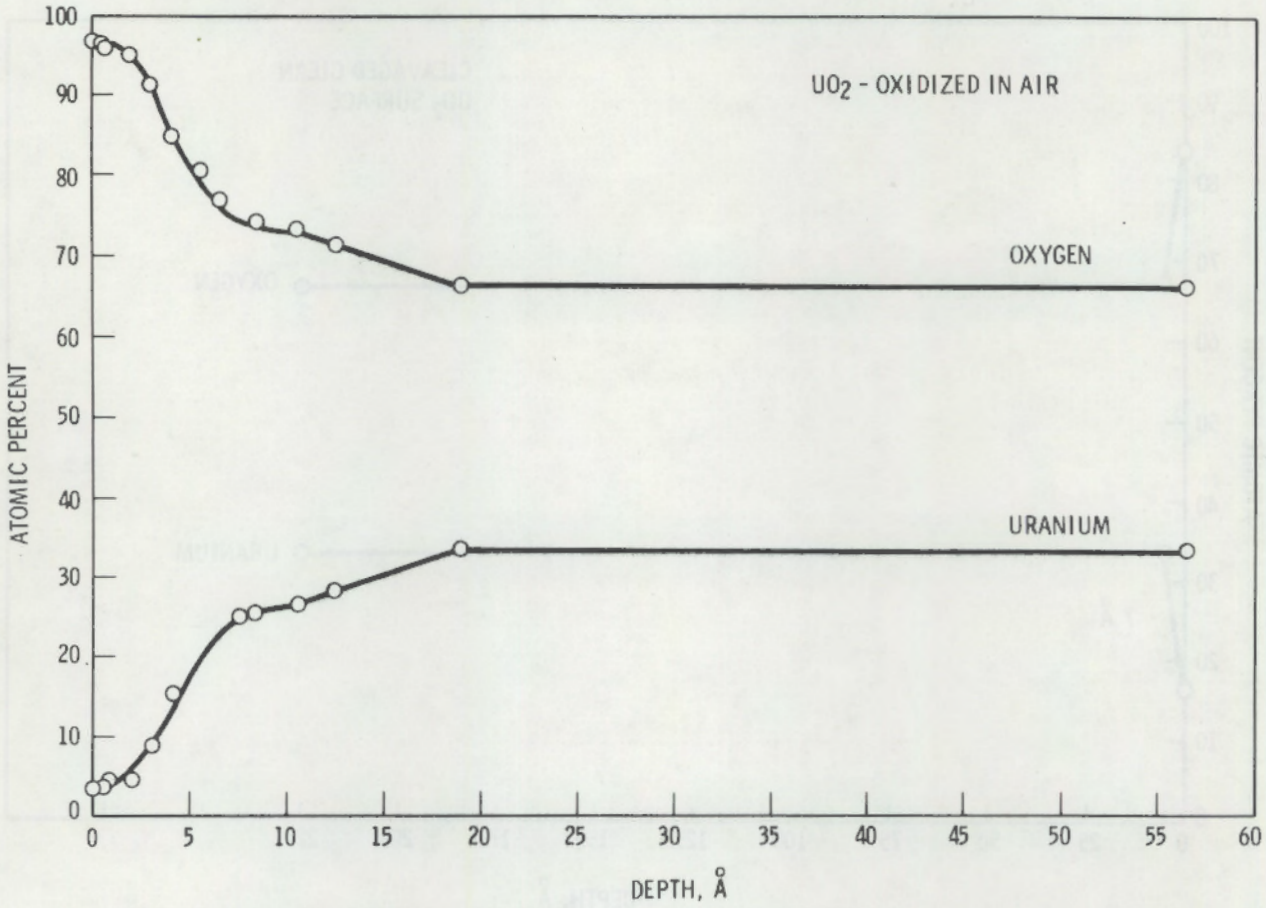

FIGURE 5. Surface Oxidation of Single-Crystal UO_2 Studied by Auger Analysis

have a smaller lattice parameter than the bulk but does not transform into the tetragonal phase. Since the bulk of most of the single crystals was not oxidized, changes in the structure of the oxidized region may be restrained by the bulk structure, preventing transformation from the cubic form. Since a restraint would create a large stress field on the oxidized surface region, this might explain the disorientation of the subgrain microstructure in terms of the stress buildup near the subgrain boundaries during the initial oxidation process.

Stressed oxide layers will imply a high surface energy or enhanced surface reactivity and potential mechanical failure by disintegration. Further investigations are needed to understand the relationship between the surface stress and the rate of dissolution of UO_2 in oxidizing solutions.

TABLE 2. Structure and Lattice Parameter of Uranium Oxides After Air Oxidation of Crushed Single-Crystal UO_2 Powders

Crushed UO_2 Powders		Phases and Lattice Parameter Observed			
Particle Size	Hours at 250°C	UO_2 [a_o, (Å)]	U_3O_7 [a_o, C_o, (Å)]	U_2O_5	U_3O_8
-400 mesh	0	5.470	---	---	---
	16	5.469	5.36, 5.52	trace	---
	40	5.467	5.38, 5.55	trace	trace
	64	---(a)	5.38, 5.55	trace	trace
-325 mesh	0	5.470	---	---	---
	16	5.469	5.38, 5.54	---	---
	40	5.467	5.38, 5.49	trace	strong
	64	---	5.38, 5.49	trace	strong
-200 mesh	0	5.470	---	---	---
	16	5.469	5.38, 5.52	---	trace
	40	5.466	5.37, 5.53	---	strong
	64	---	5.38, 5.49	---	strong

(a) (---) = Not detectable.

DISSOLUTION OF UO_2 IN OXYGENATED SOLUTIONS

The objective of this study is to identify the dissolution mechanisms for UO_2 surfaces in oxygenated solutions. Results reported here are based on autoclave experiments at 75°C and 150°C for times up to 81 d in three solutions supersaturated with dissolved O. We studied the oxidation-dissolution mechanism as a function of temperature and time by characterizing these UO_2 surface features: microstructure, structure, and composition of the surface being dissolved. We then correlated these observations with the changes of the U concentration in the solution.

EXPERIMENTAL PROCEDURES

Single-crystal UO_2 samples weighing about 3 to 6 g with surface areas of ~4 cm^2 were selected. The dissolution experiments were made in a 1-gal Hastelloy-C autoclave with three titanium capsules of UO_2 prepared as shown in Figure 6. The Ti capsules have a volume of ~70 ml and have threaded tip closures with provisions for pressurizing lines. The Ti capsules were enclosed in a Ti screen holder and a volume (in cm^3) of leachant 10 times the estimated surface area (in cm^2) of the samples was prepared (about 40 ml of solution). Three leachant solutions were used in the study: 1) deionized water, 2) 0.03 M synthetic bicarbonate ground water, and 3) Waste Isolation Pilot Plant (WIPP) "8" salt brine. These solutions were prepared in accordance with WISAP Task 2 standards. Each leach solution was pressurized with pure O at different pressures so that a 200 ppm dissolved-oxygen level was anticipated (Needham, Jr. et al. 1975) (Figure 7). Because substantial overpressures were used and there was some refluxing action during the test, O was not sparged before and during the test.

After loading the capsules with samples, the three solutions were added to each capsule and the capsules were placed in the autoclave. Before start of heating, the desired O overpressure was established for each capsule. A run was measured from the time at which the autoclave reached the test temperature.

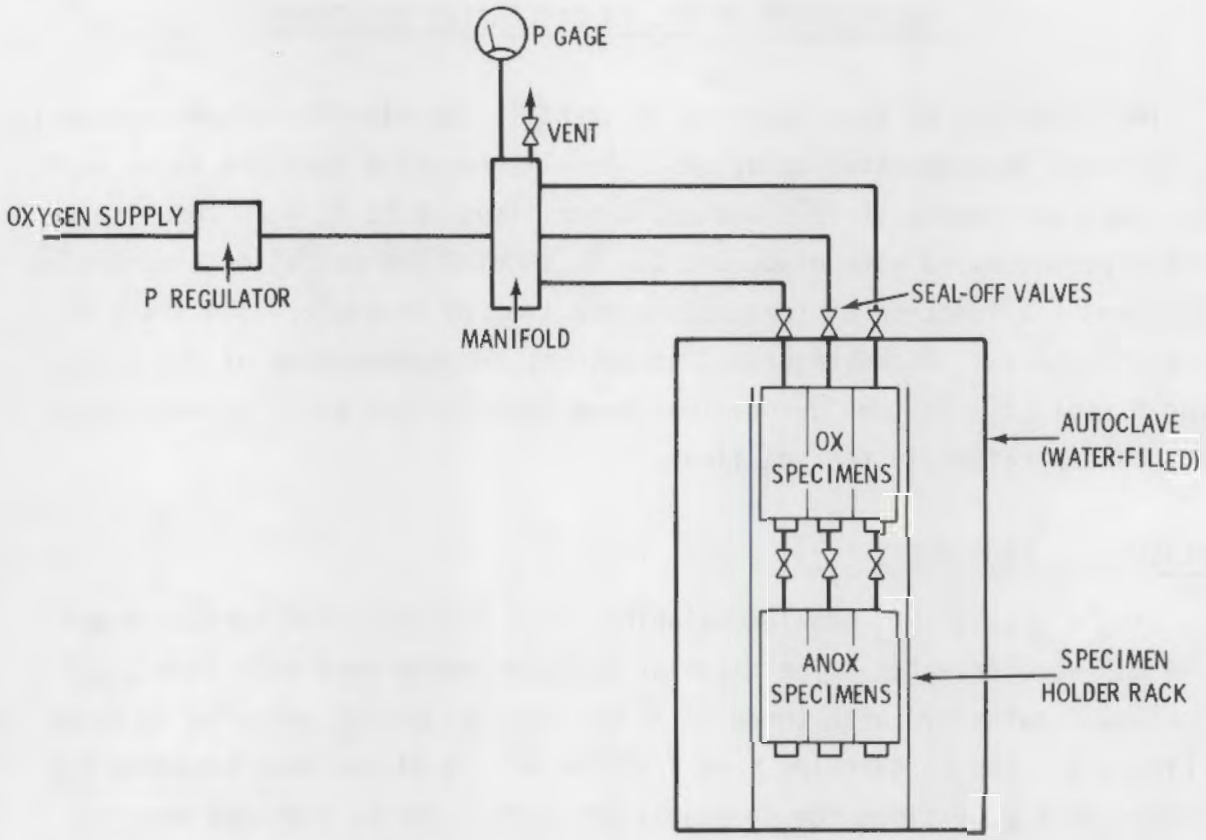

FIGURE 6. Autoclave Experiment for Dissolution of UO_2 in Solutions With 200 ppm Dissolved Oxygen

Upon completion of the test for a designated time, the autoclave power was shut off and the overpressure was maintained until the autoclave had cooled for disassembly. The test solutions were transferred to a glass container for U and pH analysis. The UO_2 samples were undisturbed and the capsules refilled with new solutions for the next test.

The test solutions were analyzed by an isotopic dilution/mass spectrometer technique. Blank solutions in Ti capsules at these temperatures were also prepared for background U content.

After 11, 30 and 60 d, a small sample weighing about 50 mg placed previously with the large samples in the capsules was removed for surface structure and composition analyses. The surfaces of the samples were studied with

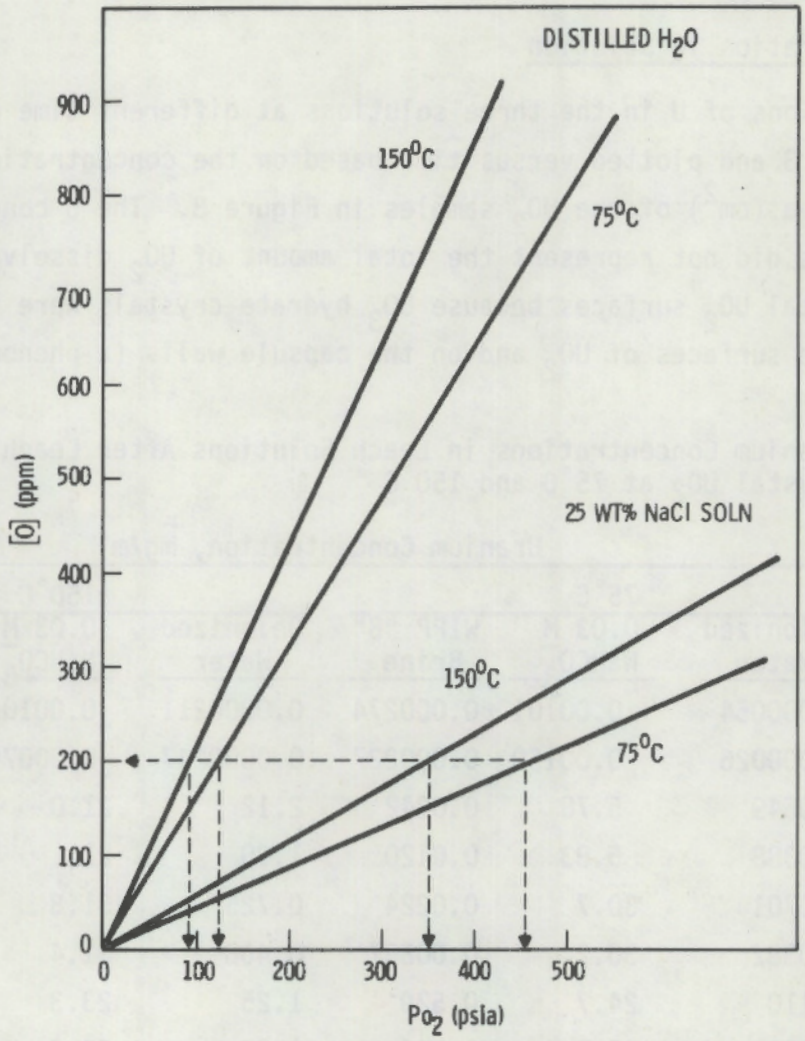

FIGURE 7. Relationship of Pressure and Oxygen Solubility in Water and NaCl Solutions (from Needham, Jr. et al. 1975)

an SEM for surface morphology and surface-film formation. The composition of the surface film and crystals was determined by x-ray energy analysis. The phase of the surface film was investigated by x-ray diffraction.

RESULTS AND DISCUSSION

Uranium Concentration in Solution

Concentrations of U in the three solutions at different time periods are listed in Table 3 and plotted versus time based on the concentration of U per unit surface area (cm^2) of the UO_2 samples in Figure 8. The U concentrations in the solutions did not represent the total amount of UO_2 dissolved from the single-crystal UO_2 surfaces because UO_3 hydrate crystals were found deposited on the surfaces of UO_2 and on the capsule walls (a phenomenon

TABLE 3. Uranium Concentrations in Leach Solutions After Leaching Single-Crystal UO_2 at 75°C and 150°C

	Uranium Concentration, mg/ml					
	75°C			150°C		
Time, d	Deionized Water	0.03 M $NaHCO_3$	WIPP "B" Brine	Deionized Water	0.03 M $NaHCO_3$	WIPP "B" Brine
2.8 Blanks	0.000054	0.00101	0.000274	0.0000211	0.00103	0.000713
9.8 Blanks	0.000026	0.00150	0.000227	0.0000247	0.000792	0.000166
0.5(a)	0.0649	5.78	0.0242	2.12	21.0	0.0171
0.5(b)	0.0388	5.83	0.0120	1.98	21.1	0.00196
2.4(a)	0.0701	30.7	0.0224	0.725	31.8	0.0956
2.4(b)	0.0382	30.2	0.00867	0.468	31.4	0.0655
6.3(a)	0.110	24.7	0.529	1.25	23.3	0.0345
6.3(b)	0.0831	25.5	0.294	1.08	23.2	0.00115
11.1(a)	0.694	41.3	0.178	0.313	28.5	0.0122
15.9(a)	1.08	36.1	0.0585	0.0680	37.8	0.00654
23(a)	2.09	54.4	0.0589	0.0624	32.5	0.0520
31(a)	2.07	49.4	0.0354	0.0579	28.6	0.0162
43(a)	0.550	69.8	0.0455	0.113	26.2	0.0351
58(a)	0.722	90.4	0.0107	0.488	26.0	0.0251
81(a)	0.482	102.0	0.0175	0.163	25.5	0.176

(a) As-received solution.
(b) Centrifuged solution.

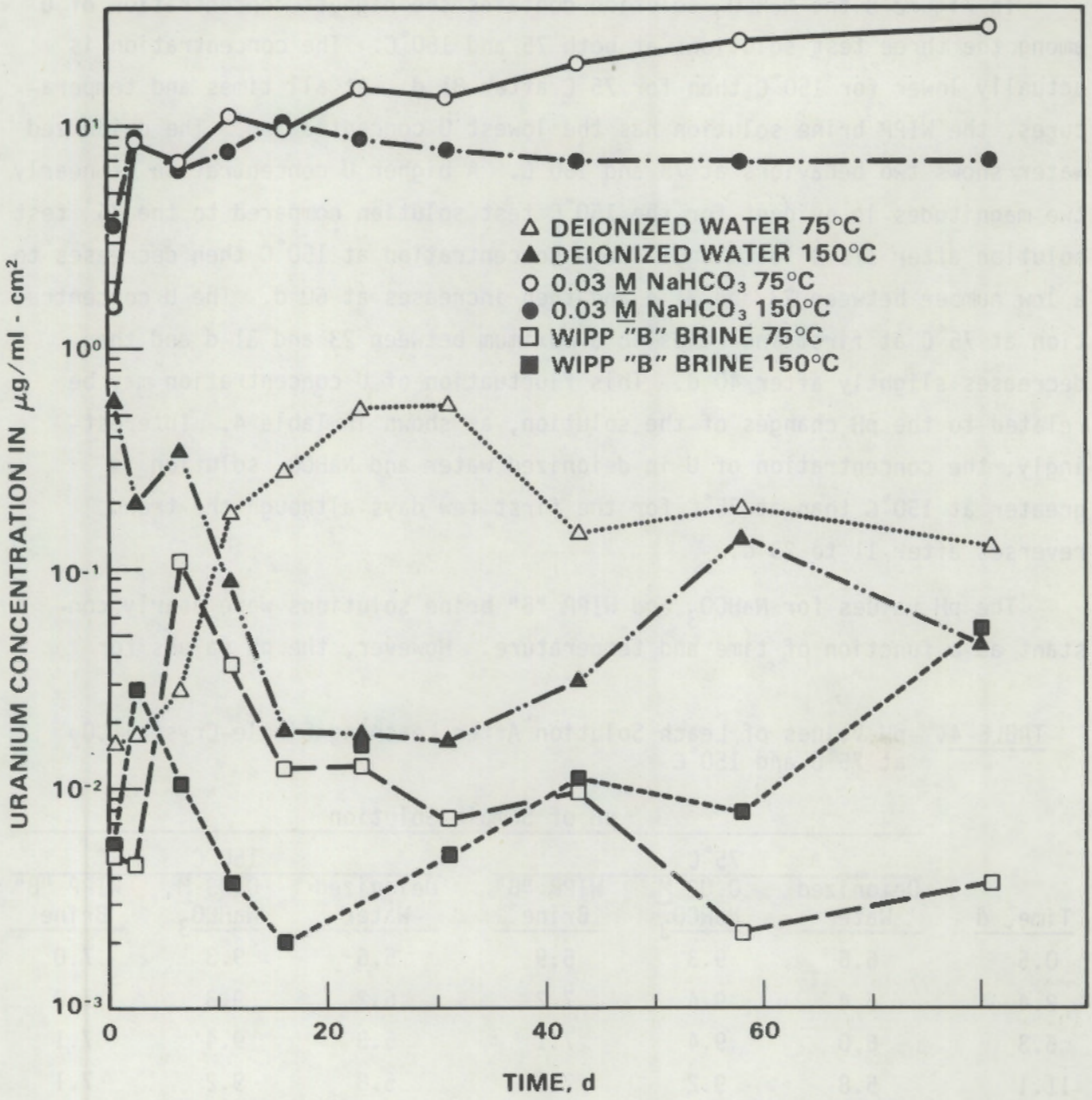

FIGURE 8. Uranium Concentration Versus Time for Single-Crystal UO_2 Surfaces

called "plate-out"). Furthermore, up to one half of the U in the solution may be associated with solid particulates as illustrated by the results of centrifuge tests in Table 3.

In Figure 8 the $NaHCO_3$ solution contains the highest concentration of U among the three test solutions at both 75 and 150°C. The concentration is actually lower for 150°C than for 75°C after 81 d. At all times and temperatures, the WIPP brine solution has the lowest U concentration. The deionized water shows two behaviors at 75 and 150°C. A higher U concentration of nearly two magnitudes is evident for the 150°C test solution compared to the 75° test solution after 1/2 d leaching. The U concentration at 150°C then decreases to a low number between 23 and 31 d and then increases at 60 d. The U concentration at 75°C at first increases to a maximum between 23 and 31 d and then decreases slightly after 40 d. This fluctuation of U concentration may be related to the pH changes of the solution, as shown in Table 4. Interestingly, the concentration of U in deionized water and $NaHCO_3$ solution is greater at 150°C than at 75°C for the first few days although the trend reverses after 11 to 23 d.

The pH values for $NaHCO_3$ and WIPP "B" brine solutions were nearly constant as a function of time and temperature. However, the pH values for

TABLE 4. pH Values of Leach Solution After Leaching Single-Crystal UO_2 at 75°C and 150°C

	pH of Sample Solution					
	75°C			150°C		
Time, d	Deionized Water	0.03 M $NaHCO_3$	WIPP "B" Brine	Deionized Water	0.03 M $NaHCO_3$	WIPP "B" Brine
0.5	6.6	9.3	6.9	5.6	9.3	7.0
2.4	6.4	9.4	7.2	6.2	9.3	7.0
6.3	6.0	9.4	7.1	5.8	9.4	7.1
11.1	5.8	9.2	7.1	5.8	9.2	7.1
15.9	5.6	9.1	7.1	6.1	9.2	7.0
23	5.6	9.2	7.0	6.1	9.2	7.1
31	5.5	9.2	7.3	6.1	9.2	7.3
43	6.0	9.3	7.5	6.3	9.2	7.2
58	6.3	9.2	7.1	6.8	9.1	7.2
81	5.9	9.2	7.3	6.3	9.1	7.0

deionized water fluctuated at the first 31 d for the 75°C solution and the first 11 d for the 150°C solution. These pH changes in deionized water would be a good indicator of the oxidation-dissolution of UO_2 and the solubility limits of the uranyl ions. The low pH values found between 11 and 31 d for the 75°C solution correspond to the high U concentrations in the solution for the same time period. Also, the sudden increase of pH from 5.6 to 6.2 for the 0.5 to 2.4 d period may cause the peak at 6.3 d for the 150°C solution. Apparently, the high U concentration is due mainly to the increase of solubility of uranyl ions at lower pH values as indicated by Holland and Brush (1979). The reason for the pH fluctuation was not identified.

The plate-out problem was examined by rinsing the Ti capsules after the test with 50 ml of 1 M HNO_3 for 1 h at room temperature. Table 5 shows the seriousness of the plate-out problem, especially for the $NaHCO_3$ and deionized water at 150°C. Although the solution analysis did show lower U concentration for $NaHCO_3$ at 150°C compared to the 75°C test, the large amount of U removed from the Ti capsules indicates that the dissolution rates of UO_2 surfaces for 150°C are far more than those of 75°C.

TABLE 5. Post-Experiment Acid Rinse[a] of Capsules

Capsule	Solution and Temperature of Leach Experiment	Uranium Removed, µg
A1	H_2O, 75°C	58.0
B1	$NaHCO_3$, 75°C	23.9
C1	WIPP "B" Brine, 75°C	4.06
A2	H_2O, 150°C	103.0
B2	$NaHCO_3$, 150°C	2280.0
C2	WIPP "B" Brine, 150°C	21.8
Spare	Not used in experiment	0.026
Blank	Glassware and reagents	0.000527

(a) Rinse Procedure: 50 ml of 1 M HNO_3 in each capsule for 1 h at room temperature.

It is possible that the deionized water and $NaHCO_3$ solutions were supersaturated with uranyl ions near the UO_2 surface region at all times and the dissolution of UO_2 continued even when the solution was saturated. In this case, the U concentration in the solution will be related to the solubility of the uranyl ions. Oxidation-dissolution will proceed even if the solution is supersaturated, and the excess uranyl ions over the solubility limit will be transferred into the solid form of deposits and plate-out. The following examination of the surface features of the test samples confirms this conclusion.

Surface Features

Although solution analysis of U concentrations did not show a clear picture of the oxidation-dissolution mechanism, much can be learned from the studies of the surface features of the UO_2 samples. The surface deposits clearly illustrate that oxidation-dissolution is promoted by higher temperatures, such as 150°C, and that a great difference exists between the dissolution rates for these two temperatures.

Deionized Water

A layer of well-defined crystals was deposited onto the UO_2 surface after 11 d at 150°C (see Figure 9). The deposited crystals had both cubic and cone shapes about 1 μm in size. X-ray diffraction indicates that these crystals are UO_3 hydrates. Table 6 shows powder diffraction patterns for those deposited crystals at 11 and 30 d. The diffraction patterns resemble those of $UO_2(OH)_2$ (Debets and Loopstra 1963) and sodium polyuranite I and II (Brush 1980), Figure 10.

No visible deposition of crystals and films on the surface of UO_2 is evident in the 75°C tests (Figure 11). After 30 d at 150°C, the deposited crystals had grown in size into the shape of a plate ~5 μm thick (Figure 12). These crystals were not as perfect as those observed after 11 d, which indicates an effect of redissolution and redeposition of the UO_3 hydrates during a long period of time. Again, no evidence of deposition was observed for UO_2 tested at 75°C for 30 d (Figure 13). After 60 d of autoclave testing, the

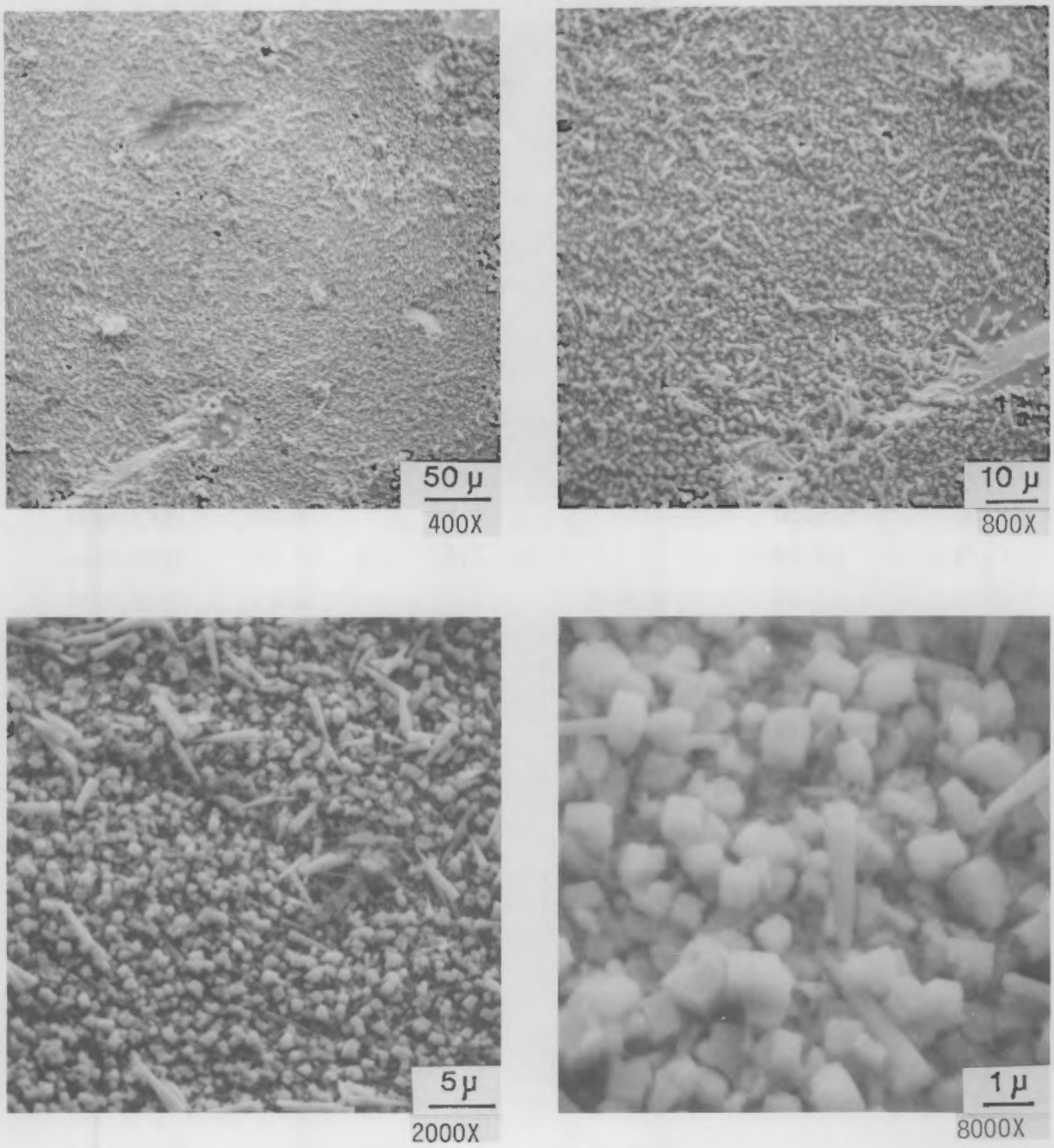

FIGURE 9. SEM Micrographs of UO_2 Surfaces After 11 Days at 150°C in Deionized Water Containing 200 ppm Dissolved Oxygen

TABLE 6. X-Ray Powder Diffraction Data for UO_2 Surface-Deposited Crystals in Deionized Water at 150°C

Deposited Crystal After 11 d			Deposited Crystal After 30 d		
D Spacing	Theta	I/I_o	D Spacing	Theta	I/I_o
7.46	5.92	Strong	7.48	5.91	Strong
5.78	7.65	---(a)	5.68	7.79	---
5.34	8.30	---	5.34	8.29	---
3.72	11.94	Medium	3.72	11.93	Medium
3.51	12.65	Medium	3.52	12.63	Medium
3.40	13.07	Medium	3.40	13.08	Medium
3.19	13.96	---	3.17	14.06	Medium
3.16	14.12	Medium	3.06	14.57	Weak
3.05	14.63	Weak	2.87	15.55	---
2.88	15.50	---	2.57	17.39	Very Weak
2.74	16.32	---	2.47	18.12	Very Weak
2.57	17.45	Very Weak	2.22	20.26	Very Weak
2.48	18.10	Weak	2.05	22.08	Very Weak
2.22	20.23	Very Weak	2.01	22.53	Weak
2.15	20.96	---	1.95	23.24	Very Weak
2.06	21.97	Very Weak	1.86	24.40	Very Weak
2.01	22.52	Weak	1.81	25.17	---
1.95	23.20	Very Weak	1.76	25.91	Very Weak
1.87	24.31	Very Weak	1.70	26.84	---
1.80	25.28	---	1.61	28.53	Very Weak
1.76	25.85	Very Weak	2.73	16.34	---
1.70	26.82	---	1.66	27.62	---
1.66	27.63	---			
1.61	28.57	Very Weak			

(a) --- = Very Very Weak

deposited hydrate crystals of the 150°C sample became rough in shape but showed no evidence of further growth of the crystal size (Figure 14), which suggests that an equilibrium of crystal deposition and dissolution was reached. The

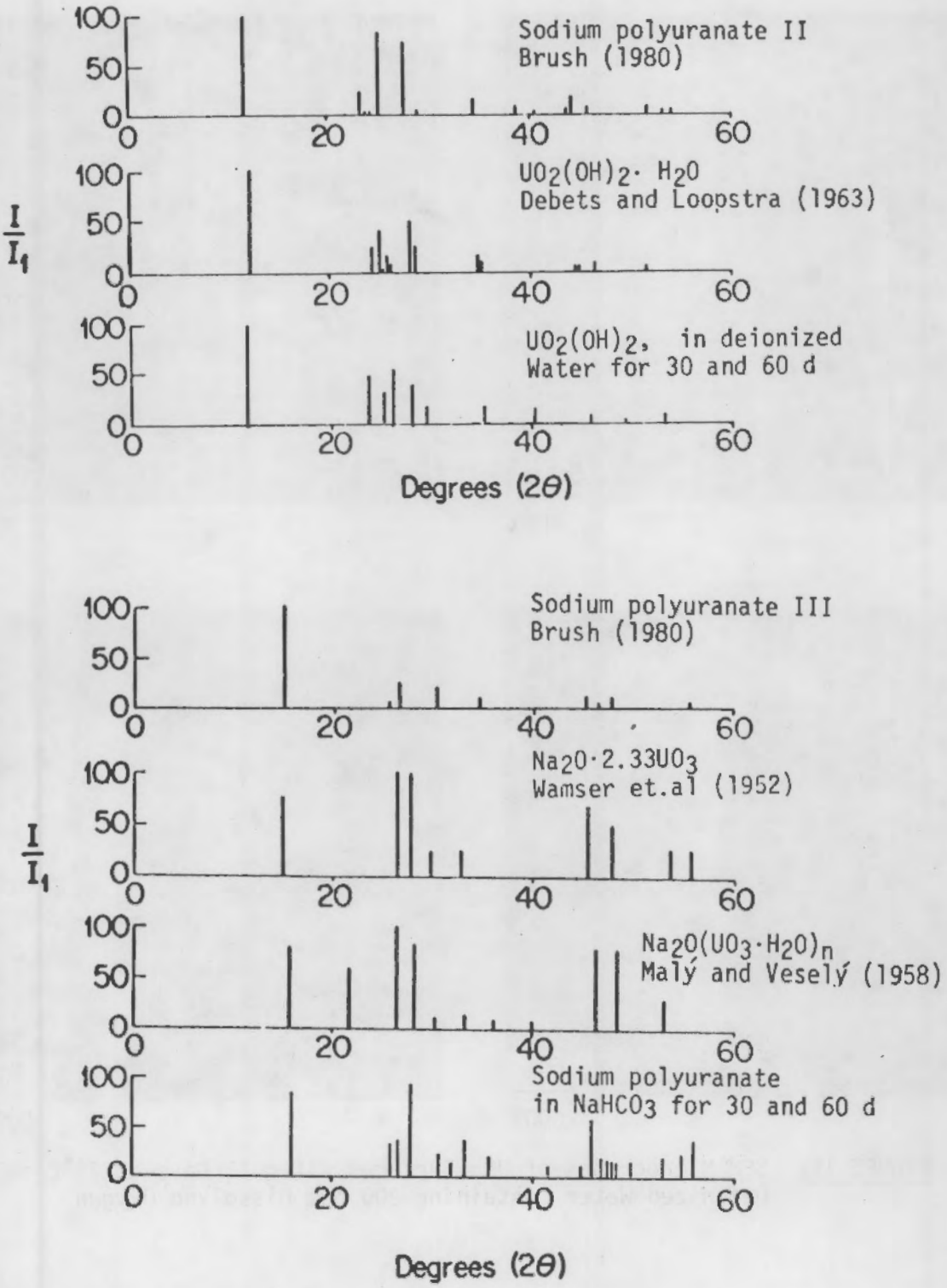

FIGURE 10. Schematic Diffractograms for UO_2 Surface-Deposited Crystals at 150°C in Deionized Water and 0.03 M $NaHCO_3$ Solution

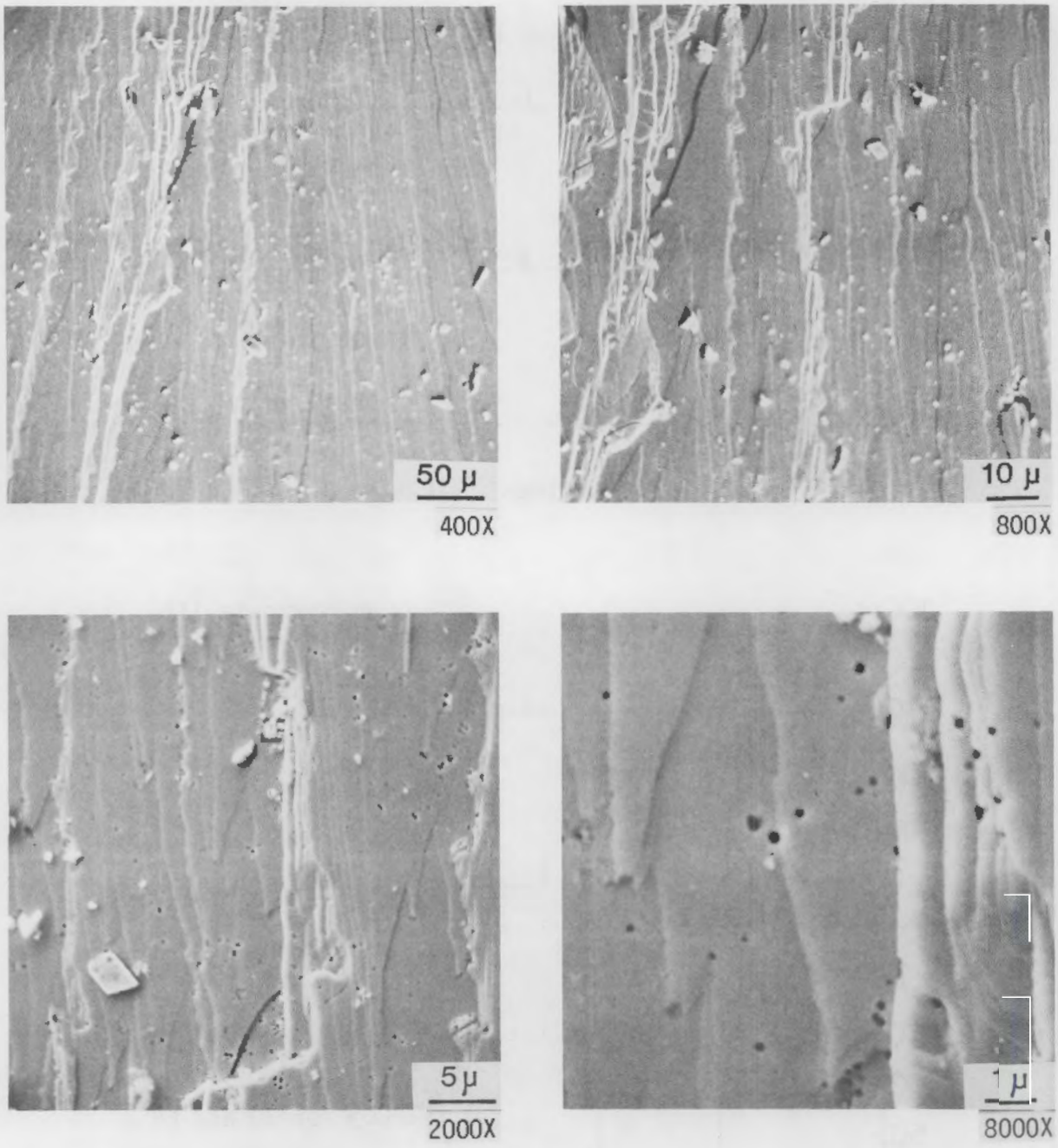

FIGURE 11. SEM Micrographs of UO_2 Surfaces After 11 Days at 75°C in Deionized Water Containing 200 ppm Dissolved Oxygen

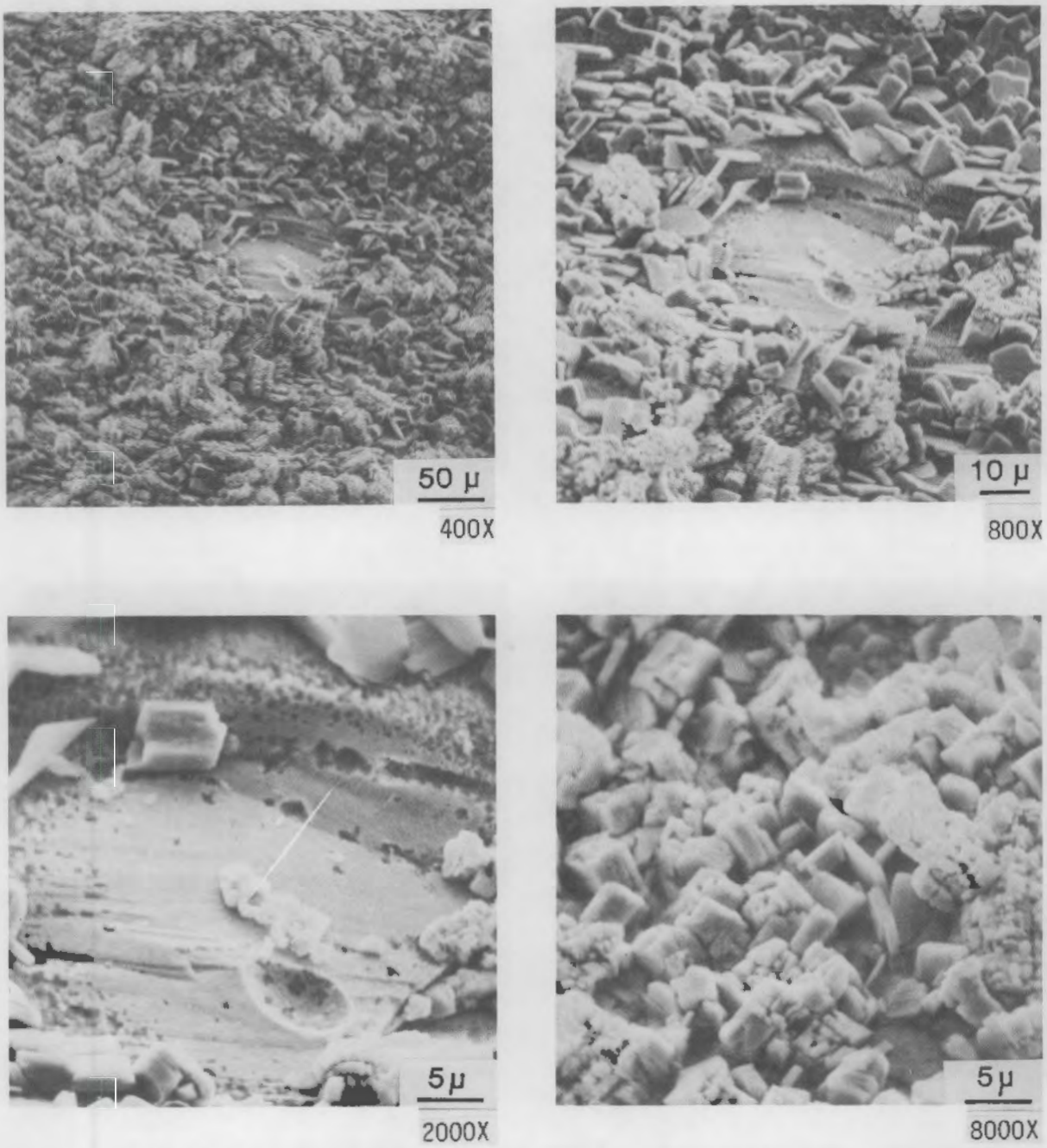

FIGURE 12. SEM Micrographs of UO_2 Surfaces After 30 Days at 150°C in Deionized Water Containing 200 ppm Dissolved Oxygen

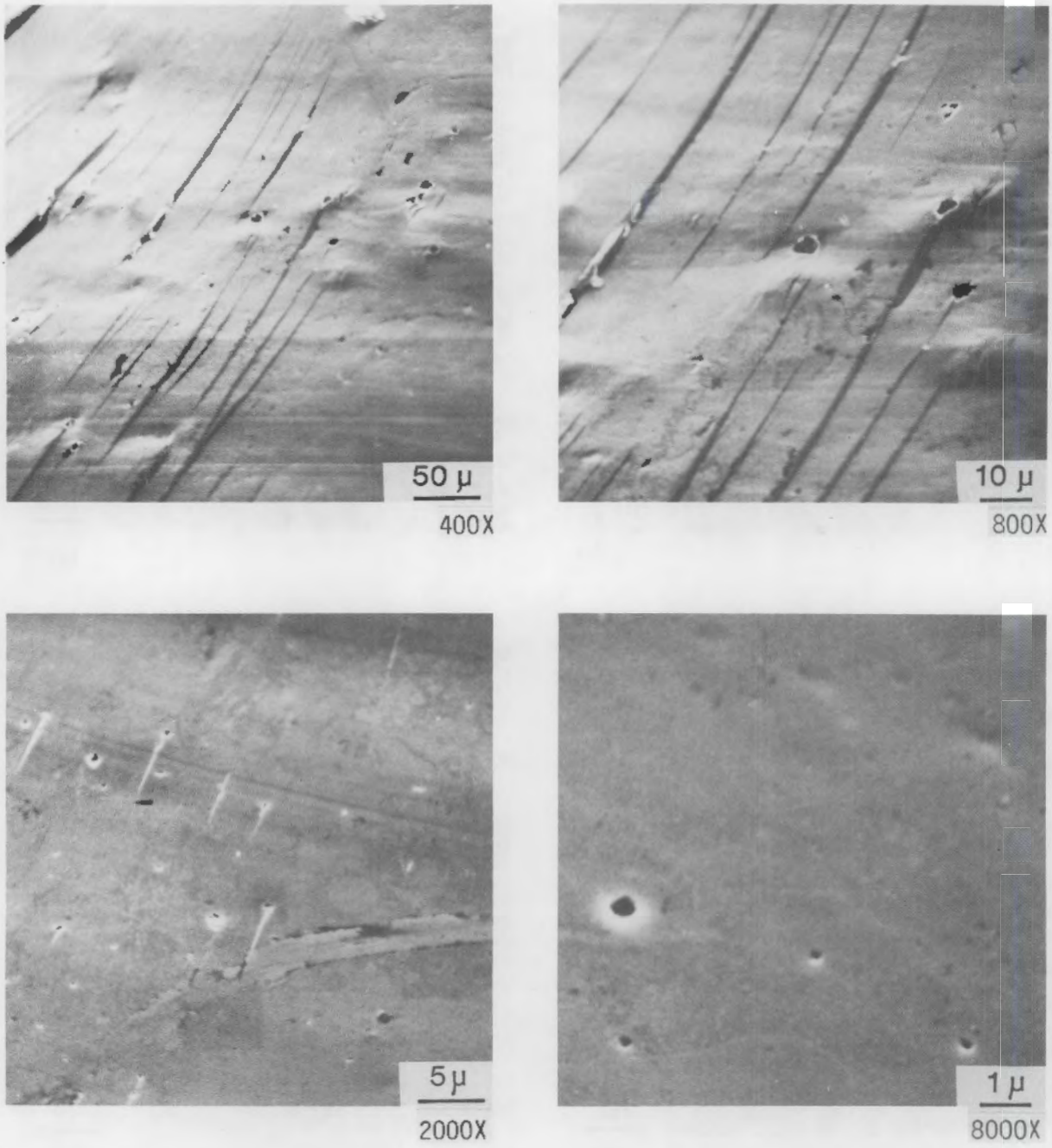

FIGURE 13. SEM Micrographs of UO_2 Surfaces After 30 Days at 75°C in Deionized Water Containing 200 ppm Dissolved Oxygen

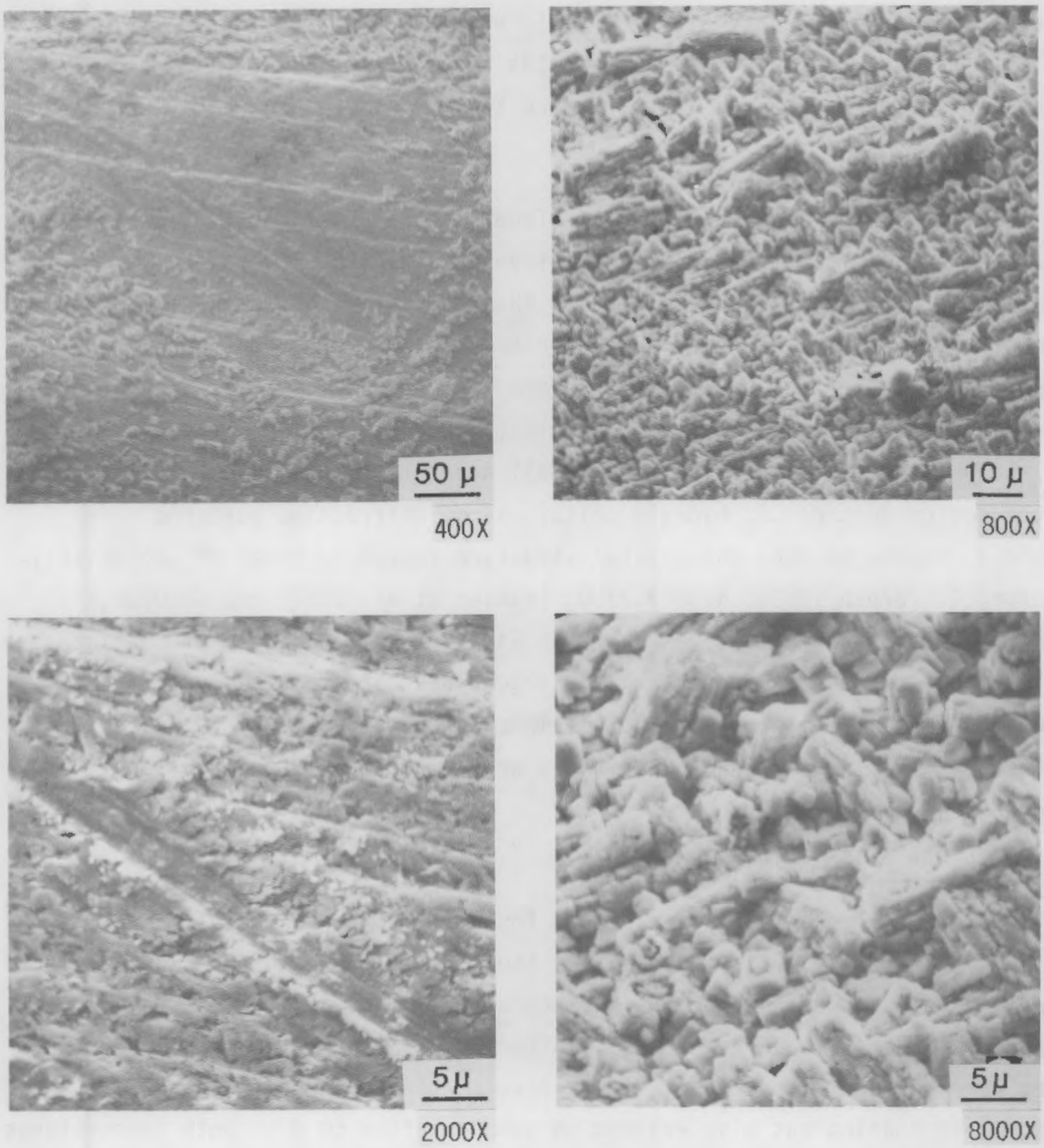

FIGURE 14. SEM Micrographs of UO_2 Surfaces After 60 Days at 150°C in Deionized Water Containing 200 ppm Dissolved Oxygen

75°C-tested sample surface after 60 d did have a few needle-shaped crystals and the surface was rough, which indicates the apparent dissolution and thin deposition of a UO_3 hydrate layer (Figure 15).

0.03 M $NaHCO_3$

Figures 16 and 17 show the UO_2 surface after 11 d of dissolution in 0.03 M $NaHCO_3$ at 75°C and 150°C, respectively. The 150°C sample had a greater dissolution and surface etching than had the 75°C sample. No deposition of crystals was observed for either temperature. However, after 30 d, dissolution of the surface was more severe, and a thick layer of deposited crystals was observed on the 150°C sample (Figures 18 and 19). X-ray elemental analysis of the crystal showed a small quantity of sodium or the formation of the sodium form of UO_3 hydrate salts. X-ray diffraction patterns (Table 7) indicated that the crystal structure resembled those of sodium polyuranite III (Brush 1980), $Na_2O \cdot 2.33UO_3$ (Wamser et al. 1952) and $Na_2O(UO_3 \cdot H_2O)_n$ (Malý and Veselý 1958) as shown in Figure 10. After 60 d of testing, the 150°C sample surface was covered with large plate-like crystals nearly 5 μm wide (Figure 20). Although the 75°C sample was pitted and etched heavily throughout this time period, no crystals were deposited on the surface (Figure 21).

WIPP "B" Brine Solution

Only a few deposited crystals were found on the UO_2 surface after 11 d at 150°C (Figure 22). Also, etching of the surface was evident. For the 75°C sample surface, no etching of the surface was evident, and few crystals were attached to the surface (Figure 23). After 30 d, both the 75°C and 150°C surfaces were covered with a thin, sponge-like coating (Figures 24 and 25). The sponge-like coating was also evident on samples after 60 d at both temperatures (Figures 26 and 27). No apparent differences existed in surface roughness and coating layer between the 30- and 60-d samples, which indicates a low dissolution and deposition rate. The thin coating layer may have a passive nature, which protects the surface from further oxidation-dissolution.

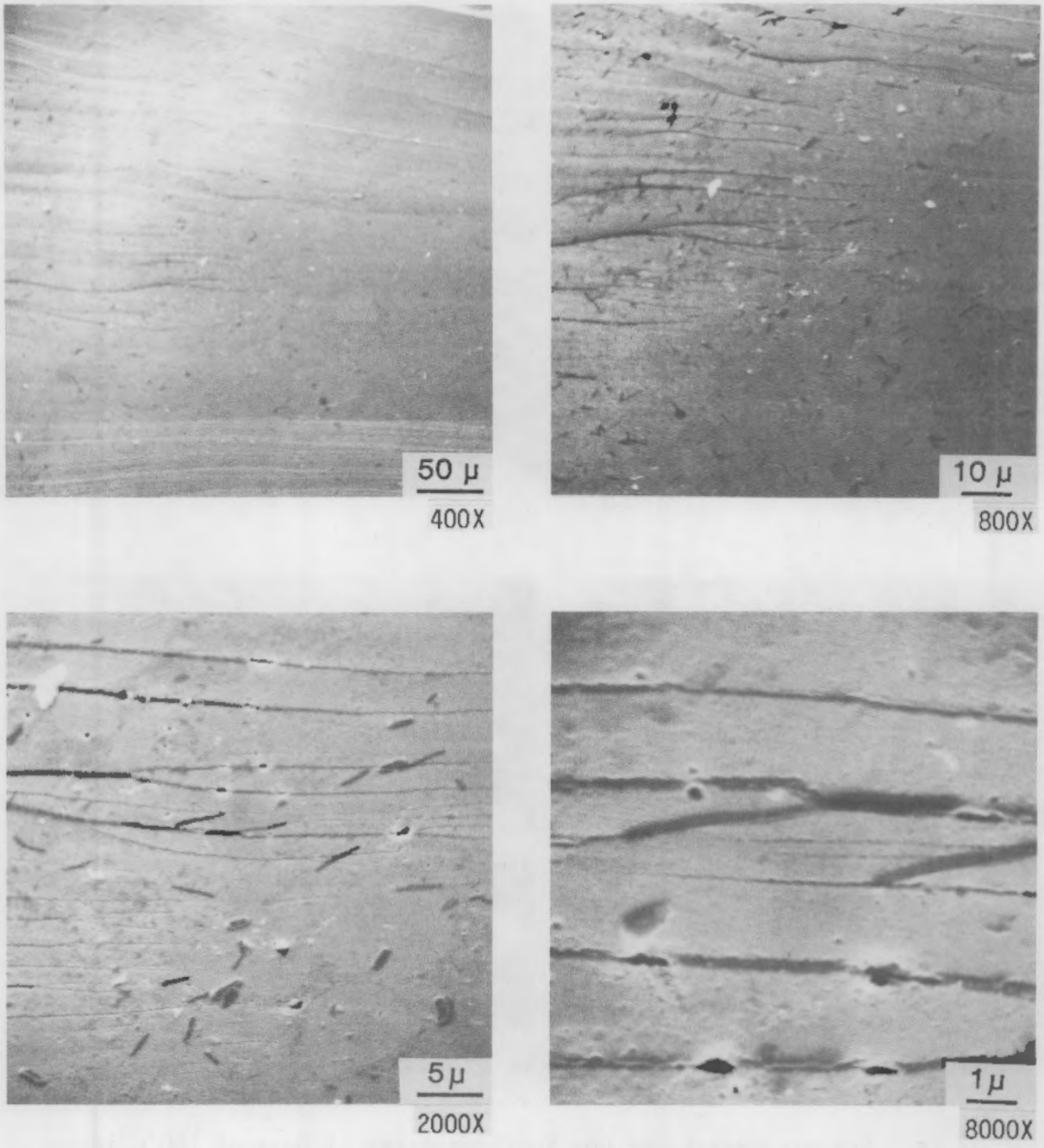

FIGURE 15. SEM Micrographs of UO_2 Surfaces After 60 Days at 75°C in Deionized Water Containing 200 ppm Dissolved Oxygen

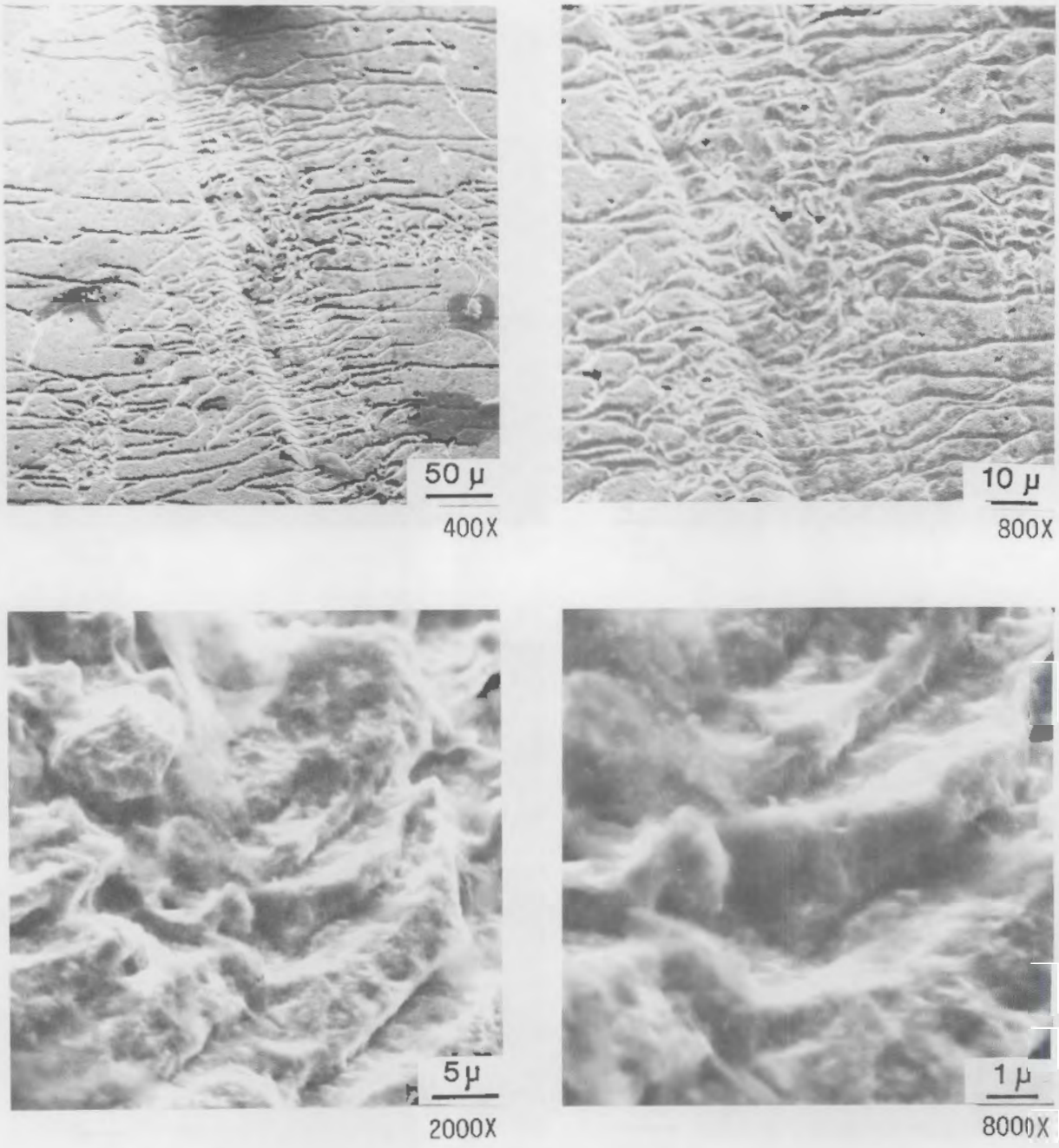

FIGURE 16. SEM Micrographs of UO_2 Surfaces After 11 Days at 150°C in $NaHCO_3$ (0.03 M) Containing 200 ppm Dissolved Oxygen

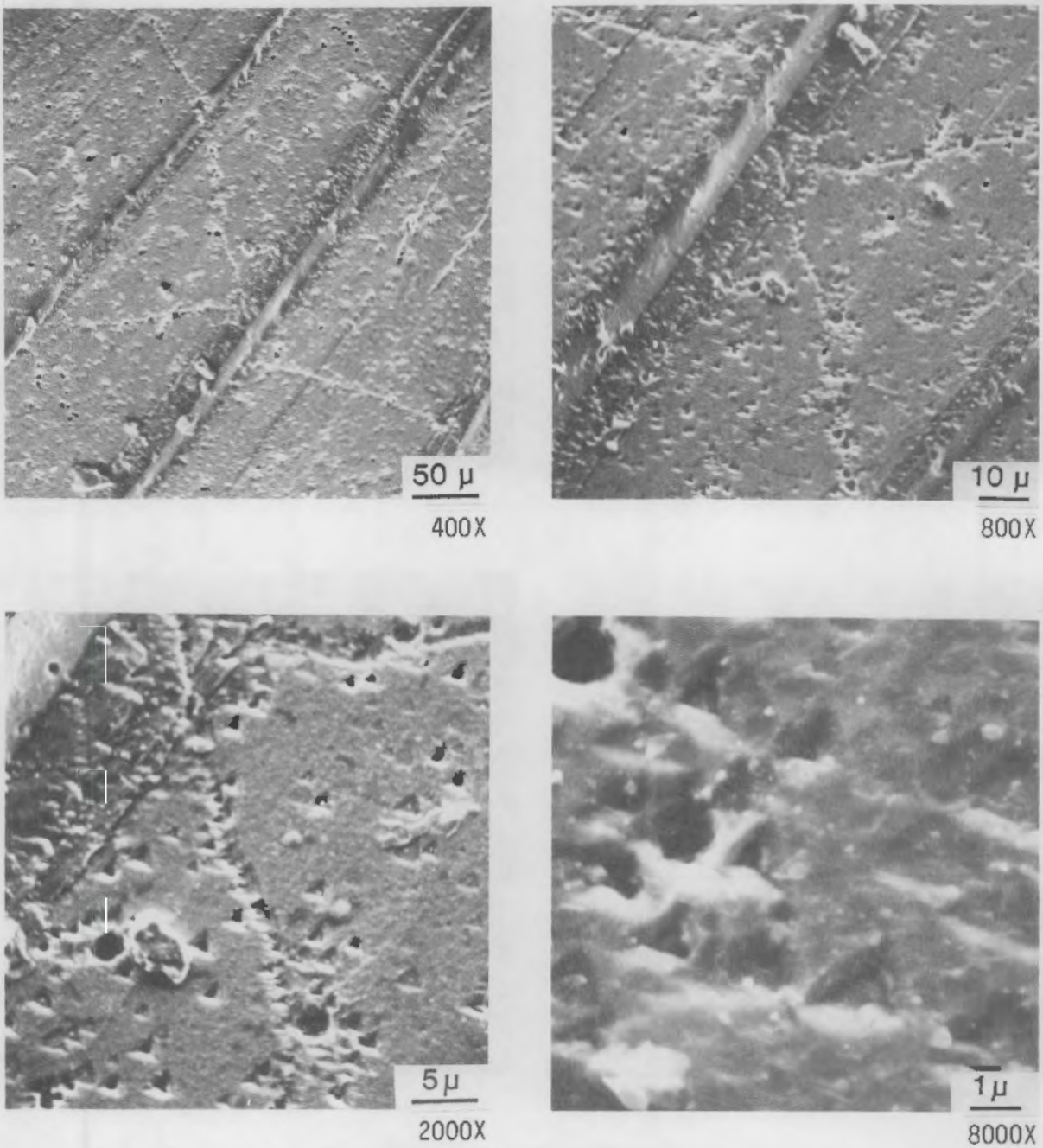

FIGURE 17. SEM Micrographs of UO_2 Surfaces After 11 Days at 75°C in $NaHCO_3$ (0.03 M) Containing 200 ppm Dissolved Oxygen

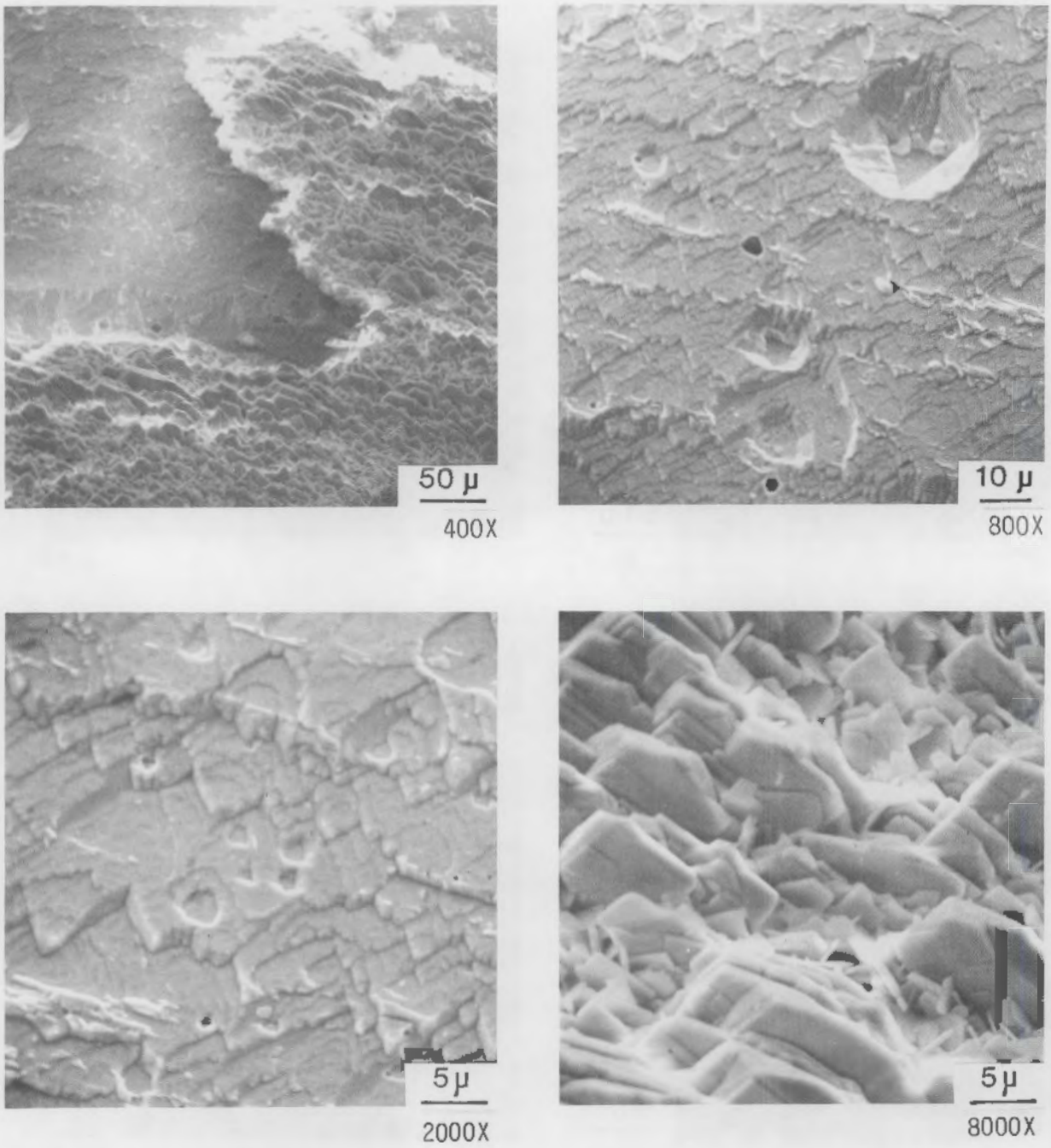

FIGURE 18. SEM Micrographs of UO_2 Surfaces After 30 Days at 150°C in $NaHCO_3$ (0.03 M) Containing 200 ppm Dissolved Oxygen

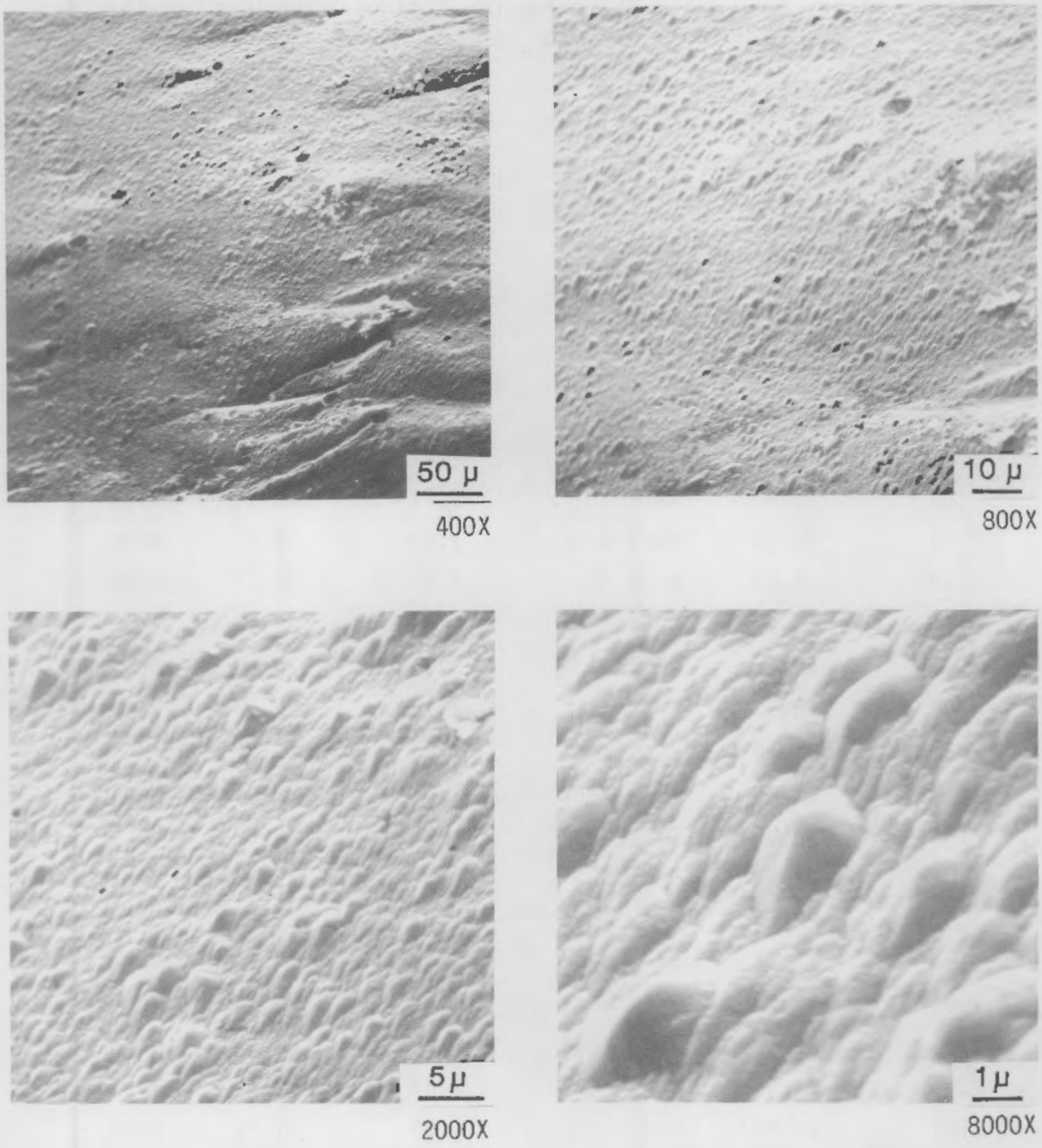

FIGURE 19. SEM Micrographs of UO_2 Surfaces After 30 Days at 75°C in $NaHCO_3$ (0.03 M) Containing 200 ppm Dissolved Oxygen

TABLE 7. X-Ray Diffraction Data for UO_2 Surface-Deposited Crystals in 0.03 M $NaHCO_3$ Solution at 150°C

Deposited Crystal After 30 d			Deposited Crystal After 60 d		
D Spacing	Theta	I/I_o	D Spacing	Theta	I/I_o
5.84	7.58	Strong	5.83	7.59	Strong
5.08	8.73	---(a)	4.18	10.61	---
4.18	10.62	---	3.68	12.09	---
3.69	12.04	---	3.45	12.90	Medium
3.45	12.89	Medium	3.36	13.24	Medium
3.37	13.22	Medium	3.22	13.83	Strong
3.22	13.84	Strong	2.78	16.0B	---
2.90	15.40	Medium	2.91	15.34	Weak
2.85	15.68	---	2.77	16.13	Weak
2.76	16.18	Very Weak	2.69	16.62	Weak
2.69	16.64	Weak	2.46	18.24	Weak
2.45	18.27	Weak	2.33	19.24	---
2.33	19.25	---	2.25	20.03	Very Weak
2.28	19.74	---	2.18	20.63	Very Weak
2.24	20.10	Very Weak	2.06	21.92	---
2.19	20.60	Very Weak	2.01	22.49	Medium
2.05	22.06	Very Weak	1.98	22.88	Very Weak
2.01	22.48	Medium	1.94	23.31	Very Weak
1.97	22.96	Very Weak	1.91	23.68	Very Weak
1.94	23.36	Very Weak	1.88	24.14	Very Weak
1.91	23.72	Very Weak	1.86	24.43	Very Weak
1.89	24.05	Very Weak	1.72	26.53	Very Weak
1.85	24.51	Very Weak	1.67	27.32	Very Weak
1.83	24.80	---	1.64	27.98	Weak
1.72	26.47	Very Weak	1.61	28.53	Very Weak
1.67	27.36	Very Weak	1.58	29.16	Very Weak
1.64	28.01	Weak	1.55	29.73	---
1.61	28.54	Very Weak	1.54	29.98	---

(a) --- = Very Very Weak

TABLE 7. (contd)

Deposited Crystal After 30 d			Deposited Crystal After 60 d		
D Spacing	Theta	I/I_o	D Spacing	Theta	I/I_o
1.57	29.22	Very Weak	1.49	30.97	---
1.55	29.73	Very Weak	1.45	31.98	---
1.53	30.10	Very Weak	1.43	32.49	---
1.49	31.07	Very Weak	1.41	32.92	---
1.45	32.02	Very Weak	1.38	33.69	---
1.43	32.46	Very Weak	1.37	34.19	---
1.41	33.02	---	1.34	35.05	---
1.38	33.79	Very Weak	1.32	35.65	---
1.37	34.19	---	1.30	36.16	Very Weak
1.34	35.09	Very Weak	1.27	37.17	---
1.32	35.65	Very Weak	1.24	38.13	---
1.30	36.21	Very Weak	1.22	38.85	---
1.27	37.08	---			
1.25	38.05	---			
1.23	38.52	---			
1.19	40.24	---			
1.18	40.77	---			
1.17	41.13	---			
1.16	41.54	---			
1.13	42.79	---			

CONCLUSIONS

Autoclave studies of the dissolution of single-crystal UO_2 surfaces at 75 and 150°C indicate that the dissolution of the UO_2 surface in oxygenated solution is a function of temperature. Oxygen, present near the UO_2 surface, assists in this dissolution. Initially, due to the high dissolution rate of the UO_2 surface, the solution near the UO_2 surface quickly approaches saturation within a short incubation period, probably 20 d at 150°C for the $NaHCO_3$ solution and <11 d for deionized water. Basically an oxidation process, the oxidation-dissolution of UO_2 is controlled by the availability of O near

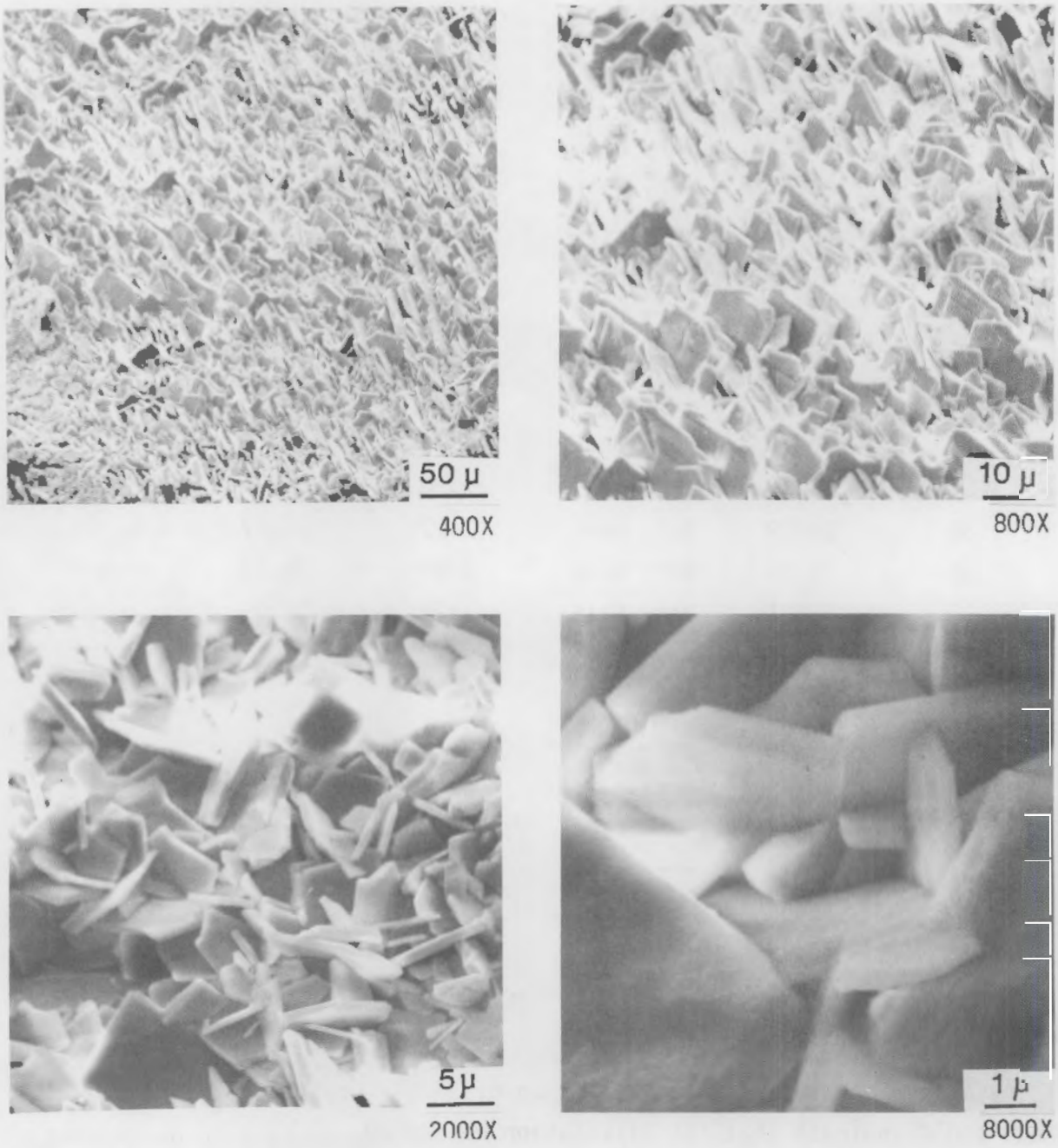

FIGURE 20. SEM Micrographs of UO_2 Surfaces After 60 Days at 150°C in $NaHCO_3$ (0.03 M) Containing 200 ppm Dissolved Oxygen

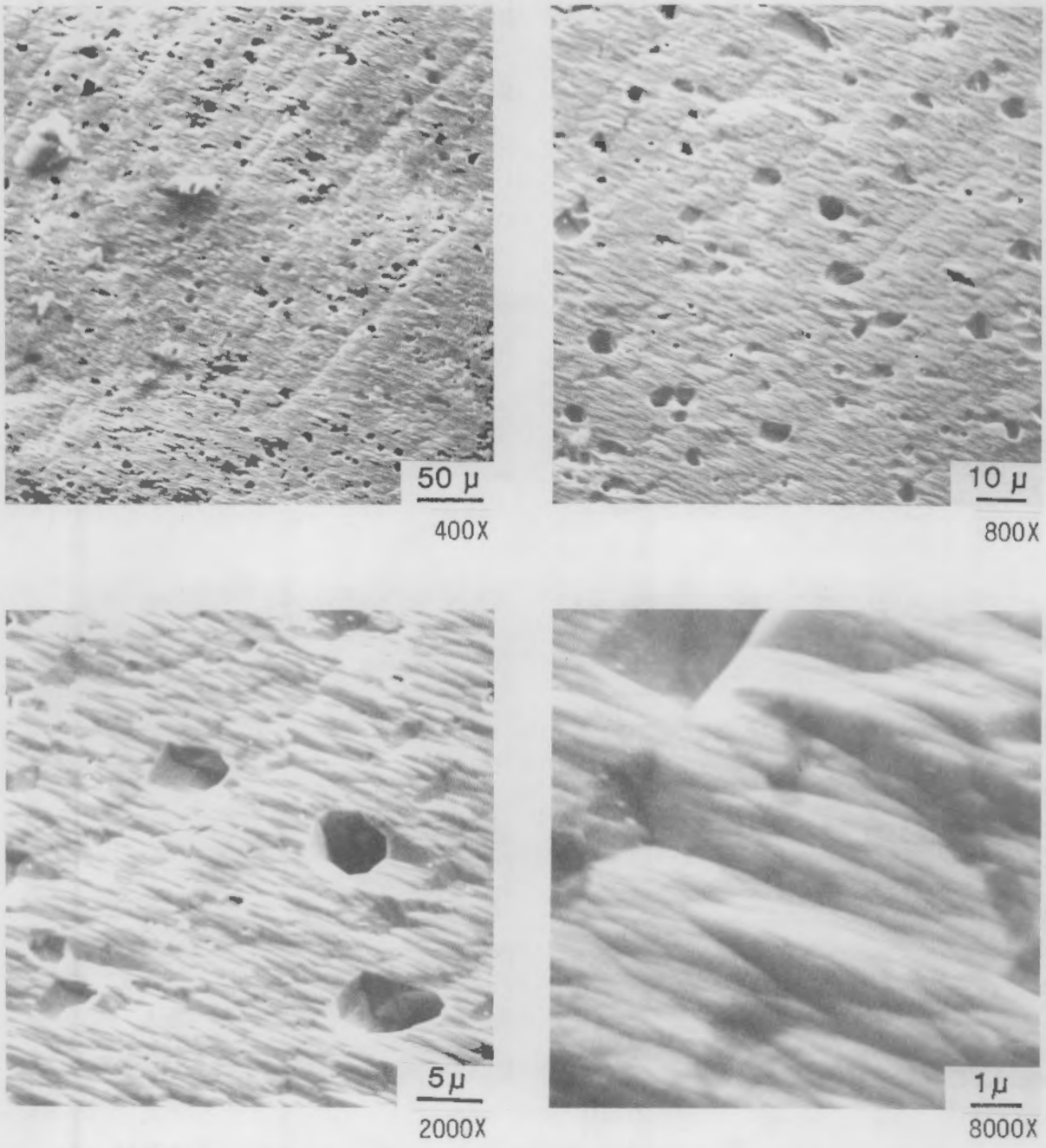

FIGURE 21. SEM Micrographs of UO_2 Surfaces After 60 Days at 75°C in $NaHCO_3$ (0.03 M) Containing 200 ppm Dissolved Oxygen

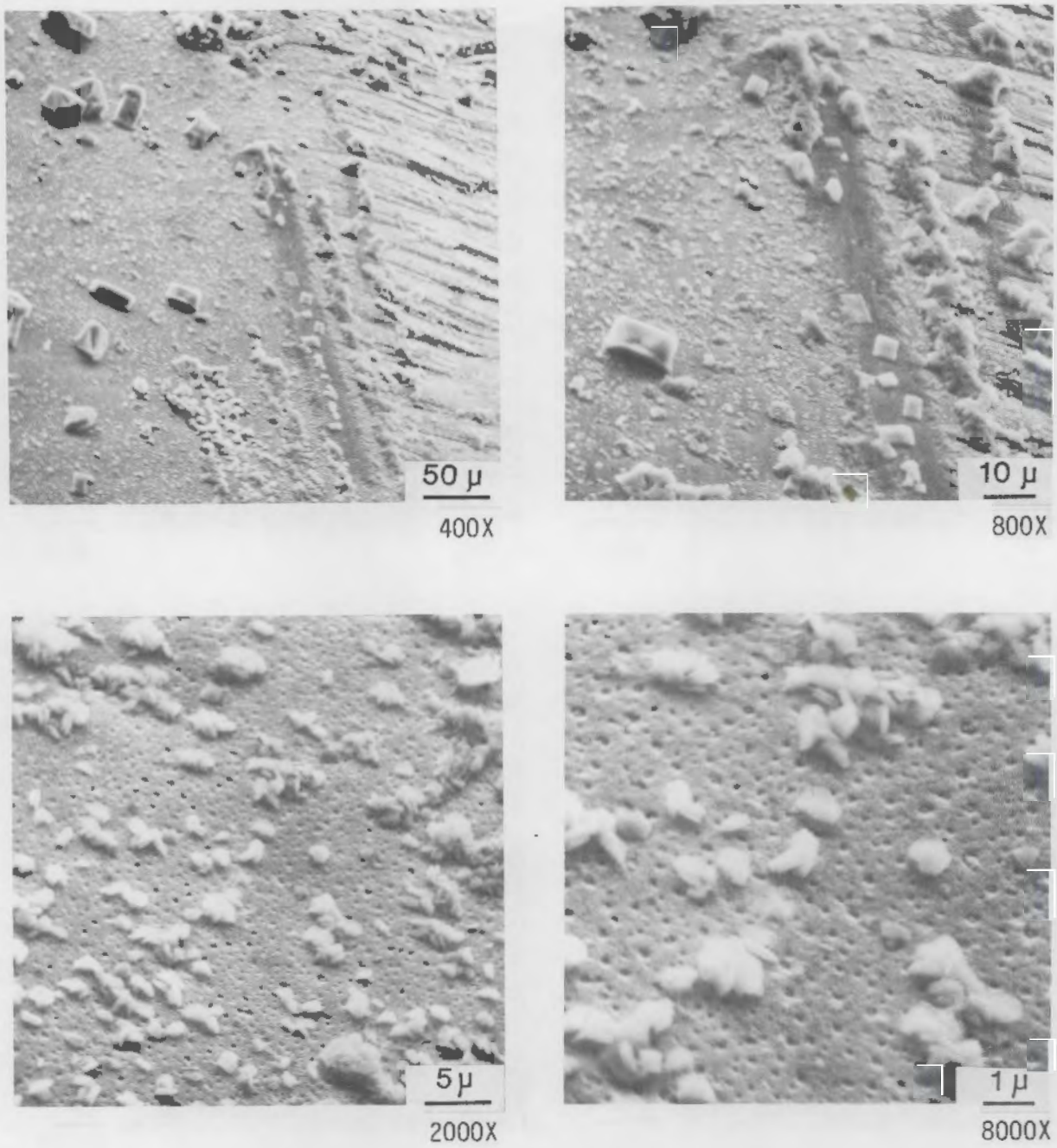

FIGURE 22. SEM Micrographs of UO_2 Surfaces After 11 Days at 150°C in WIPP "B" Brine Solution Containing 200 ppm Dissolved Oxygen

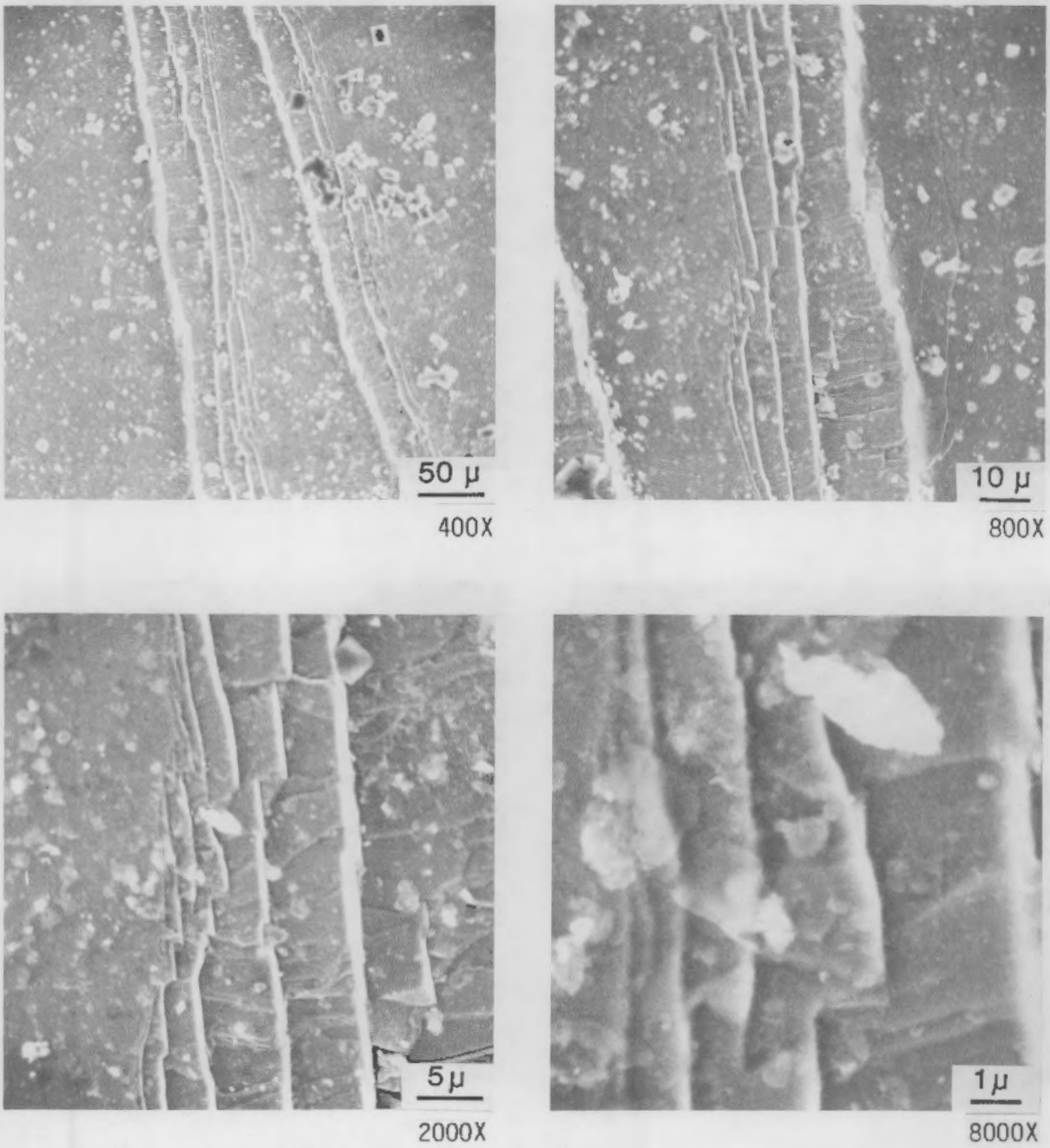

FIGURE 23. SEM Micrographs of UO_2 Surfaces After 11 Days at 75°C in WIPP "B" Brine Solution Containing 200 ppm Dissolved Oxygen

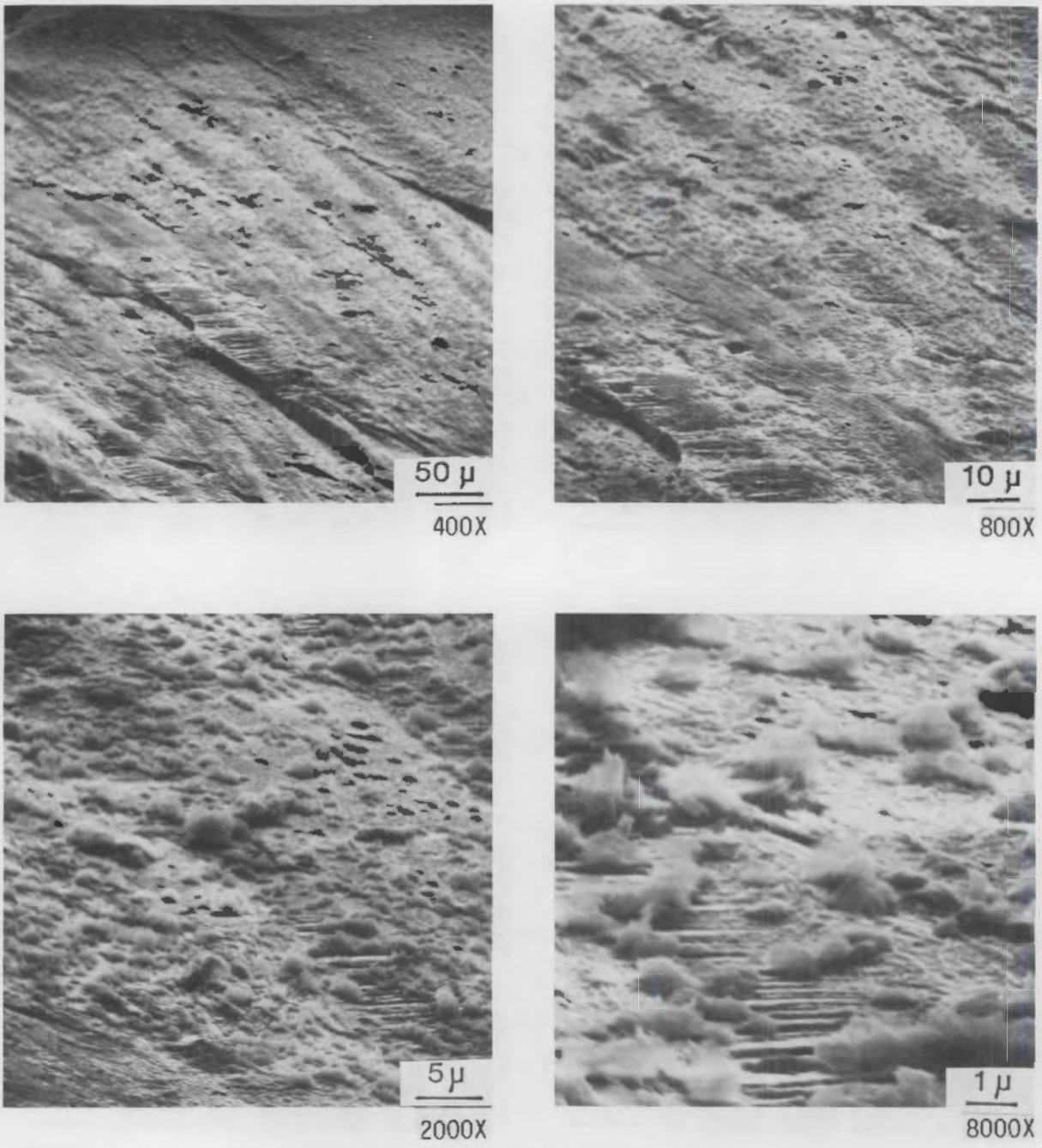

FIGURE 24. SEM Micrographs of UO_2 Surfaces After 30 Days at 150°C in WIPP "B" Brine Solution Containing 200 ppm Dissolved Oxygen

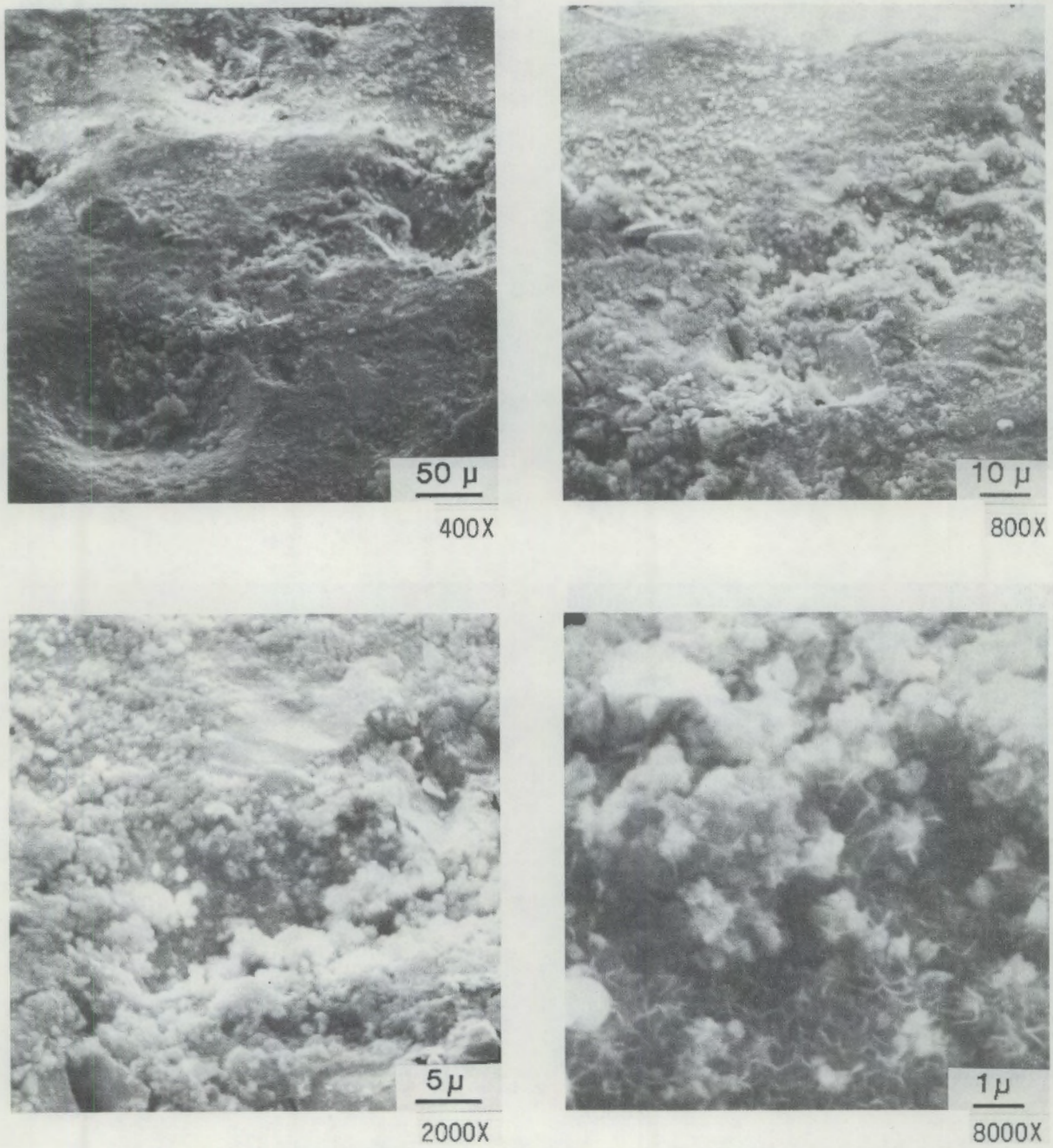

FIGURE 25. SEM Micrographs of UO_2 Surfaces After 30 Days at 75°C in WIPP "B" Brine Solution Containing 200 ppm Dissolved Oxygen

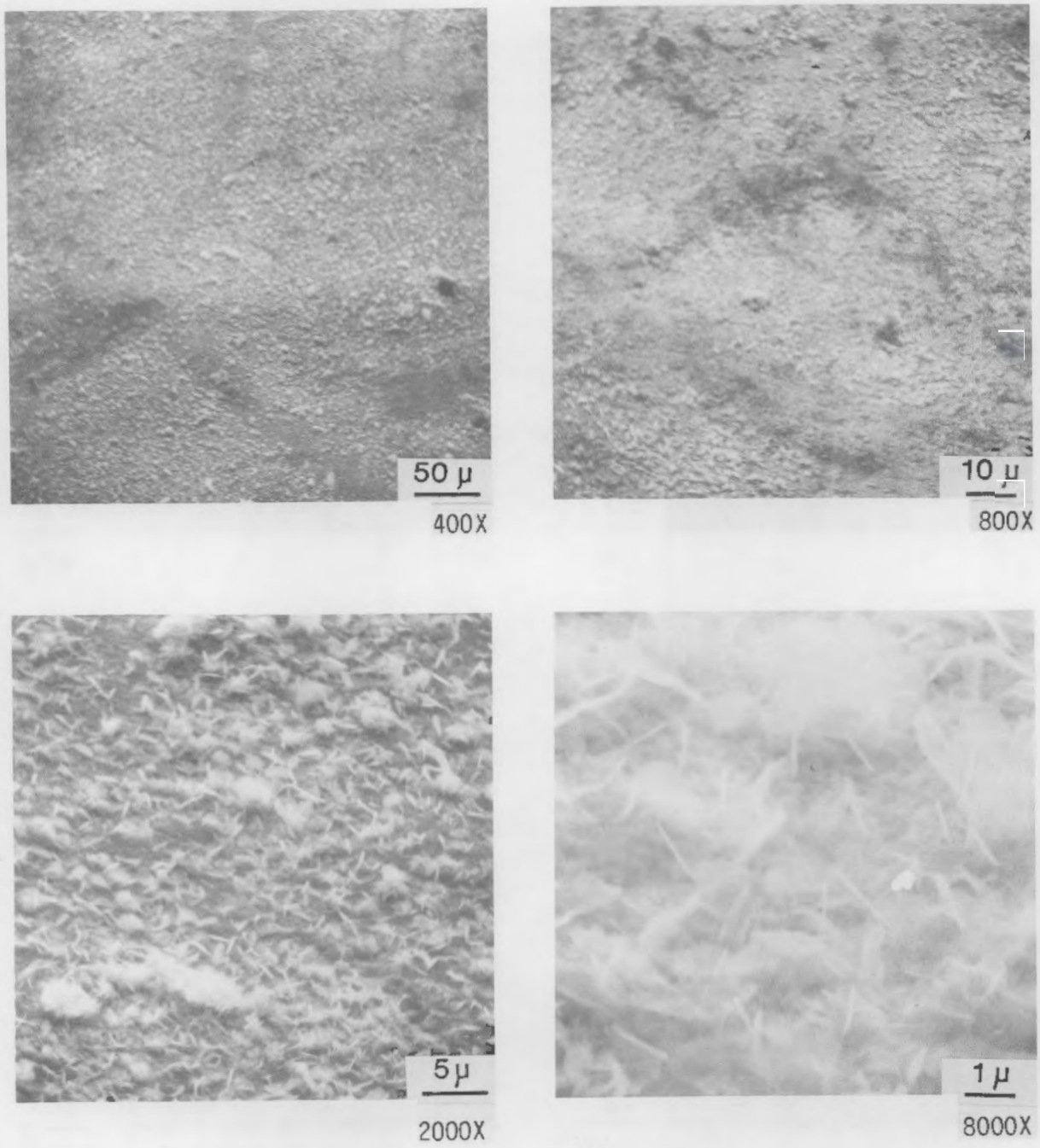

FIGURE 26. SEM Micrographs of UO_2 Surfaces After 60 Days at 150°C in WIPP "B" Brine Solution Containing 200 ppm Dissolved Oxygen

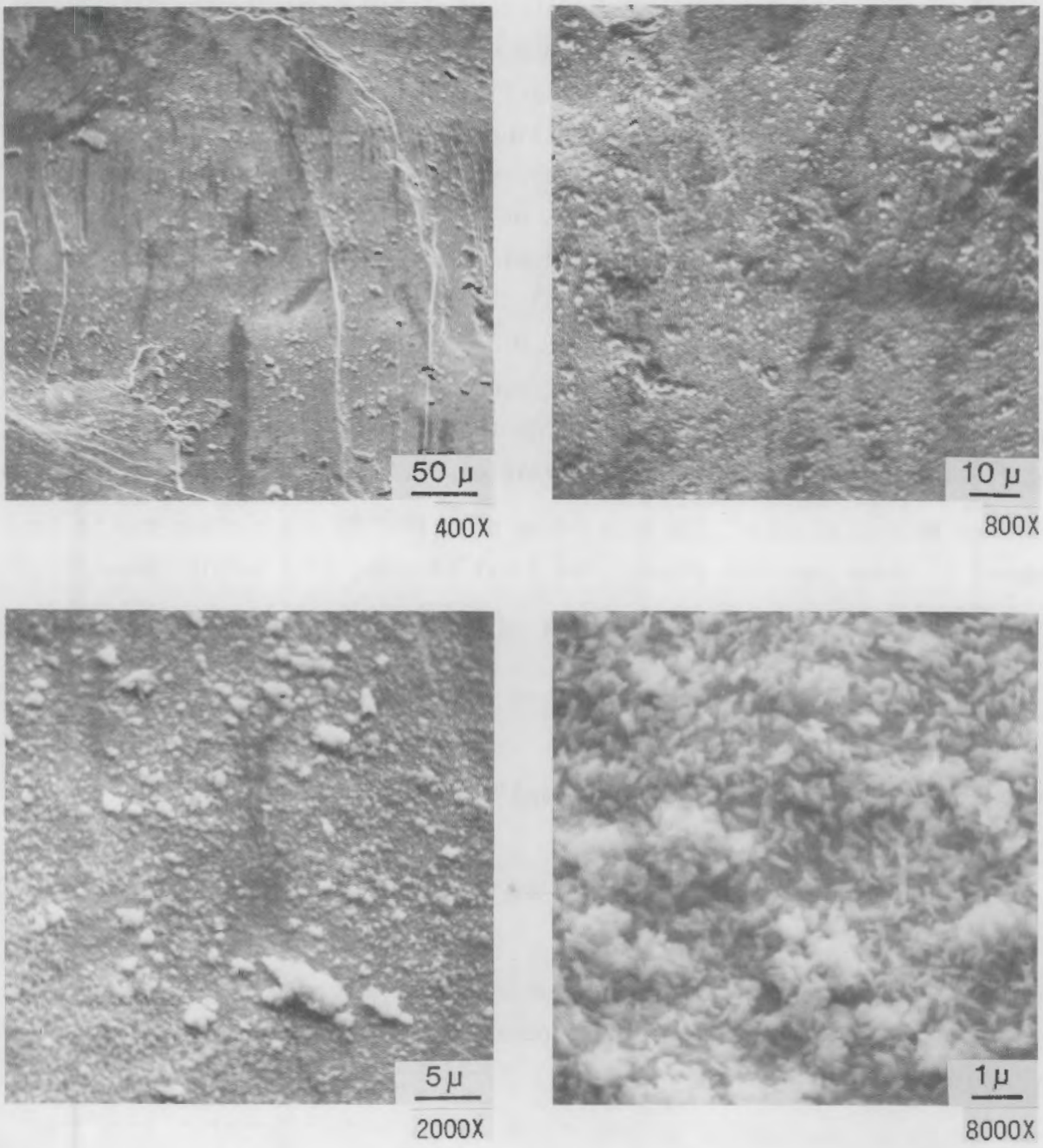

FIGURE 27. SEM Micrographs of UO_2 Surfaces After 60 Days at 75°C in WIPP "B" Brine Solution Containing 200 ppm Dissolved Oxygen

the UO_2 surface. As long as an unlimited supply of O exists, the dissolution of UO_2 will continue even if the surface region of the solution has been supersaturated. In addition, uranyl ions are deposited as solid UO_3 hydrate crystals onto the UO_2 surface and container wall. Interestingly, a temperature increase from 75 to 150°C also favors the formation of deposited hydrate crystals because the solubility limits of uranyl ions reduce in respect to the increase of temperature, e.g., the solubility of uranyl ions is higher at room temperature than at 90°C (Holland et al. 1979). Therefore, the concentration of U in solutions such as $NaHCO_3$ and H_2O decreased with the function of time at 150°C since hydrated crystals were found on the UO_2 surface. This implies that the concentration of uranyl ions in these solutions may not be directly related to the oxidation-dissolution rate of the UO_2.

For deionized water, the mechanisms of oxidation-dissolution may be considered in three reaction steps. The first step may be a simple oxidation of the surface, such as:

$$UO_2 + X/2\ O_2 \longrightarrow UO_{2+x} \qquad (1)$$

The second step involves dissolved O and H^+ ions:

$$UO_{2+x} + H^+ + (1-x)/2\ O_2 \longrightarrow UO_2(OH)^+, \qquad 4 \leq pH \leq 7 \qquad (2)$$

This reaction is consistent with our observation that dissolution of UO_2 in 75°C deionized water increases with increased hydrogen ions (decreased pH values).

The third reaction is the deposition of UO_3 hydrate crystals onto the UO_2 surface and capsule walls. For a low-temperature reaction, such as 75°C test, the reaction possibly is a hydrolysis and involves H^+ ions, such that:

$$UO_2(OH)^+ + 2\ H_2O \rightleftharpoons UO_3 \cdot 2H_2O + H^+, \qquad 4 \leq pH \leq 7 \qquad (3)$$

For a higher temperature, such as 150°C or greater, the hydrolysis reaction may take the form of:

$$UO_2(OH)^+ + H_2O \rightleftharpoons UO_2(OH)_2 + H^+, \qquad 4 \leq pH \leq 7 \qquad (4)$$

In both cases, the release of H^+ ions during the hydrolysis reactions will compensate for the consumption of H^+ during the oxidation-dissolution reactions (2), and the oxidation-dissolution reaction will be carried on as the deposition of hydrate crystals begins. It is not clear whether the incubation time required for the alternation of reaction (2) and subsequent reactions (3) and (4) cause the fluctuation of the pH in the deionized water, but this question is certainly worthy of further investigation.

ELECTROCHEMICAL OXIDATION AND DISSOLUTION OF UO_2

We initiated a study of the oxidation and dissolution of UO_2 using electrochemical methods with two objectives in mind:

- to determine the principal mechanism and kinetics of the oxidation and dissolution process
- to develop electrochemical methods for accelerated leaching of spent fuel to assess the stability of the spent fuel in different environments.

Electrochemical methods are attractive because they offer a "clean" way to accelerate oxidation and dissolution processes. Either they can increase or control the oxidizing potential of an environment, and thereby reveal specific characteristics of the UO_2 without the addition of chemical oxidizing agents, or they can measure dissolution rates without the removal of the solution or the UO_2 sample from the environment, thus avoiding significant disturbance of the environment.

Further, the dissolution rate obtained from electrochemical methods would be directly proportional to the amount of materials removed from the UO_2 surface since the charge transfer involved in the electrochemical reaction can be determined. Therefore, we can determine the total amount of UO_2 dissolved from the surface precisely at each moment even if redeposition and container plate-out of UO_3 hydrates occur. Dissolution kinetics can also be continuously monitored for detection of rapid and minor changes of dissolution characteristics, which may be impossible by solution analysis. Finally, the most attractive advantage of the electrochemical method would be its application to spent-fuel studies. In this case, in-situ measurement and monitoring of the leach rate for spent fuel can be obtained directly with control performed outside the hot cell. Combined with other techniques, such as acoustic emission, impedence measurement and photoelectrochemical measurement and ellipsometry, the microstructure, composition and optical properties of the surface films can be studied in-situ while the leaching processes are in progress.

DISSOLUTION RATE DETERMINATION

Several reactions occur at a metal surface during electrochemical dissolution experiments:

- Dissolution:

$$M \longrightarrow M^{+Z} + Ze^{-} \qquad (5)$$

- Surface oxidation and formation of oxide film

$$M + Z/2\ H_2O \longrightarrow MO_{Z/2} + ZH^{+} + Ze^{-} \qquad (6)$$

- Formation of surface salt film

$$M + ZX^{-} \longrightarrow MX_z + Ze^{-} \qquad (7)$$

Dissolution of UO_2 would be correlated to reaction (5). However, anodic conditions also favor reactions (6) and (7). If the reaction rate of (5) is far below the rates for reactions (6) and (7), the surface of the material will be covered by oxidation and salt-film products, and the dissolution of the material will then be controlled by surface-film characteristics.

In this case, the measurement of the dissolution rate by electrochemical methods should be limited to the region of overpotential where the surface oxidation and surface salt film will not interfere with the dissolution of the new surface. This can be done by applying a very small overpotential over the open-circuit potential, such as below 50 mV used to determine the Tafel plot.

With polarization techniques, the rates of both cathodic and anodic reaction usually follow Tafel behavior, that is:

$$E = a + b \log i \qquad (8)$$

where E is the electrode potential of the sample, i is the current density of the electrochemical reaction, and a and b are the constants.

The dissolution current can be estimated if the electrochemical dissolution processes follow the Tafel behavior. The net current density on the

sample is related to the current densities of the electrochemical reactions occurring on the sample surface by the equation:

$$i\ (net) = i\ (anode) - i\ (cathode) \qquad (9)$$

The exponential behavior of current density with potential means that the anodic contribution to the net current density can generally be ignored if the sample potential is 50 mV more negative than the open-circuit value, while the cathodic contribution is usually negligible at a potential 50 mV more positive than the open-circuit value. These relationships are shown schematically in Figure 28. For a sample of single-crystal UO_2 in deionized water, it is clear that the dissolution of UO_2 can be obtained based on the Tafel relationship (see Figure 29).

Assuming the dissolution current density obtained from Equation (8) is i_o as 1 $\mu A/cm^2$, according to Faraday's law, the current is equivalent to:

$$\frac{10^{-6}\ A/cm^2 \times 8.64 \times 10^4\ s/d \times 10^4\ cm^2/m^2}{1.6 \times 10^{-19}\ Coul/electron} = 5.4 \times 10^{21}\ electrons/m^2\text{-}d \qquad (10)$$

If the dissolution of one molecule requires two electrons, based on the probable oxidation-dissolution mechanisms for UO_2 described in the previous section, this can be expressed by the following electrochemical reactions:

$$UO_2 + H_2O \longrightarrow UO_2(OH)^+ + H^+ + 2e, \qquad 4 \leq ph \leq 7 \qquad (11)$$

Therefore, the dissolution rate of UO_2 will be:

$$\text{Dissolution rate } UO_2\ (g/m^2\text{-}d) = \frac{5.4/2 \times 10^{21}\ UO_2\ molecules \times 270\ g\ UO_2/mole}{0.602 \times 10^{24}\ UO_2\ molecules/mole}$$

$$\times\ (i_o) = 1.21 \cdot i_o\ (\mu A/cm^2) \qquad (12)$$

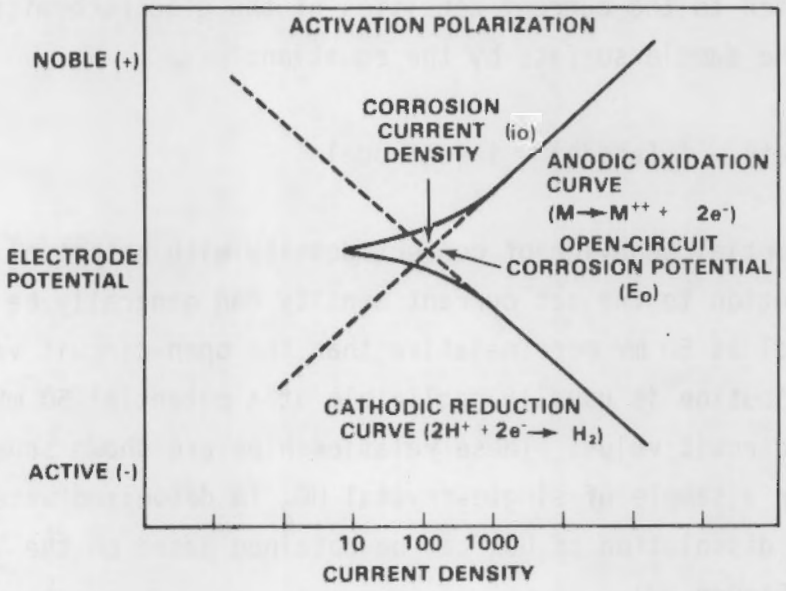

FIGURE 28. Electrochemical Methods of Corrosion Measurements

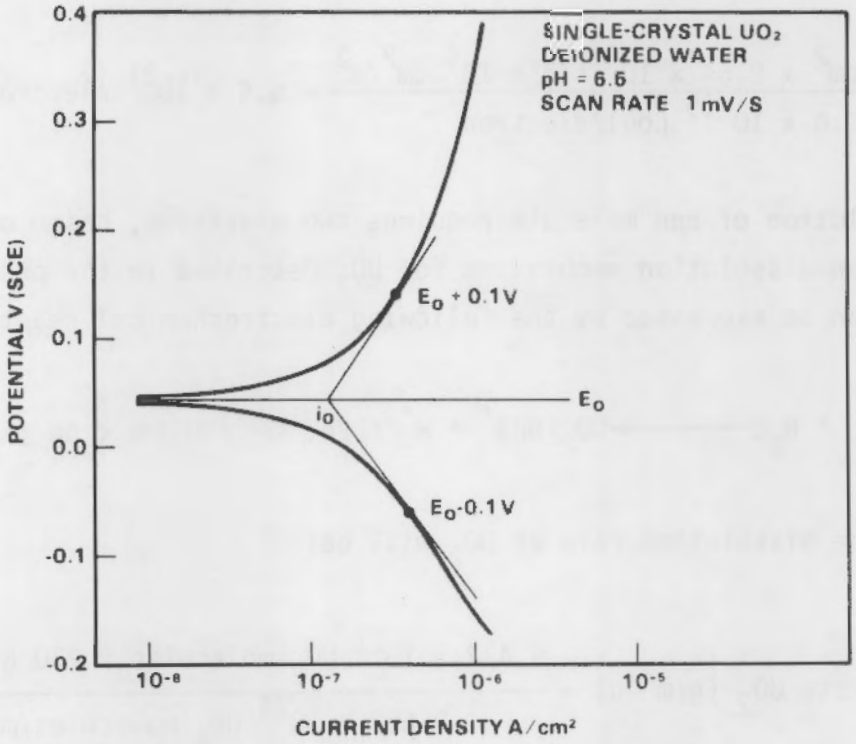

FIGURE 29. Cathodic and Anodic Polarization Curves for Single-Crystal UO_2 Surface in Deionized Water

This expression assumes that all the component elements dissolve based on one type of dissolution reaction and at essentially a uniform rate. This assumption is suitable for a single-crystal UO_2 surface containing no grain boundary.

POLARIZATION OF UO_2 SURFACE

The oxidation and dissolution behavior of single-crystal UO_2 surfaces was studied by polarization techniques to characterize the dissolution mechanism and kinetics in specific environments. The polarization technique provides information about the dissolution current as a function of oxidation potential, which is particularly sensitive to small changes of the UO_2 surface condition and the solution chemistry. We studied the dissolution of UO_2 in deionized water, $NaHCO_3$ (0.03 M) and WIPP "B" brine solution at room temperature and 75°C.

The experimental setup for polarization of UO_2 surfaces is shown in Figures 30 and 31. Princeton Applied Research Models 350 and 173 potentiostats were used. The electrochemical cell was a standard multineck flask with a standard Calomel reference electrode and graphite counter-electrode. A single crystal of UO_2 with a (111) surface area of nearly 0.2 cm^2 was selected for the experiments. Electrical contact was made with copper wire attached with conducting epoxy, and the sample was then mounted with epoxy resin, leaving the (111) surface exposed to the solution. The surface of the sample was polished between tests with 600 grit paper and cleaned with water to remove loose particles. This surface preparation procedure gave us reproducible results.

DISSOLUTION RATE

The dissolution current, i_o, was obtained from Tafel plots between E_o, the open-circuit potential of the UO_2 surface for a selected solution, and 200 mV above E_o. Polarization curves were obtained by scanning between -1 and 1 V (SCE) at a scanning rate of 1 mV/s. The solution was not stirred. pH readings were recorded before and after the electrochemical polarization experiment.

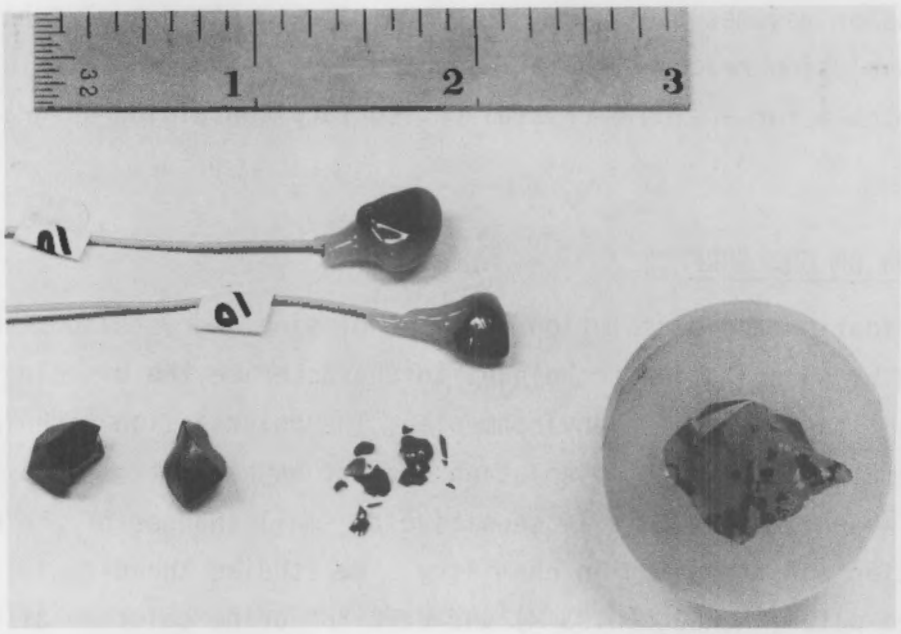

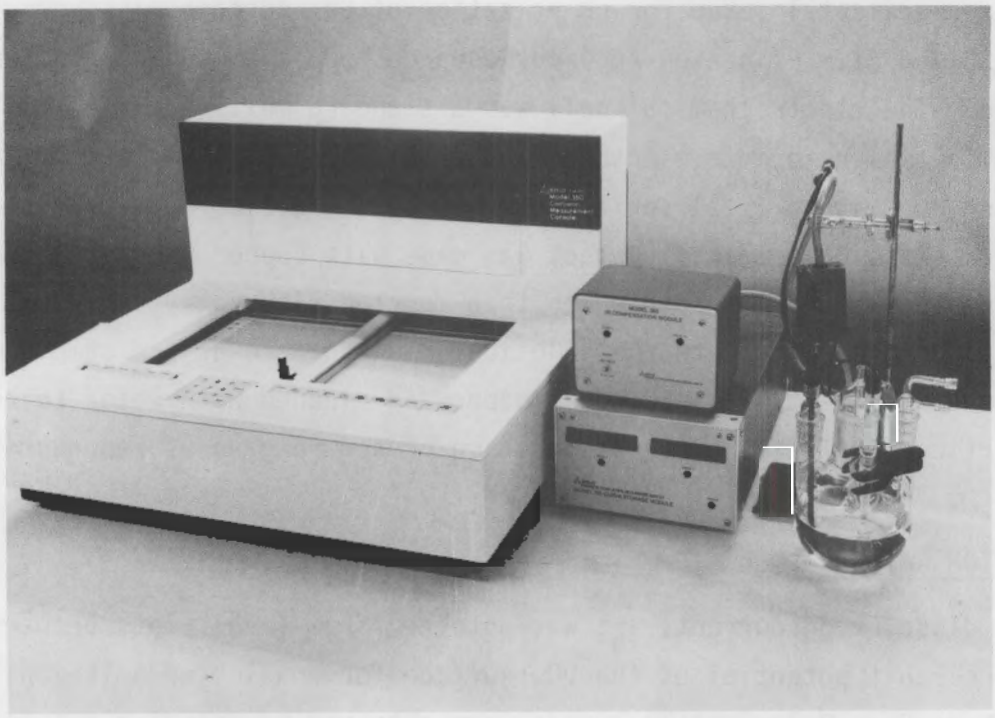

FIGURE 30. UO_2 Specimen and Laboratory Setup for Electrochemical Oxidation and Dissolution Experiments

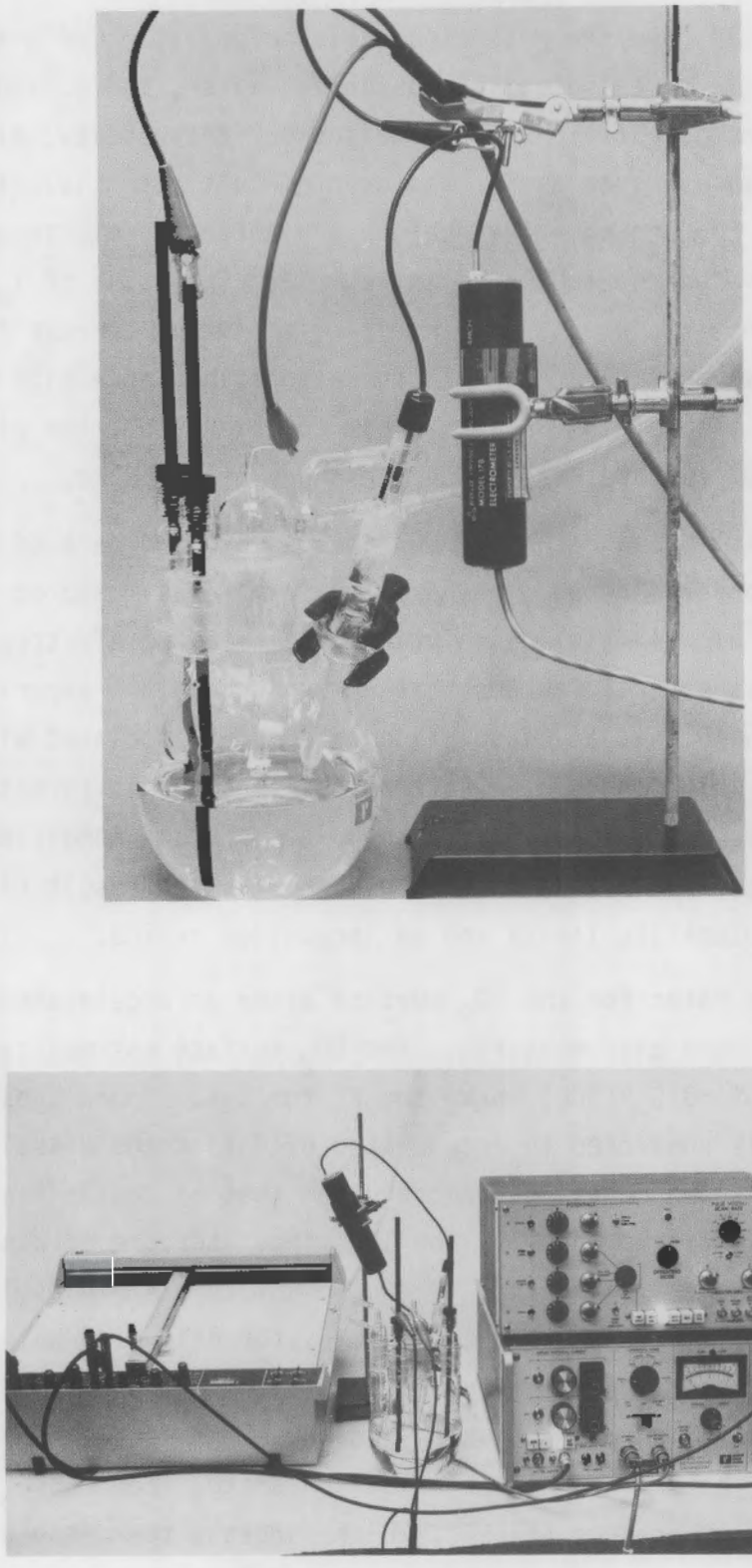

FIGURE 31. Electrochemical Cell for UO_2 Oxidation and Dissolution Studies

Figures 32 and 33 show the potentiodynamic polarization of a single-crystal UO_2 surface in three solutions--deionized water, $NaHCO_3$ and WIPP "B" brine--plotted as potential, V(SCE), versus current density, A/cm^2. The parameters and variables, such as E_o, the open-circuit potential, i_o, the dissolution current at E_o, and pH values before and after the electrochemical dissolution are measured and tabulated in Table 8. The value of i_o determined from Tafel plots represents the initial dissolution current from a clean UO_2 surface within several minutes. All three solutions have high initial dissolution currents, about 10^{-6} A/cm^2. From Equation (10), the dissolution rates for a clean UO_2 surface will be on the order of 1 g/m^2-d.

The initial dissolution rates for UO_2 are about two orders of magnitude higher than those observed for UO_2 powder, 10^{-2} g/m^2-d as measured from solution analysis. The high initial dissolution rate from the electrochemical methods may be due to several factors that are unique to the experiments. It is likely that the high initial dissolution rates are associated with the (111) surface of the UO_2, which is readily susceptible to etch pit formation. The high dissolution rate may also be due to the clean surface condition that is free from oxidized surface films, which would grow as the result of the buildup of uranyl ions to solubility limits and an incubation period.

The dissolution rates for the UO_2 surface after an accelerated dissolution of the surface were also measured. The UO_2 surface was maintained at a constant potential of ~0.5 V(SCE) above the E_o for 1 h. Under these conditions, the surface is subjected to accelerated oxidation and dissolution at a current density about two magnitudes higher than that of the initial dissolution rate at open-circuit potential. The 100 times increase of dissolution rate induced by the potential for 1 h is equivalent to a 4-d dissolution test at open-circuit condition. As shown in Table 8, for deionized water and WIPP "B" salt brine solutions, the i_o values decreased and E_o values increased after the accelerated dissolution period, which indicates the formation of a surface film with protective nature and higher oxidation state. For $NaHCO_3$ solution, both i_o and E_o were not changed at 25°C, which suggests the dissolution rate

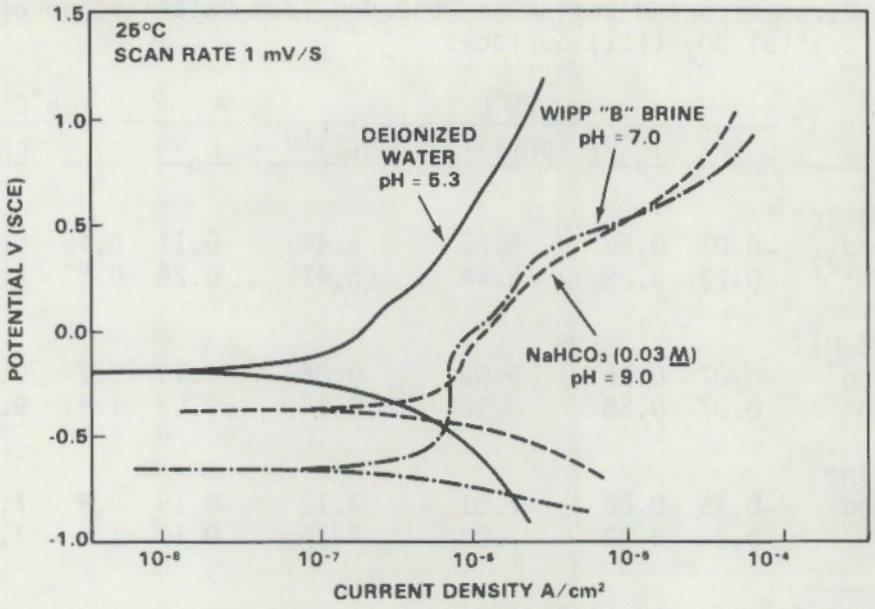

FIGURE 32. Comparison of Polarization Behaviors of Single-Crystal UO_2 Surface in Deionized Water, $NaHCO_3$ (0.03 M) and WIPP "B" Brine at 25°C

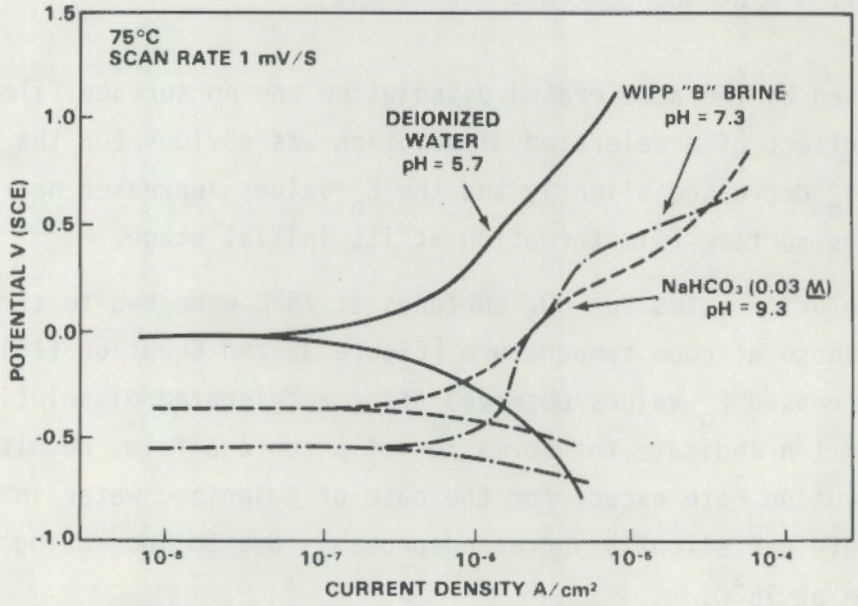

FIGURE 33. Comparison of Polarization Behaviors of Single-Crystal UO_2 Surface in Deionized Water, $NaHCO_3$ (0.03 M) and WIPP "B" Brine Solutions at 75°C

TABLE 8. Parameters and Variables Observed from Polarization of Single-Crystal UO_2 (111) Surfaces

Solution	25°C				75°C			
	E_o[a]	i_o[b]	pH(1)[c]	pH(2)[d]	E_o	i_o	pH(1)	pH(2)
Deionized Water								
As-polished	-0.01	0.56	5.27	5.44	0.11	0.46	5.67	5.81
0.5 V, 1 h[e]	0.23	0.28	5.44	5.47	0.24	0.53	5.83	5.87
$NaHCO_3$ (0.03 M)								
As-polished	-0.07	0.96	9.02	0.06	-0.13	3.2	9.35	9.41
0.5 V, 1 h	0.07	0.58	9.12	9.14	0.03	1.8	9.52	9.54
WIPP "B" Brine								
As-polished	-0.15	0.86	7.01	7.12	-0.15	2.9	7.34	7.39
0.5 V, 1 h	0.2	0.63	7.20	7.26	0.17	1.5	7.13	7.29

(a) E_o = open-circuit potential (SCE)
(b) i_o = dissolution current at E_o, $\mu A/cm^2$
(c) pH(1) = pH value before test
(d) pH(2) = pH value after test
(e) 0.5 V, 1 h = Sample surface was maintained at 0.5 V(SCE) above E_o for 1 h. The surface dissolution rate was increased nearly 100 times or nearly 4 d at open-circuit condition.

was not affected by the accelerated dissolution and no surface film was formed. However, the effect of accelerated dissolution was obvious for the 75°C test in which the i_o decreased slightly and the E_o values increased nearly 0.2 V, which indicates surface-film formation at its initial stage.

The dissolution rates for UO_2 surfaces at 75°C were two to three times greater than those at room temperature [Figure 32 and Equation (10)]. Similarly, the increased E_o values observed after accelerated dissolutions at 0.5 V + E_o for 1 h indicate the formation of a surface film, resulting in a reduced dissolution rate except for the case of deionized water in which the dissolution rate was slightly increased probably due to increasing solubility of UO_3 hydrate at 75°C.

SURFACE FEATURES

Although the studies were primarily with the (111) surface of the UO_2 single crystal, we did observe varying etch patterns for the other

crystallographic planes under identical conditions, which indicated the possibility of differing dissolution rates. The surface micrographs obtained from the SEM techniques (Figure 34) did not reveal the surface film (the film was too thin to be observed by SEM). For most cases, the surface was corroded and etched and the surface morphology varied depending on the type of the crystallographic plane observed.

Based on polarization behavior of UO_2 in three solutions at 25 and 75°C (shown in Figures 32 and 33), only the surface in the brine solution was passivated to some degree between -0.6 and -0.2 V(SCE). This passivation correlates with a low dissolution rate of the UO_2 samples and the absence of a thick uranyl hydrate coating observed in the autoclave tests. After a prolonged accelerated dissolution at about 0.5 V(SCE) above E_o for several hundred hours, this passive nature of the surface films in brine solution is illustrated in Figure 35 with the UO_2 surface in $HaHCO_3$ solution (Figure 35A). Here, the severely corroded surface of UO_2 in $NaHCO_3$ was due to lack of protecting surface film, whereas the surface of UO_2 in brine solution was covered with a uniform hydrate film which contained a few cracks probably caused by dehydration after the sample was dried in the SEM viewing chamber.

CONCLUSIONS

From these preliminary electrochemical oxidation and dissolution studies, we conclude that electrochemical methods may be useful in the detection of initial dissolution and accelerated dissolution rates. Also, the electrochemical methods can monitor the dissolution rate change during a long-term leaching study. In addition, electrochemical methods are sensitive to surface conditions and information related to the characteristics of the surface film, which can be analyzed based on E_o, i_o and potentiostatic polarization behaviors. The shapes of the polarization curves for UO_2 in the test solutions (smooth increases of current as a function of applied potential) indicate that the dissolution of UO_2 can be accelerated with electrical potential. We are comparing surface characteristics and dissolution rates for static dissolution and electrochemical-accelerated dissolution to evaluate the use of accelerated

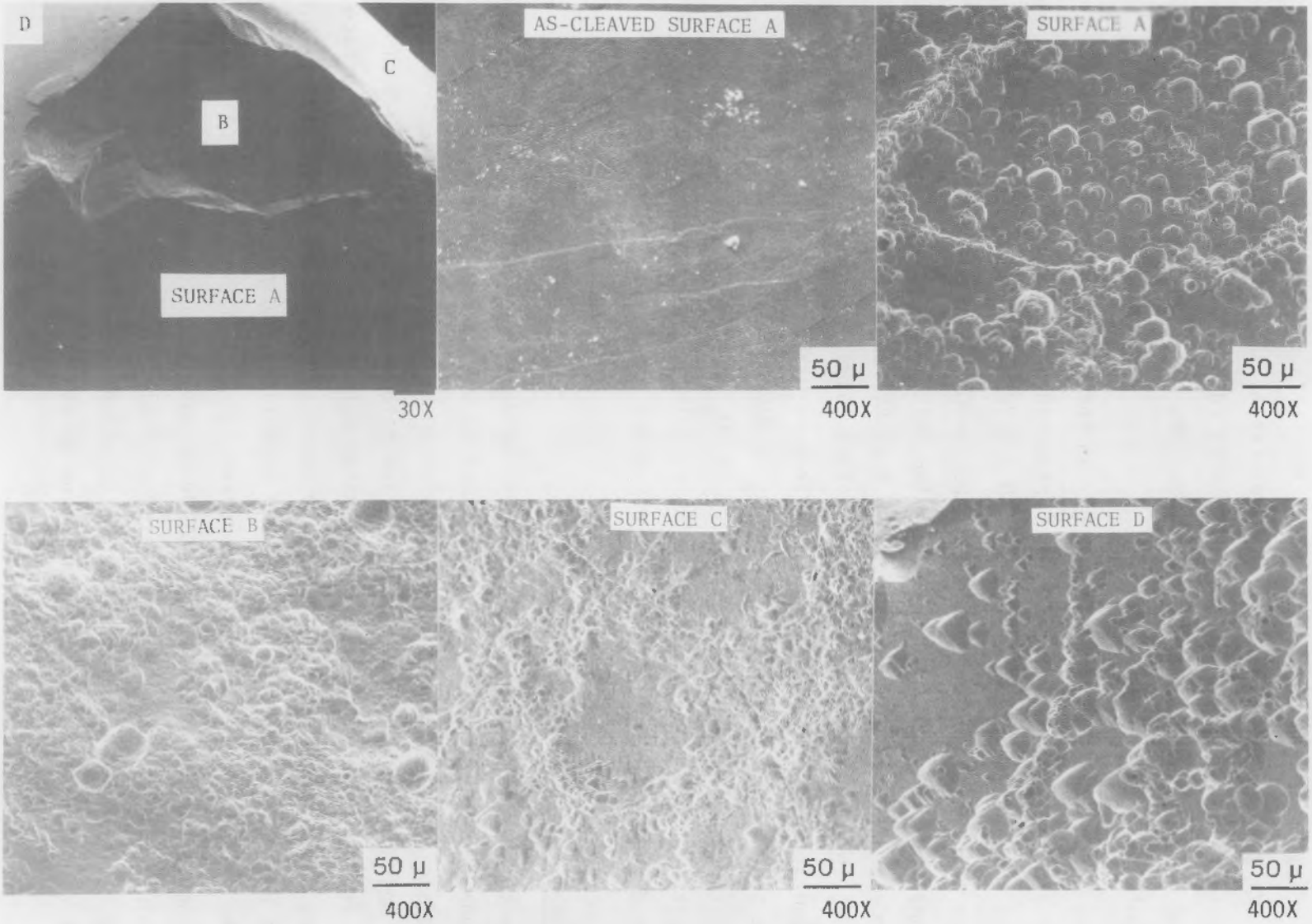

FIGURE 34. Different Surface Morphologies After Electrochemical Dissolution of UO_2 Crystal in Deionized Water at 25°C

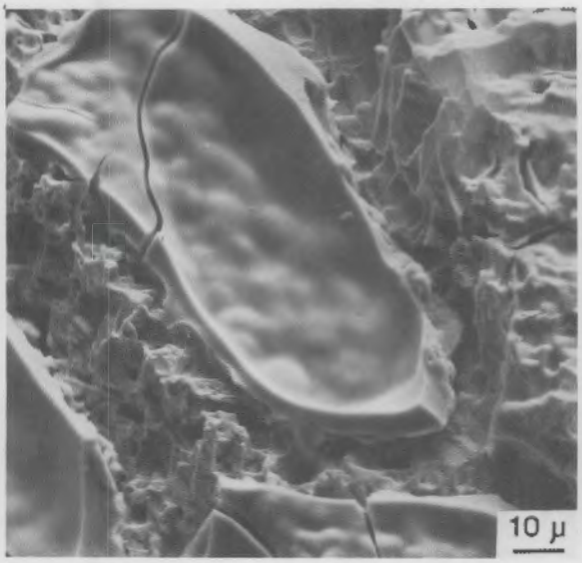

A. Surface Film Formed in NaHCO3 (0.03 M) Solution 144 h at 0.4 V(SCE)

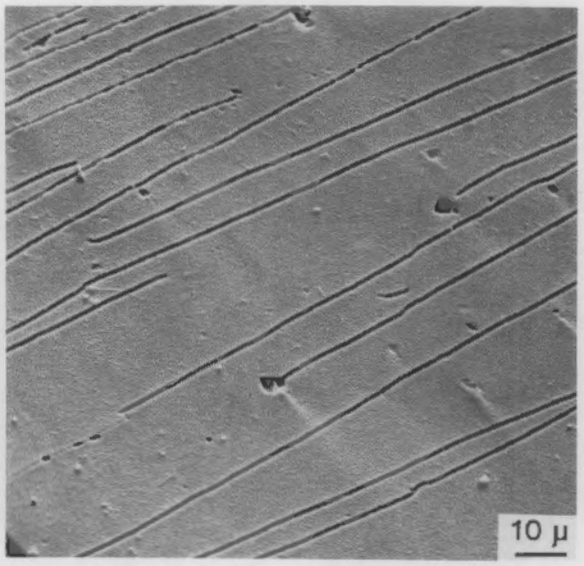

B. Surface Film Formed in WIPP "B" Brine Solution After 120 h at 0.5 V(SCE)

FIGURE 35A,B. Formation of Hydrated Films After Long-Term Electrochemical Dissolution of UO_2 Surfaces

dissolution for studying the leaching rates and mechanisms for both UO_2 and spent fuel. Due to the different dissolution rates associated with crystallographic planes, UO_2 pellets should be used with electrochemical methods to obtain data that are compatible with the spent fuel.

EFFECTS OF H_2O_2 ON SINGLE-CRYSTAL UO_2 SURFACE

Hydrogen peroxide can be formed by radiolysis of water at or near the spent fuel-water interface even within a reducing environment, and localized regions of the spent-fuel surface could become highly oxidized. Hiskey (1980) reported that the effect of H_2O_2 on the dissolution of UO_2 in 0.5 M CO_3^{2-} solutions at pH 9.8 and 25°C increases the dissolution rate 100 times over dissolved O_2 in equivalent concentrations. We investigated the effects of H_2O_2 on single-crystal UO_2 surfaces in deionized water. The study was based on both dip-reaction and electrochemical reaction. After the reactions, the surface of the UO_2 was characterized by x-ray diffraction, SEM, Auger and optical microscopy.

DIP REACTION

Dip-reaction studies of UO_2 were made in deionized water at 25°C and 75°C with additions of 50 to 3000 ppm H_2O_2 by volume. At room temperature with 50 ppm H_2O_2 for 24 h, the growth of a thin surface film was identified by SEM (Figure 36). The film had many cracks that may be due to the dehydration of the film during SEM analysis. With 300 ppm of H_2O_2 for 3 h, the surface of the UO_2 was covered with a thicker, brownish-colored hydrate film. The dip reaction indicates that the surface film formed rapidly and that a small amount of H_2O_2 was present.

The dip reaction was rapid at 75°C, 300 ppm H_2O_2. Several UO_2 crystals were placed in a gold container within a reaction bomb and filled with 300 ppm H_2O_2 solution for reaction at 75°C for 4 d. The weight of one crystal increased from 1.8633 g to 1.8634 g, and the surface was coated with a gray deposit. This deposit was identified by x-ray diffraction as a mixture of $UO_4 \cdot 4H_2O$ and $UO_3 \cdot 2H_2O$ phases. The solution, when evaporated, left a very small amount of bright yellow deposit identified as amorphous UO_3 hydrate that may be formed by decomposition of $UO_4 \cdot 4H_2O$ as suggested by Cordfunke and Van Der Giessen (1963). Apparently, UO_2 dissolved in great quantity, but the weight loss was not apparent due to the deposition of the surface film. The deposition phenomenon based on H_2O_2 was similar to that observed in static autoclave dissolution experiments at 150°C.

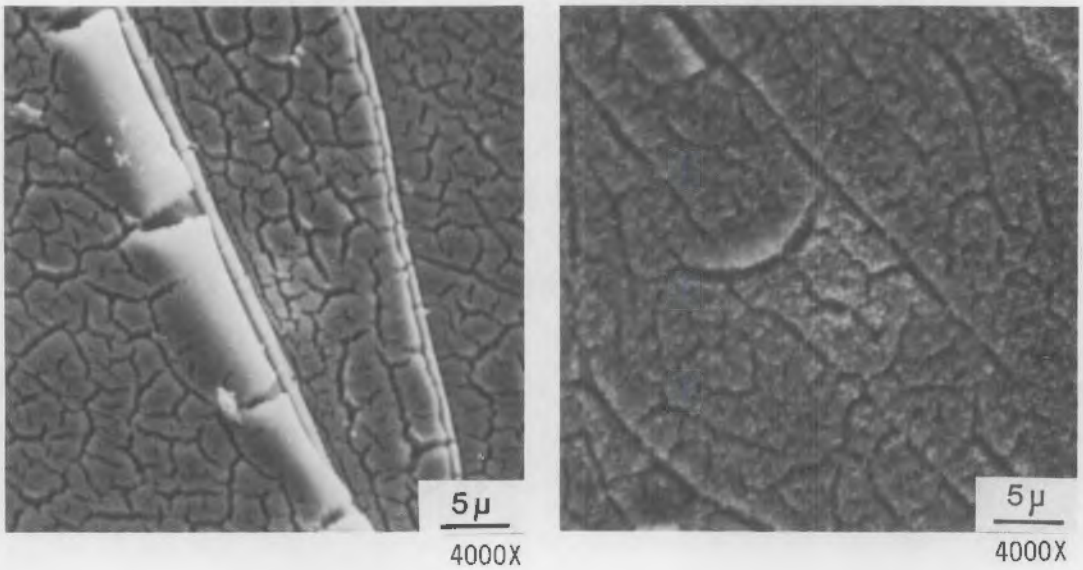

A. Surface Dipped in 50 ppm H_2O_2 at 25°C for 24 h

B. Surface of (A) After Electrochemical Dissolution in Deionized Water

FIGURE 36A,B. The Surface Feature of Single-Cyrstal UO_2 After Dip-Reaction at Room Temperature With 50 ppm H_2O_2 for 24 Hours

After the removal of the deposited UO_3 hydrate film, the UO_2 surface was studied by x-ray topography. Analysis indicates that there is no significant substructure change. Apparently, H_2O_2 only enhances the dissolution of the UO_2, and the crystal surface was not attacked directly by H_2O_2. The result suggests that the effect of H_2O_2 is mostly on enhanced uniform dissolution of UO_2 and formation of UO_3 hydrate deposits.

In another test, 3000 ppm H_2O_2 in H_2O, the crystal became fragmented. Figure 37A shows a crystal face before fragmentation in a H_2O_2 solution. This crystal was then exposed 6 h at 75°C, and we retrieved a large fragment for examination. The fracture surface is a (111) cleavage plane passing through the subgrain matrix. Close examination shows that the fracture begins and ends at substructure boundaries but does not coincide with any subgrain boundaries in the interior (Figure 37B).

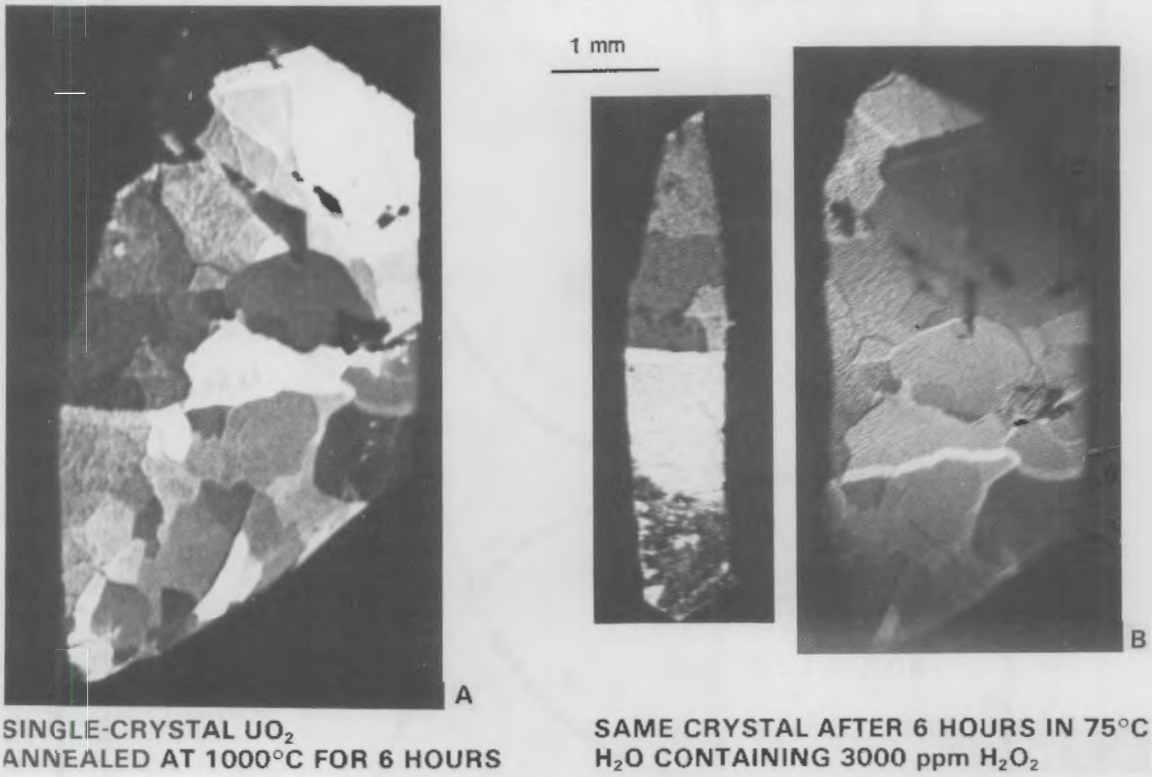

FIGURE 37A,B. X-Ray Lang Topographs of Single-Crystal UO_2 Surface Before and After Treated With 3000 ppm H_2O_2 at 75°C for 6 Hours

Large fragments such as these are rare. Usually, the sample "sheds" into very small fragments also cleaved on a (111) plane. Perfect tetrahedras, whose faces are the four (111) planes, are seen most often. This effect, the apparent change of (111) surface energy by H_2O_2, is a very interesting phenomenon and merits further study.

ELECTROCHEMICAL REACTIONS

With electrochemical oxidation and dissolution, we can observe the growth of UO_3 hydrate films at 25°C. The polarization behavior of UO_2 in deionized water + 300 ppm of H_2O_2 by volume at a pH of 9 is illustrated in Figure 38 along with a comparison of the polarization behavior in deionized water with a pH of 9.9, both adjusted by NaOH. It is clear that the open-circuit potential

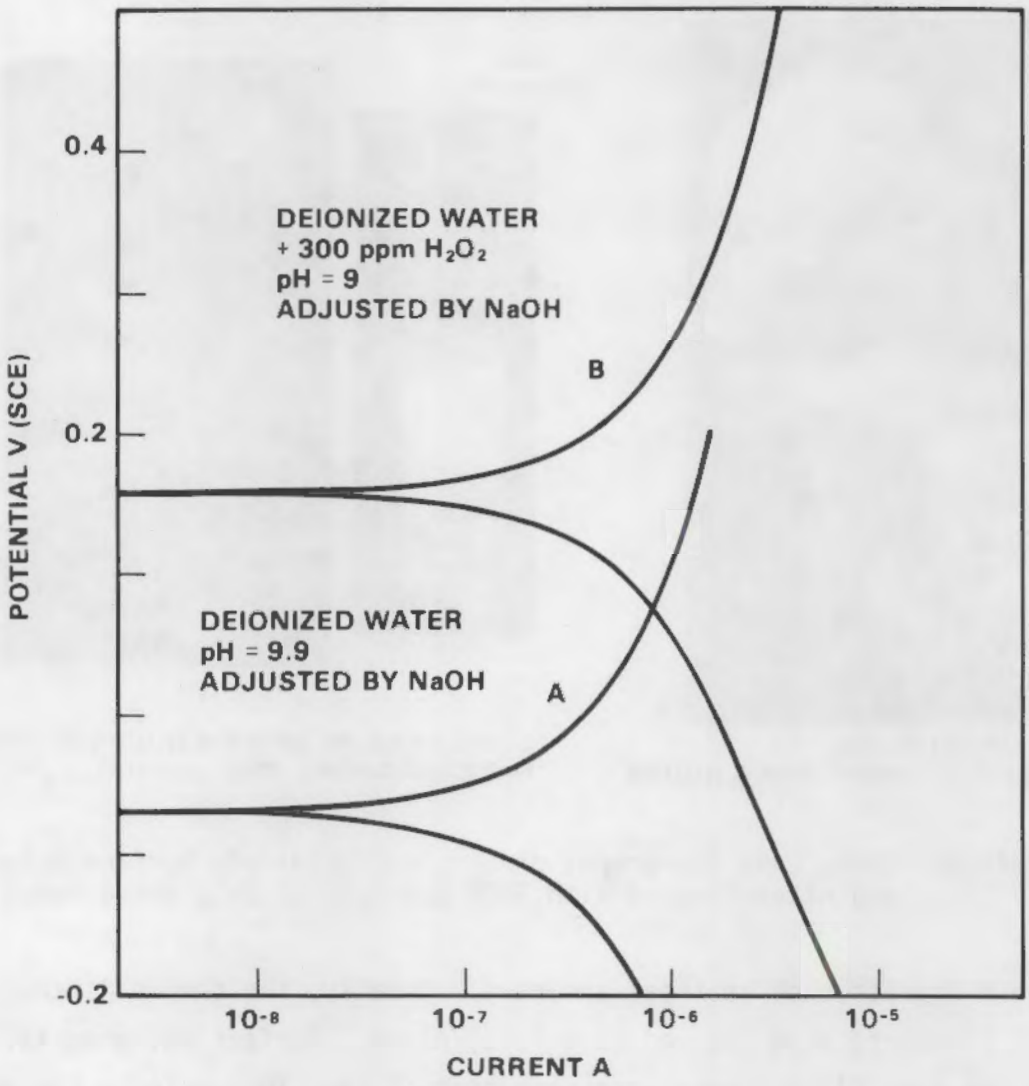

FIGURE 38. Polarization Behavior of UO_2 in Deionized Water and in Deionized Water Plus 300 ppm by Volume of H_2O_2

of UO_2, E_o, was greatly increased by the presence of H_2O_2, but the dissolution current was only decreased slightly. This is indicative of the formation of a surface film of higher oxidation state with some protective nature for the bare UO_2 surface. A UO_2 surface was then placed in deionized water with 500 ppm H_2O_2 at a pH of 6.8, and a potential of nearly 0.5 V(SCE) was applied for 24 h. The surface was then removed from the solution and examined by SEM and optical microscopy. The surface was covered with a layer of porous film about 1 to 5 μm thick and contained numerous cracks that may be due to the dehydration during viewing in the SEM vacuum chamber (Figure 39).

400X

Solution: Deionized H_2O
Voltage: 0.5 V (SCE)
Time: 64 h

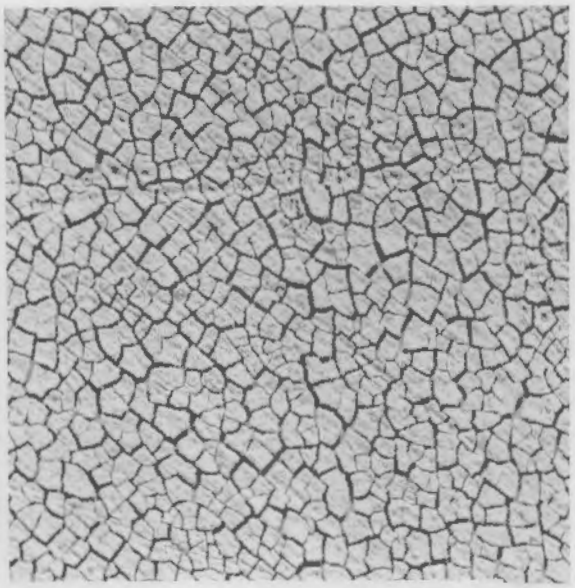

400X

Solution: 500 ppm H_2O_2 in Deionized H_2O
Voltage: 0.5 V (SCE)
Time: 26 h

FIGURE 39. A Single-Crystal UO_2 Surface After Electrochemical Oxidation Dissolution in Deionized Water and Deionized Water With Addition of 500 ppm H_2O_2

X-ray diffraction indicated that the film had a crystal structure resembling that of hydrated $UO_2(OH)_2$, except that the film grown on the (111) surface of UO_2 was highly textured with preferred orientation (Figure 40). There is no explanation as to why the film grown on the UO_2 single-crystal surface by electrochemical methods has a textured structure. We hypothesize that the electrochemical overpotential may create a surface charge to align the linear UO_2^{+2} complex ions during the crystal deposition process. The film was loosely attached to the surface and was easily peeled off. The surface under the film was very smooth indicating the growth of the film was made by deposition from the solution.

The surface of UO_2 containing the UO_3 hydrate film was studied by Auger analysis as a function of depth (Figure 41). The surface film had a high O/U

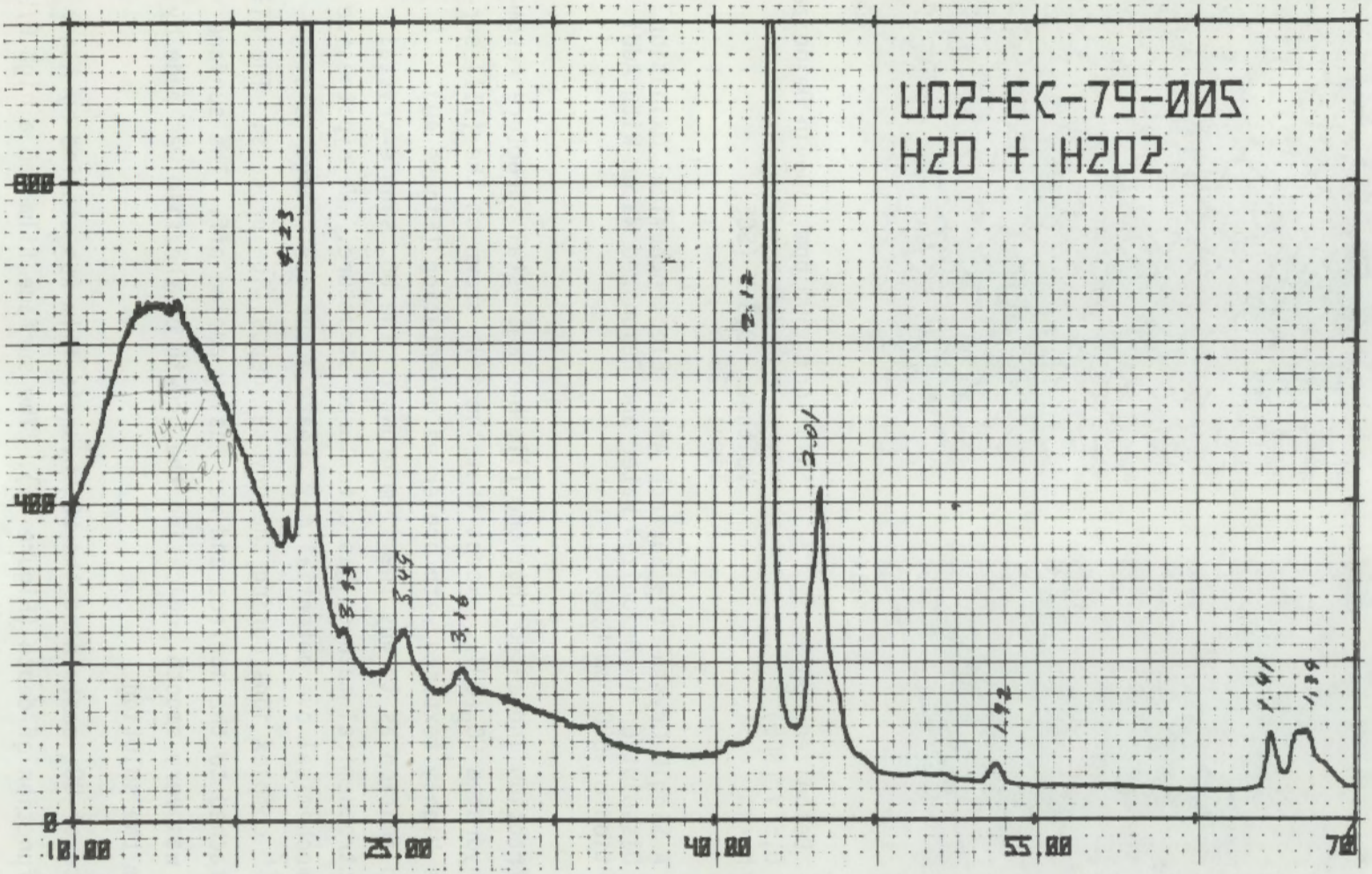

FIGURE 40. The X-Ray Diffraction Pattern of the Surface Film Grown on UO_2 by Electrochemical Oxidation and Dissolution in Deionized Water With Addition of 500 ppm H_2O_2

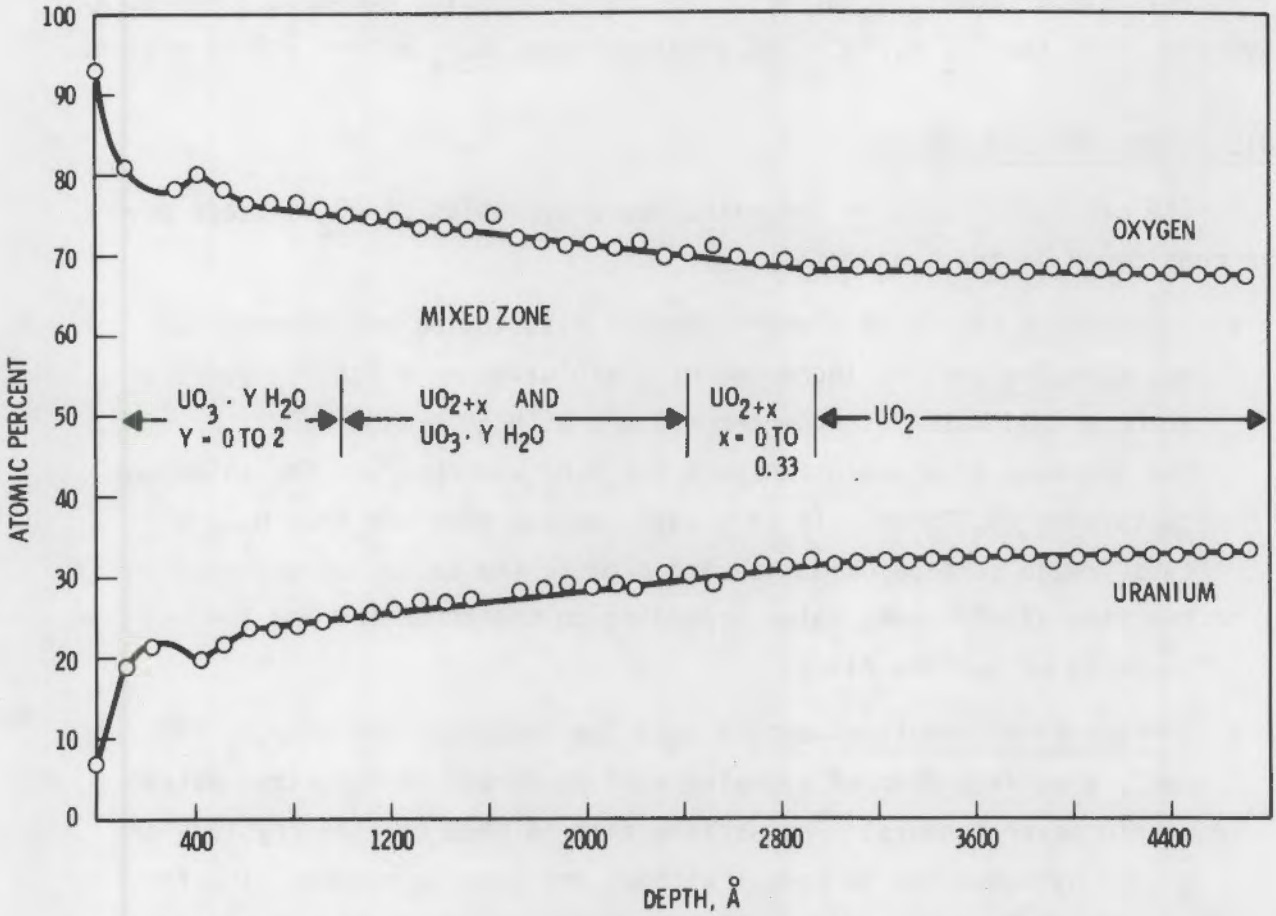

FIGURE 41. Auger Analysis of the Surface Composition Profile for Single-Crystal UO_2 Surface After Electrochemical Oxidation and Dissolution in Deionized Water With 500 ppm H_2O_2 Addition

ratio near four and gradually reduced as a function of the depth until an O/U ratio of two was reached for the UO_2 matrix. The high O/U ratio of four also confirmed the formation of $UO_2(OH)_2$ or $UO_3 \cdot H_2O$ surface film. The graded O/U ratios between two and three would be due to a mixture of UO_3 hydrate and UO_{2+x} phases, where x = 0 to 0.33. The surface of the UO_2 may be schematically described as follows:

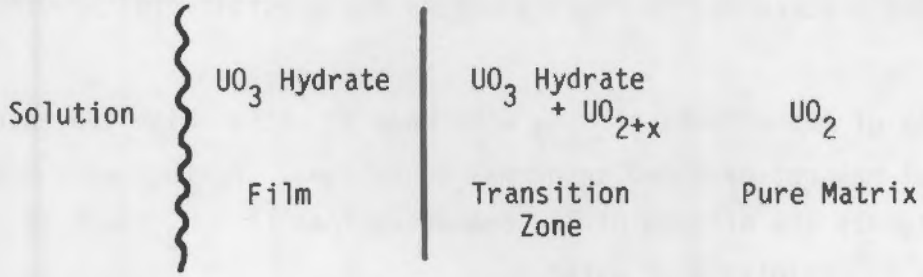

This study suggests that prior to the dissolution and deposition of a hydrate film, the UO_2 surface was oxidized into UO_{2+x} within a thin region.

DISCUSSION AND CONCLUSIONS

The effects of H_2O_2 on the oxidation-dissolution of UO_2 surface may be considered in these aspects:

- Dissolution Rate--The electrochemical dissolution measurement did not show the obvious increases of dissolution rate for UO_2 surface in deionized water at room temperature with 50 ppm of H_2O_2. However, the increase of dissolution rate for H_2O_2 was observed for solutions containing CO_3^{--} ions. In this case, we can conclude that H_2O_2 will cause rapid surface oxidation and promote the oxidation-dissolution reaction at different rates depending on the formation and the property of surface films.
- Surface-Film Formation--With a very low concentration of H_2O_2 (40 ppm), a surface film of hydrates will be formed in deionized water within several hours. The surface film is made of fine crystals of uranyl hydrates and is porous without any passive nature. The formation of the thin surface film may be due to the decrease of the solubility of the uranyl ions in the deionized water by H_2O_2.
- UO_2 Crystal Disintegration--Crystals of UO_2 will disintegrate into fine fragments in a high concentration of H_2O_2 (3000 ppm) within hours. The disintegration of the crystals may be due to combined causes associated with the defects and microcracks on the UO_2 surface. The H_2O_2 will first rapidly oxidize the cracked surfaces and extend the crack depth by oxidation-dissolution. The oxidation of the surface creates a stress field, and the formation of fine oxygen bubbles in the cracked region finally breaks the crystal into fragments.

These observations of the effects of H_2O_2 were made at rather high concentrations of H_2O_2 that may not be found in normal conditions. Further work may be needed to characterize the effects of low concentrations of H_2O_2, such as would be produced by radiolysis of water.

EFFECTS OF RADIATION ON SINGLE-CRYSTAL UO_2 SURFACE

A strong radiation field can produce defects, voids and segregations in the solid-state structures and microstructures of the materials undergoing study. In addition, radiation effects can change the surface conditions of the UO_2 and the solution chemistry. We initiated studies to identify the effects of radiation on UO_2 dissolution based on possible surface-property modifications and solution chemistry changes caused by the radiation of the spent fuel. Three types of radiation effects considered were:

- oxidation of air
- radiolysis of water
- surface activation.

Other possible radiation effects, such as ionization of dissolved or suspended chemical species in the solution, were not included in this study.

OXIDATION OF AIR

Radiation can oxidize the nitrogen in the air and form gaseous NO_x and HNO_3 in water. The HNO_3 in water will decrease the pH value of the solution and increase the dissolution of UO_2, as indicated by Holland and Brush (1979) and Rai, Strickert and Ryan (1980). The effects of oxidation of air by radiation can be simulated by adding HNO_3 to the solution. Using electrochemical methods, experimental evaluation of the pH effects caused by the oxidation and dissolution of single-crystal UO_2 surfaces is progressing.

RADIOLYSIS OF WATER

The effects of radiation on water were analyzed by Burns and Moore (1976) using computer simulation of the radiolysis of water by fast neutron and $\beta\gamma$ radiation at 25°C and 305°C. As Figure 42 shows, the radiolysis of water based on $\beta\gamma$ (5 W g^{-1}) intensity would mean that within 10 s the H_2, O_2 and H_2O_2 concentrations would reach about 0.4 ppm for each species. The 0.4 ppm/10 s formation rate of H_2O_2 would be particularly important because the H_2O_2

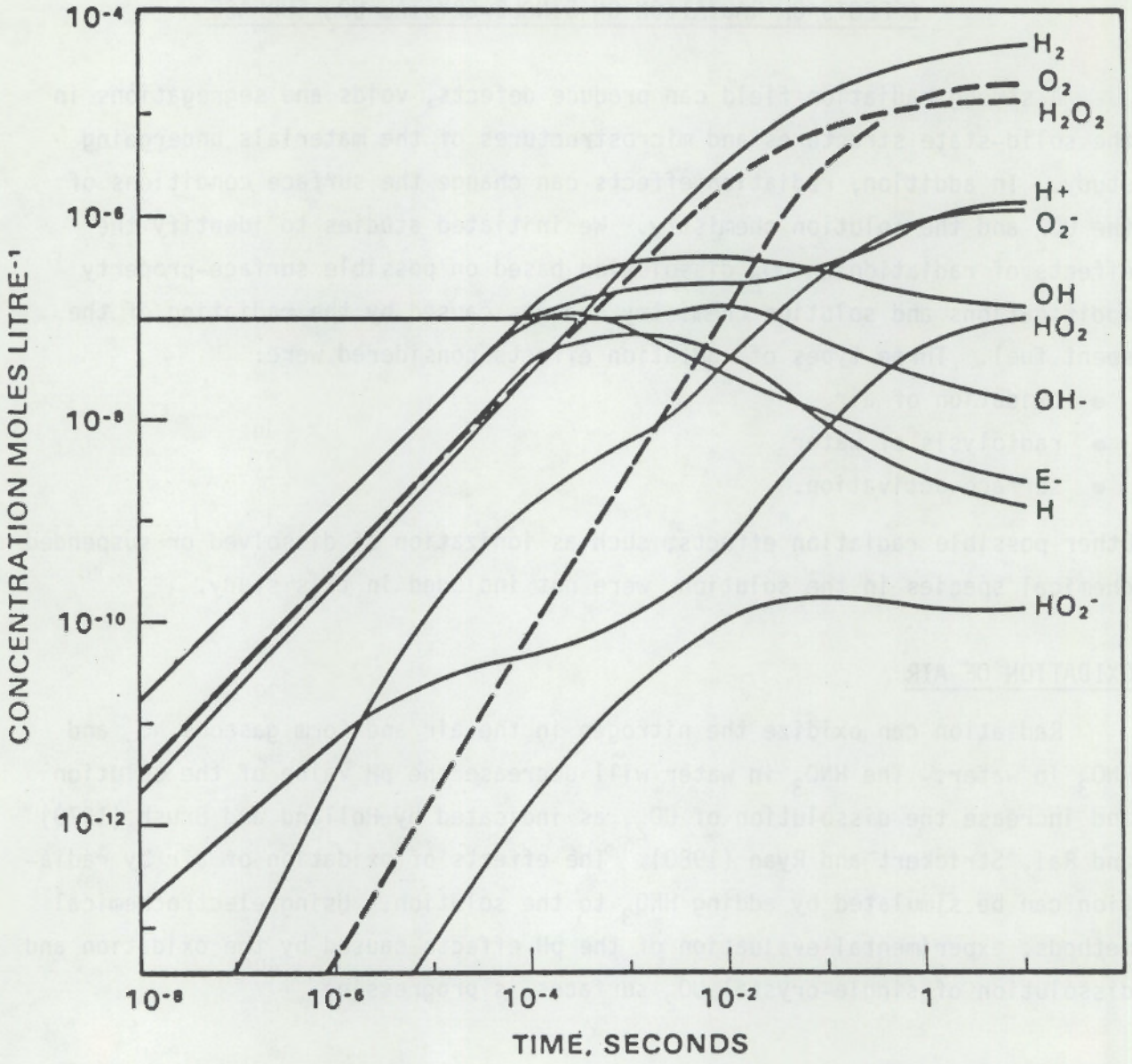

FIGURE 42. Radiolysis (5 W g^{-1}) of Water at 25°C (from Burns and Moore 1976)

would be quickly consumed by the UO_2 surface through oxidation and dissolution, even if H_2 and other reducing ions were near the surface of the UO_2. Thus, the effects of radiolysis would be an important source for enhanced oxidation and dissolution of spent fuel even at reducing conditions.

We are now designing experiments to 1) detect the formation of H_2O_2 by radiolysis of water, and 2) determine the effects of H_2O_2 and other oxidation species, produced by radiolysis of water, on the surface of UO_2. It is not easy to detect H_2O_2 formed by radiolysis of water because of its low concentration and the problems of analyzing the solution during irradiation. We are designing an oxygen sensor based on UO_2 material because we have demonstrated that the oxidation potential of the UO_2 is extremely sensitive to the presence of H_2O_2. Measurement of the oxidation potential change of the UO_2 single-crystal surface would be a good way to detect H_2O_2 formed by radiolysis. Also, the effects of the H_2O_2 on the UO_2 surface can be determined by surface analyses of the UO_2 surface after the irradiation for comparison of the surface film with those obtained from deionized water by addition of controlled amounts of H_2O_2. The electrochemical methods, coupled with gamma ray facilities, have many advantages for determining the effects of radiation due to radiolysis of water.

SURFACE ACTIVATION

Surface activation is commonly observed at the semiconductor-electrolyte interface. Radiation, usually in the form of light, can activate the surface if the incoming radiation has an energy greater than the bandgap of the semiconductor. The electrons from the valence band will be excited into the conduction band and separated by the surface charge created by the band bending at the semiconductor-electrolyte interface. The activated surface would have improved activity and usually show enhanced anodic dissolution.

All the uranium oxides and their hydrates have some semiconducting properties in nature (Figure 43). The mean bandgap for UO_2 was measured as 13.5 eV, but the covalent contribution in bonding cannot be excluded based on about 0.8 ionicity for both UO_2 and U_4O_9 [Naegele, Manes and Birkholz (1975)]. The covalent bonding contribution may be related to the small gap between 5f state to the conduction band, about 4 to 5 eV for both UO_2 and U_4O_9; the uranium oxides all show low activation energies for intrinsic conduction [Manes and Naegele (1976)]. In this case, radiation will cause the surface to be

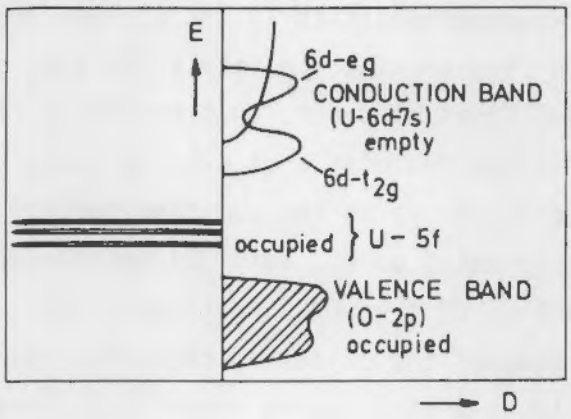

Suggested Band Model for UO_2

Oxide	Resistivity, ohm-cm	Conduction Type	Activation Energy Extrinsic Conduction, eV
UO_{2-x}	10^4 to 10^7	n	1.2
UO_2	10^3 to 10^6	p	0.2
UO_{2+x}	10^3 to 10^7	p	0.1 to 0.4
U_4O_9	10^2 to 10^7	n	0.2 to 0.9
U_3O_8	10^3 to 10^4	n	0.2 to 0.5
PuO_{2-x}	10^2 to 10^{11}	p	0.2 to 1.8

FIGURE 43. Electronic Properties of Uranium Oxides (from Manes and Naegele 1976)

more active than the surface without radiation. The creation of an electron-hole pair at the surface region would mean that the electron will be carried into the material and that the hole will move into the electrolyte in the case of an n-type semiconductor, such as UO_{2-x}, U_4O_9, or UO_3 hydrates. The chemical reactions on the surface involving the radiation-induced holes may be described as 1) direction oxidation, 2) oxidation of the water, and 3) anodic dissolution, as shown in Figure 44.

Through another DOE program, we have demonstrated the effects of surface activation by radiation based on photoelectrochemical measurements (Figure 45) of single-crystal UO_2 with ultraviolet radiation (UV) of ~40 mW/cm^2 intensity with a wavelength of less than 300 nm (greater than 3 ev). The as-cleaved

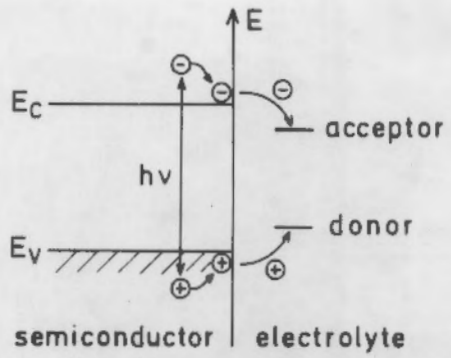

Radiation-Induced Redox Reactions at a Semiconductor-Electrolyte Interface.

1. Direct Oxidation

$$U^{+4} + 2p^{+} \longrightarrow U^{+6}$$

2. Oxidation of Water

$$2(OH)^{-} + 2p^{+} \longrightarrow H_2O_2$$

3. Anodic Dissolution

$$UO_{2+2}\ p^{+} + H_2O \longrightarrow UO_2\ (DH)^{+} + H^{+}$$

FIGURE 44. Probable Surface Reaction Induced by Radiation

UO_2 did not show enhanced anodic dissolution with the UV radiation due to the p-type conduction of the UO_2 crystal. However, we observed enchanced anodic dissolution with the UO_2 crystal covered with UO_3 hydrate film (Figure 46). The dissolution current was increased nearly two-fold when the light was turned on. Apparently the UD_3 hydrate film is a n-type semiconductor and can have enhanced dissolution by surface activation with radiation.

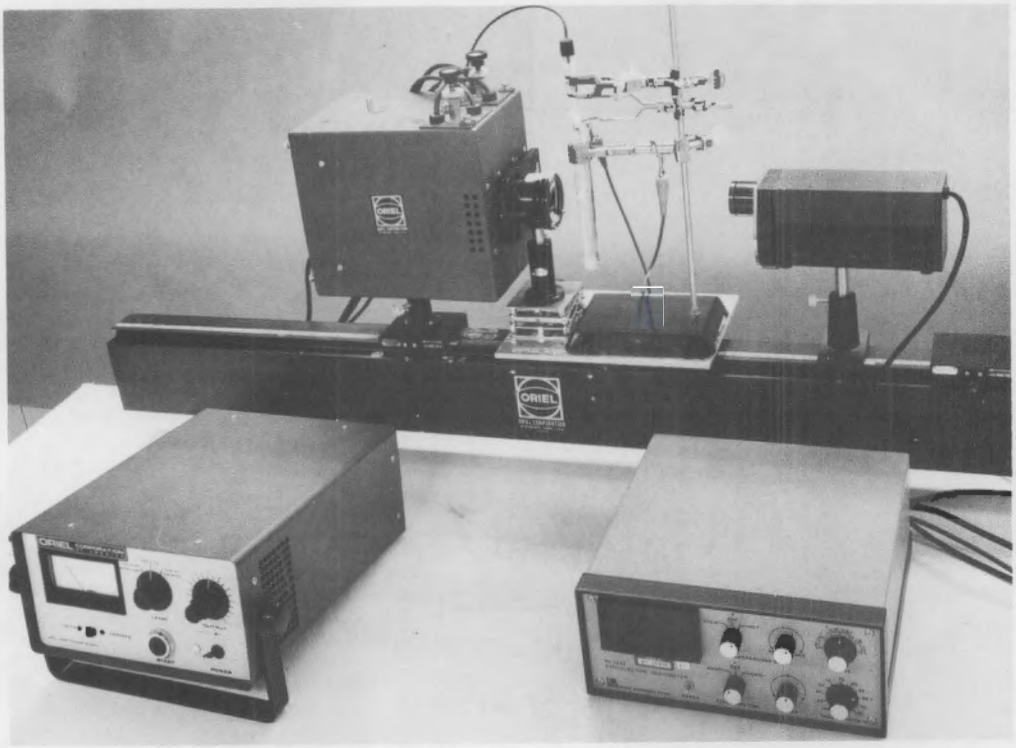

FIGURE 45. Experimental Setup for Studies of Radiation-Enhanced Dissolution of Single-Crystal UO_2 Surface With Ultraviolet Light (UV)

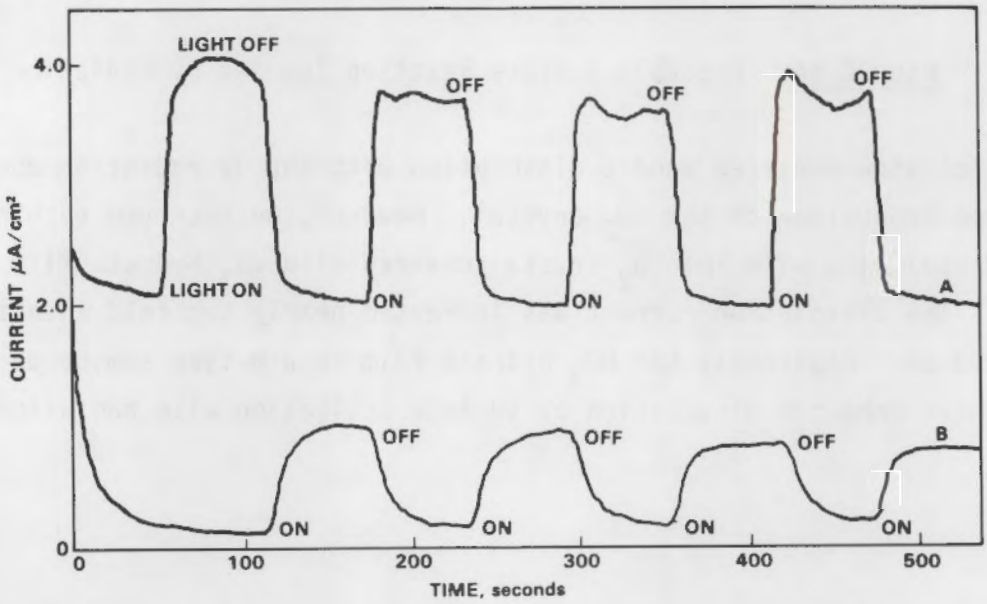

FIGURE 46. UV-Induced Enhanced Dissolution on UO_2 Single-Crystal Surfaces

DISCUSSION OF UO_2 OXIDATION-DISSOLUTION

The experimental evidence described in this report suggests that the oxidation-dissolution mechanisms for single-crystal UO_2 surfaces are rather complex. Even though the data and observations presented here are based on accelerated dissolution with high concentrations of O and H_2O_2 for the purpose of identifying the detailed oxidation-dissolution processes, we anticipate that oxidation of UO_2 as a result of low O concentrations poses serious questions about surface modifications and enhanced dissolution. Also, oxidation conditions can be created by the presence of dissolved O, chemical species and radiolysis of water. If the effects of radiation as observed in our laboratory studies are considered, it may be rather difficult to maintain neutral or reducing conditions at the surfaces of spent fuel.

OXIDATION-DISSOLUTION OF UO_2

The oxidation-dissolution process may be one of the main mechanisms for UO_2 dissolution in aqueous solutions. In neutral or reducing conditions, dissolution of UO_2 only involves the U(IV) valence state (Langmuir 1978; Lemire and Tremaine 1980), as shown in Figure 47. The equilibrium solubility is extremely low, and is usually below the detection limits of the chemical analysis of 2×10^{-8} mol/kg (Johnson et al. 1980).

However, in solutions containing O and oxidizing species, the dissolution mechanisms for single-crystal UO_2 surfaces may be considered as a rate-controlled oxidation and phase transformation of U(IV) (solid) into U(VI) (liquid and solid) state via the liquid media. The probable oxidation-dissolution steps and reactions, based on solubility and stability of various uranyl ions [Holland and Brush (1978)] (Figure 48), are generalized in Figure 49 for deionized water.

A clean, single-crystal UO_2 surface exposed to oxidizing species in the solution rapidly oxidizes to form a thin, oxide layer of UO_{2+x}, where x ranges from 0 to 1 [reaction (15) in Figure 48]. This layer is only a few angstroms thick at the single-crystal UO_2 surface and forms along the grain

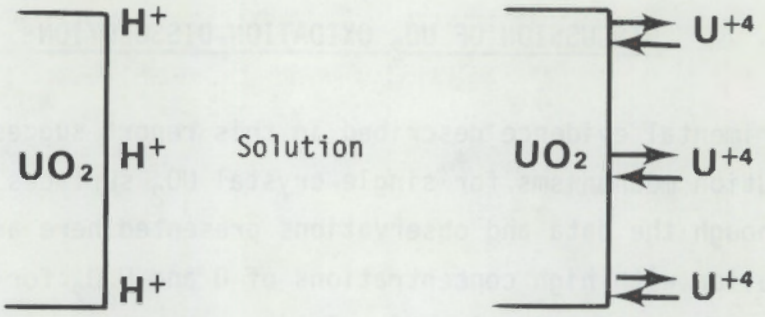

(a) Neutral Condition (b) Dissolution

At 25°C:

$$UO_2 + 3H^+ \rightleftharpoons U(OH)^{+3} + H_2O \quad (13)$$

Up to 200°C

$$UO_2 + 4H^+ \rightleftharpoons U^{+4} + 2H_2O \quad (14)$$

FIGURE 47. Dissolution of UO_2 in Neutral or Reducing Conditions

boundary several micrometers deep from the surface of the polycrystalline pellets. This oxidized layer, combined with dissolved O or oxidizing species, rapidly dissolves to form uranyl ions (UO_2^{+2} and $UO_2(OH)^+$) and solution species of $UO_2(OH_2^o)$, depending on the pH of the water. For deionized water, three oxidation-dissolution reactions are postulated: (16), (17) and (18). Thus, the dissolution of the UO_2 is strongly dependent on both the available O and H^+ ions.

The uranyl ions are transported throughout the solution but are concentrated mostly at the solution/UO_2 interface region. The rapid increase of uranyl ion concentration near this region leads to hydrolysis reactions (19) to (24) as functions of pH and temperature. For lower temperatures such as 25 to 75°C (Wadsten 1976), uranyl hydrates form as thin films consisting mainly of $UO_3 \cdot 2H_2O$ phases. At elevated temperatures, such as 150°C, deposition of large uranyl crystals of $UO_2(OH)_2$ occur. The deposition of these thin films

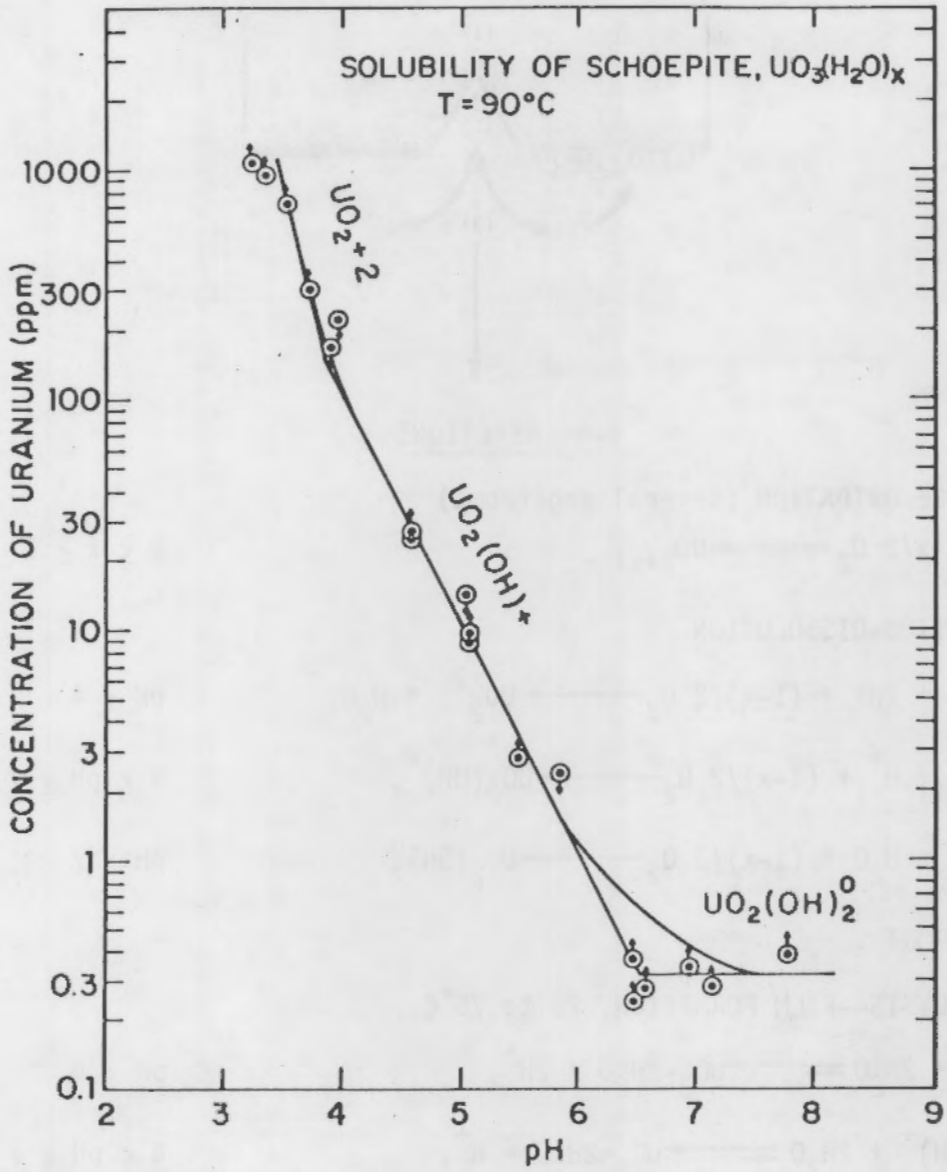

FIGURE 48. Solubility of Schoepite, $UO_3(H_2O)_x$, at 90°C in NaCl-Free Solutions (from Holland and Brush 1978)

and crystals is based on the solubility limits of the uranyl ions and pH (Figure 48). In this case, the concentration of uranyl ions in the solution can be determined by the reactions (19) to (24), rather than reactions (16) to (18). Because the hydrolysis reactions release the H^+ ions consumed by the

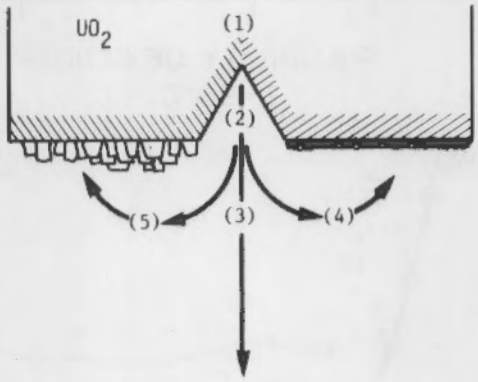

REACTIONS

(1) SURFACE OXIDATION (several angstroms)

$$UO_2 + x/2\ O_2 \longrightarrow UO_{2+x}, \qquad 0 \le x \le 1 \qquad (15)$$

(2) OXIDATION-DISSOLUTION

$$UO_{2+x} + 2H^+ + (1-x)/2\ O_2 \longrightarrow UO_2^{+2} + H_2O, \qquad pH < 4 \qquad (16)$$

$$UO_{2+x} + H^+ + (1-x)/2\ O_2 \longrightarrow UO_2(OH)^+, \qquad 4 \le pH \le 7 \qquad (17)$$

$$UO_{2+x} + H_2O + (1-x)/2\ O_2 \longrightarrow UO_2(OH)_2^o \qquad pH \ge 7 \qquad (18)$$

(3) TRANSPORT

(4) HYDROLYSIS--FILM FORMATION, 25 to 75°C

$$UO_2^{+2} + 3H_2O \rightleftharpoons UO_3 \cdot 2H_2O + 2H^+, \qquad pH \le 4 \qquad (19)$$

$$UO_2(OH)^+ + 2H_2O \rightleftharpoons UO_3 \cdot 2H_2O + H^+, \qquad 4 \le pH \le 7 \qquad (20)$$

$$UO_2(OH)_2^o + H_2O \rightleftharpoons UO_3 \cdot 2H_2O, \qquad pH \ge 7 \qquad (21)$$

(5) HYDROLYSIS--CRYSTAL GROWTH, 150°C

$$UO_2^{+2} + 2H_2O \rightleftharpoons UO_2(OH)_2 + 2H^+, \qquad pH \le 4 \qquad (22)$$

$$UO_2(OH)^+ + H_2O \rightleftharpoons UO_2(OH)_2 + H^+, \qquad 4 \le pH \le 7 \qquad (23)$$

$$UO_2(OH)_2^o \rightleftharpoons UO_2(OH)_2, \qquad pH \ge 7 \qquad (24)$$

FIGURE 49. Oxidation and Dissolution Mechanisms for UO_2 in Deionized Water

oxidation-dissolution reactions, the dissolution of the UO_2 surface will continue as long as O is available. Grandstaff (1976) found that the dissolution rate of UO_2 powders is directly proportional to the partial pressure of O at least for 23°C.

The oxidation-dissolution of UO_2 increases as a function of temperature because the diffusion of O and H^+ ions to the UO_2 surface increases. However, the solubility of uranyl ions is inversely related to temperature; thus, most of the dissolution products end up in the uranyl hydrates as those observed at 150°C in the autoclave experiments.

Interestingly, the presence of H_2O_2 enhances the oxidation-dissolution reaction as well as the hydrolysis reaction. Since the formation of H_2O_2 is expected from radiolysis of water, the dissolution mechanism for UO_2 may continue at the UO_2-solution interface region even when the solution has reducing or neutral conditions.

Continuous oxidation and dissolution of UO_2 surfaces after the formation of $UO_2(OH)_2$ or UO_3 hydrates depends on the porosity and thickness of the deposited film. When the deposited film is thick and dense, oxidation and dissolution are greatly reduced and solubility is then controlled by the surface film. However, as the surface film buildup increases, chances for cracking and spalling increase and fresh UO_2 surface is exposed again to the solution. Oxidation-dissolution reactions resume until the deposited film is thick enough to prevent further oxidation and dissolution of the UO_2 surface. Fluctuation of pH and solution of U concentration may be associated with this film formation cycle.

The polarization behavior of UO_2 in WIPP "B" brine solution indicated that the UO_2 surface was passivated to some degree between -0.6 and -0.2 V(SCE). This passivation correlates with the low dissolution rate of the UO_2 samples determined by electrochemical measurement and with the low U concentration in the solution at both 75 and 150°C in the autoclave tests. The passive nature of the surface film on the UO_2 may be due to a thin and protective uranyl hydrate film formed at the early stages of the oxidation-

dissolution process. We would need to study the structure and the property of this surface film in order to understand the passive nature of the UO_2 surface film.

IMPLICATIONS OF RESULTS TO SPENT-FUEL PROBLEMS

The results of this study provide only guidelines for the probable leaching mechanisms of spent fuel. We are not certain whether spent fuel would behave similarly to single-crystal UO_2 because of the vast difference in the compositions, microstructures and radiation levels of spent fuel. The leaching mechanisms of spent fuel may be more complex and require direct evaluation.

However, recent studies have indicated that initial leaching of spent fuel may be due to leaching of the grain boundary region, and after a long period, mainly due to matrix dissolution (Katayama 1979; Katayama, Bradley and Harvey 1980; Bradley 1979; Johnson et al. 1980). In this case, oxidation-dissolution mechanisms of UO_2 will play an important part in both leaching processes of spent fuel. The leaching of the grain boundary region is associated with the oxidation-dissolution process because the initial surface oxidation of the spent fuel will mainly occur at the grain boundary area up to several micrometers deep from the surface area. This short-term leaching rate of the spent fuel would be directly associated with the rate of the oxidation-dissolution process and the protective nature of the hydrate films. Due to the large inhomogeneity of the microstructure and composition of the spent fuel, it is possible that a surface oxidation/leaching/dissolution/surface-film-formation/cracking/spalling cycle would occur at different locations and times. Therefore, assessment of the stability of the spent fuel based on short-term leaching experimental data will be very difficult.

The electrochemical methods developed here for UO_2-surface analyses are attractive for studying spent fuel. First, these methods may be used to determine the initial dissolution rate and the surface oxidation state of spent-fuel samples (Wang and Katayama 1980). Second, electrochemical dissolution may be controlled to simulate an accelerated test condition for the investigation of long-term leaching effects on spent fuel at a realistic temperature range for

the repository. Third, the electrochemical methods are simple and can be applied simultaneously in many test cells for comparison of similar and different leaching solutions and conditions. However, additional understanding and development of electrochemical methods are needed to assure measurement of realistic leach data for spent fuel under all repository conditions.

CONCLUSIONS

This report presents a current understanding of the complex oxidation and dissolution of UO_2 in three aqueous solutions: deionized water, 0.03 M sodium bicarbonate, and Waste Isolation Pilot Plant (WIPP) "B" brine solutions. Dissolution mechanisms were identified based on accelerated oxidation and dissolution tests performed in static autoclave and electrochemical dissolution experiments. Experimental results lead to these conclusions:

- Oxidation of UO_2 in air or aqueous solutions mainly occurs at the surface region. Therefore, for single-crystal UO_2, surface oxidation is limited to a depth of several angstroms and for polycrystalline UO_2 pellets to a depth of several microns along the grain boundary area.
- The initial dissolution of UO_2 and spent fuel involves the oxidation of U(IV) (solid) to U(VI) (liquid) through the formation of uranyl ions. The oxidation-dissolution is a rate-controlled process whose rate increases as temperature increases.
- The dissolved uranyl ions form solids of uranyl hydrates or related complex compounds by a hydrolysis reaction, which occurs more rapidly at high temperatures to form large hydrate crystals.
- The presence of H_2O_2, probably from radiolysis of water, enhances the oxidation-dissolution of UO_2 and also increases the formation of hydrate deposits.
- Dissolution rates for UO_2 in brine solution are low because the surface is passivated.
- Electrochemical methods may be used to compare the leaching behaviors of UO_2 and spent fuel and to perform accelerated leaching tests for spent fuel in a realistic temperature range for the repository.

REFERENCES

Aronson, S., R. B. Roff, Jr. and J. Belle. 1957. "Kinetic Study of the Oxidation of Uranium Oioxide." J. Chem. Physics. 27:137.

Bond, W. L. 1960. Acta Cryst. 13:814.

Bradley, O. J. 1979. "Waste Form Interactions." In Proceedings of the National Waste Terminal Storage Program Information Meeting, ONWI-62, October 30, 1979.

Brush, L. H. 1980. Ph. D. Thesis. The Solubility of Some Phases in the System UO_3-Na_2O-H_2O in Aqueous Solutions at 60 and 90°C. Harvard University, Massachusetts, Boston, Massachusetts.

Burns, W. G. and P. B. Moore. 1976. Radiation Effects. 30:233.

Cordfunke, E. H. P. and Van Der Giessen. 1963. J. Inorg. Nucl. Chem. 25: 553.

Debets, P. C. and B. O. Loopstra. 1963. Inorg. Nucl. Chem. 25:945.

Grandstaff, D. E. 1976. Economic Geology. 71:1493.

Gronvold, F. and H. Haraldsen. 1948. Nature. 162:69.

Henry, N. F. M. and K. Lonsdale, eds. International Tables for X-Ray Crystallography. 1959. Vol. II, p. 119, Kynoch Press, Birmingham, England.

Hiskey, J. B. 1980. "Hydrogen Peroxide Leaching of Uranium Oxide in Carbonate Solutions." Sym. of Hydrogen Peroxide ASM.

Holland, H. D. and L. H. Brush. 1979. "Uranium Oxides in Ores and Spent Fuels." In Proceedings of the Conference on High-Level Radioactive Solid Waste Forms, December 19-21, 1978, Denver, Colorado, NUREG/CP-0005.

Johnson, L. H. et al. 1980. Mechanisms of Leaching and Dissolution of UO_2 Fuel. AECL-6992.

Katayama, Y. B. 1979. Spent LWR Fuel Leach Tests. PNL-2982, Pacific Northwest Laboratory, Richland, Washington.

Katayama, Y. B., D. J. Bradley and C. O. Harvey. 1980. Status Report on LWR Spent Fuel IAEA Leach Tests. PNL-3173, Pacific Northwest Laboratory, Richland, Washington.

Lang, A. R. 1958. J. Appl. Phys. 29:597.

Langmuir, D. 1978. Geochem. Gosmochim. Acta. 42:547.

Lemire, R. J. and P. R. Tremaine. 1980. J. Chem. and Eng. Data.

Malý, J. and V. Veselý. 1958. J. Inorg. Nucl. Chem. 7:119.

Manes, L. and J. Naegele. 1976. "Electronic Properties of Uranium Oxides." In Plutonium 1975 and Other Actinides. H. Bland and R. Linder, eds., North-Holland Publishing Co., pp. 361.

Naegele, J., L. Manes and U. Birkholz. 1976. "Optical Properties of UO_2 and U_4O_9 Single Crystals and Their Relation to Chemical Bonding." In Plutonium 1975 and Other Actinides, H. Blank and R. Lindner, eds., North-Holland Publishing Co., p. 393.

Needham, P. B., Jr. et al. 1975. "Material Research and Development for Geothermal Environments." In Proceedings of 2nd Workshop on Material Properties for Geothermal Energy Systems, El Centro, California, p. 47.

Rai, D., R. G. Strickert and J. L. Ryan. 1981. Inorg. Nucl. Chem. Letters.

Rundle, R. E. et al. 1948. J. Amer. Chem. Soc. 70:99.

Taylor, P., E. A. Burgess and D. G. Owen. 1980. J. of Nuclear Materials. 88:153.

Wadsten, T. 1976. J. Nucl. Materials. 64:315.

Wamser, C. A. et al. 1952. J. Am. Chem. Soc. 74:1020.

Wang, R. and Y. B. Katayama. 1980. "Electrochemical Leaching of Spent Fuel." In Proceedings of the ORNL Conference on the Leachability of Radioactive Solids, Gatlinburg, Tennessee, December 9-12, 1980.

PNL-3566
UC-70

DISTRIBUTION

No. of Copies

OFFSITE

A. A. Churm
DOE Chicago Patent Division
9800 South Cass Avenue
Argonne, IL 60439

27 DOE Technical Information Center

B. Adams
Corning Glass Works
Technical Staffs Division
Corning, NY 14830

Allied Chemical Corporation
(File Copy)
550 2nd Street
Idaho Falls, ID 83401

J. M. Batch
Battelle Memorial Institute
505 King Avenue
Columbus, OH 43201

L. V. Benson
Lawrence Berkeley Laboratory
Bldg. 90-1140
1 Cyclotron Road
Berkeley, CA 94720

E. F. Benz
Battelle Memorial Institute
Office of Nuclear Waste
Isolation
505 King Avenue
Columbus, OH 43201

Beverly Rawles
Battelle Memorial Institute
Office of Nuclear Waste
Isolation
505 King Avenue
Columbus, OH 43201

No. of Copies

J. R. Berreth
Allied Chemical Corporation
550 2nd Street
Idaho Falls, IO 83401

R. E. Blanco
Union Carbide Corporation (ORNL)
Chemical Technology Division
P. O. Box Y
Oak Ridge, TN 37830

J. O. Blomeke
Union Carbide Corporation (ORNL)
P. O. Box Y
Oak Ridge, TN 37830

E. A. Bondietti
Oak Ridge National Laboratory
P. O. Box X
Oak Ridge, TN 37830

J. Braithwaite
Sandia Laboratories
Albuquerque, NM 87185

Brookhaven National Laboratory
Reference Section
Information Division
Upton, NY 11973

R. A. Buckham
Allied-General Nuclear Service
P. O. Box 847
Barnwell, SC 29812

H. C. Burkholder
Battelle Memorial Institute
Office Nuclear Waste
Isolation
505 King Avenue
Columbus, OH 43201

No. of Copies

B. Cahan
Department of Chemistry
Case Western Reserve University
Cleveland, OH 44106

W. A. Carbiener
Office of Nuclear Waste Isolation
505 King Avenue
Columbus, OH 43201

T. C. Chee
DOE Office of Nuclear Waste Management
Washington, DC 20545

R. B. Chitwood
DOE Division of Nuclear Power Development
Washington, DC 20545

5 D. Coles
Lawrence Livermore Laboratory
P. O. Box 808
Livermore, CA 94550

P. Colombo
Department of Applied Science
Brookhaven National Laboratory
Upton, NY 11973

C. R. Cooley
DOE Office of Nuclear Waste Management
Washington, DC 20545

George Cowan
Los Alamos Scientific Laboratory
Los Alamos, NM 87545

J. L. Crandall
E. I. duPont DeNemours and Company
Savannah River Laboratory
Aiken, SC 29801

No. of Copies

R. E. Cunningham
Deputy Director for Fuels and Materials
Nuclear Regulatory Commission
Silver Springs, MD 20910

H. Diamond
Argonne National Laboratory
9700 South Cass Avenue
Argonne, IL 60439

J. P. Duckworth
Plant Manager
Nuclear Fuel Services, Inc.
P. O. Box 124
West Valley, NY 14171

J. O. Duguid
Office of Nuclear Waste Isolation
505 King Avenue
Columbus, OH 43201

Environmental Protection Agency
Technology Assessment Division (AW-559)
Office of Radiation Programs
Washington, DC 20460

B. Erdal
Los Alamos Scientific Laboratories
CNC-11-MS-514
P. O. Box 1663
Los Alamos, NM 87545

Keith Flynn
Argonne National Laboratory
9700 South Cass Avenue
Argonne, IL 60439

A. Friedman
Argonne National Laboratory
9700 South Cass Avenue
Argonne, IL 60439

No. of
Copies

R. G. Garvin
E. I. duPont DeNemours and Company
Savannah River Laboratory
Aiken, SC 29801

H. W. Godbee
Union Carbide Corporation (ORNL)
Chemical Technology Division
P. O. Box Y
Oak Ridge, TN 37830

E. S. Goldberg
DOE Savannah River Operations Office
P. O. Box A
Aiken, SC 29801

R. L. Hahn
Oak Ridge National Laboratory
Oak Ridge, TN 37830

Mark Harwell
P. O. Box 667
Cannon Beach, OR 97110

C. A. Heath
DOE Office of Nuclear Waste Management
Washington, DC 20545

R. E. Heineman
Office of Nuclear Waste Isolation
505 King Avenue
Columbus, OH 43201

L. L. Hench
Department of Materials Science and Engineering
University of Florida
Gainsville, FL 32611

No. of
Copies

H. Henning
Electric Power Research Institute
3412 Hillview Avenue
P. O. Box 10412
Palo Alto, CA 94301

H. C. Hess
Battelle Memorial Institute
Office of Nuclear Waste Isolation
505 King Avenue
Columbus, OH 43201

Peter Hoffman
Office of Nuclear Waste Isolation
505 King Avenue
Columbus, OH 43201

H. D. Holland
Department of Geology and Geophysics
University of Hawaii
Honolulu, HI 96822

N. Hubbard
Battelle Memorial Institute
Office of Nuclear Waste Isolation
505 King Avenue
Columbus, OH 43201

J. L. Jardine
Argonne National Laboratory
9700 South Cass Avenue
Argonne, IL 60439

J. K. Johnstone
Sandia Laboratories
Albuquerque, NM 87107

J. A. Kelley
E. I. duPont DeNemours and Company
Savannah River Laboratory
Aiken, SC 29801

No. of Copies

C. J. Kershner
Monsanto Research Corporation
Mound Laboratory
P. O. Box 32
Miamisburg, OH 45342

J. F. Kircher
Office of Nuclear Waste Isolation
Battelle Memorial Institute
505 King Avenue
Columbus, OH 43201

D. A. Knecht
Allied Chemical Corporation
550 2nd Street
Idaho Falls, ID 83401

E. H. Kobish
Solid State Division
Oak Ridge National Laboratory
Oak Ridge, TN 37830

D. Lam
Argonne National Laboratory
9700 South Cass Avenue
Argonne, IL 60439

Paul W. Levy
Brookhaven National Laboratory
Upton, NY 11973

S. E. Logan
Los Alamos Technical Associates, Inc.
P. O. Box 410
Los Alamos, NM 87544

Los Alamos Scientific Laboratory (DOE)
P. O. Box 1663
Los Alamos, NM 87544

J. B. Martin
United States Nuclear Regulatory Commission
Washington, DC 20555

No. of Copies

W. C. McClain
RE/SPEC Inc.
P. O. Box 725
Rapid City, SD 57701

M. D. McCormack
E.G. & G. Idaho, Inc.
P. O. Box 1625
Idaho Falls, ID 83401

R. E. Meyer
Oak Ridge National Laboratory
P. O. Box X
Oak Ridge, TN 37830

Sheldon Meyers
DOE Office of Nuclear Waste Management
Washington, OC 20545

Don Moak
Office of Nuclear Waste Isolation
505 King Avenue
Columbus, DH 43201

M. A. Molecke
Sandia Laboratories
Albuquerque, NM 87107

W. E. Mott
DOE Division of Environmental Control Technology
Washington, DC 20545

J. Neff, Program Manager
Department of Energy
Columbus Program Office
505 King Avenue
Columbus, OH 43201

R. M. Neilson, Jr.
Department of Applied Science
Brookhaven National Laboratory
Upton, NY 11973

No. of Copies

A. E. Norris
Los Alamos Scientific Laboratory
CNC-11 Mailstop 514
Los Alamos, NM 87545

2 Oak Ridge National Laboratory (DOE)
Central Research Library
Document Reference Library
P. O. Box X
Oak Ridge, TN 37830

G. Oertel
DOE Office of Nuclear Waste Management
Washington, DC 20545

A. Ogard
Los Alamos Scientific Laboratory
CNC-11 Mailstop 514
Los Alamos, NM 87545

Al Ogle
Los Alamos Scientific Laboratory
CNC-CO Mailstop 760
Los Alamos, NM 87545

A. F. Perge
DOE Office of Nuclear Waste Management
Washington, DC 20545

M. S. Plodinec
E. I. duPont DeNemours and Company
Savannah River Laboratory
Aiken, SC 29801

John Pomeroy
Technical Secretary
National Academy of Sciences
Committee of Radioactive Waste Management
National Research Council
2101 Constitution Avenue
Washington, DC 20418

No. of Copies

R. G. Post
College of Engineering
University of Arizona
Tucson, AZ 85721

Professor Guna Salvaduray
Materials Engineering
San Jose State University
San Jose, CA 95192

L. Ramspott
Lawrence Livermore Laboratory
P. O. Box 808
Livermore, CA 94550

D. M. Rohrer
United States Nuclear Regulatory Commission
Washington, DC 20555

R. G. Romatowski
DOE Office of Nuclear Waste Management
Washington, DC 20545

R. Roy
202 Materials Research Laboratory
Pennsylvania State University
University Park, PA 16802

B. Scheetz
210 Materials Research Laboratory
Pennsylvania State University
University Park, PA 16802

T. Scott
Ames Laboratory
Iowa State University
Ames, IA 50011

W. C. Seymour
E.G. & G. Idaho, Inc.
P. O. Box 1625
Idaho Falls, ID 83401

No. of
Copies

R. J. Silva
Lawrence Berkeley Laboratory
Bldg. 70A/1160
1 Cyclotron Road
Berkeley, CA 94720

M. J. Steindler
Argonne National Laboratory
9700 South Cass Avenue
Argonne, IL 60439

D. B. Stewart
U.S. Department of Interior
959 National Center
Geological Survey
Reston, VA 22092

J. Tewhey
Lawrence Livermore Laboratory
P. O. Box 808
Livermore, CA 94550

John Van Cleve
DOE Oak Ridge Operation Office
P. O. Box X
Oak Ridge, TN 37830

E. Vejovoda, Director
Chemical Operations
Rockwell International
Rocky Flats Plant
P. O. Box 464
Golden, CO 80401

D. L. Vieth
DOE Office of Nuclear Waste
Management
Washington, DC 20545

J. W. Voss
Office of Nuclear Waste
Management
Battelle Memorial Institute
505 King Avenue
Columbus, OH 43201

No. of
Copies

R. D. Walton
DOE Office of Nuclear Waste
Management
Washington, DC 20545

W. Weart
Sandia Laboratories
Albuquerque, NM 87107

H. Weed
Lawrence Livermore Laboratory
P. O. Box 808
Livermore, CA 94550

W. White
210 Materials Research
Laboratory
Pennsylvania State University
University Park, PA 16802

J. B. Whitsett
DOE Idaho Operations Office
550 2nd Street
Idaho Falls, ID 83401

A. Williams
Allied-General Nuclear Service
P. O. Box 847
Barnwell, SC 29812

R. Williams
Electric Power Research
Institute
3412 Hillview Avenue
P. O. Box 10412
Palo Alto, CA 94304

ONSITE

5 DOE Richland Operations Office

P. A. Craig
H. E. Ransom
J. J. Schreiber
M. W. Shupe
M. J. Zamorski

No. of Copies

11 Rockwell Hanford Operations

J. Babad
G. Scott Barney
M. Bensky
R. A. Deju
R. J. Gimera
J. D. Kaser
M. J. Kupfer
W. W. Schultz
M. J. Smith
D. D. Wodrich
File Copy

Exxon Nuclear Company

S. J. Beard

Joint Center for Graduate Study

J. Cooper

2 United Nuclear Industries, Inc.

T. E. Dabrowski
A. E. Engler

8 Westinghouse Hanford Company

A. G. Blasewitz
D. M. Bosi
D. A. Cantley
R. J. Cash
R. E. Einziger
R. L. Fish
R. L. Knecht
A. C. Leaf

132 Pacific Northwest Laboratory

R. P. Allen
G. L. Benson
W. F. Bonner
D. J. Bradley (5)
J. B. Brown, Jr.
T. D. Chikalla

No. of Copies

Pacific Northwest Laboratory (contd)

D. B. Cearlock
R. A. Clark
M. O. Cloninger
S. D. Dahlgren
G. W. Dawson
W. J. Deutsch
R. L. Dillon
C. R. Hann
M. S. Hanson
C. O. Harvey
O. F. Hill
J. H. Jarrett
E. A. Jenne
A. B. Johnson
Y. B. Katayama
R. S. Kemper
H. E. Kissinger
H. E. Kjarmo
D. E. Knowlton
K. M. Krupka
M. R. Kreiter
W. L. Kuhn
D. E. Larson
G. B. Long (3)
J. L. McElroy
G. L. McVay (5)
G. B. Mellinger
J. E. Mendel
M. D. Merz
R. D. Nelson
R. E. Nightingale
C. R. Palmer
J. W. Patten
R. D. Peters
L. R. Pederson
A. M. Platt
D. Rai
J. F. Relyea
F. P. Roberts
G. R. Robinson
W. A. Ross
J. M. Rusin
J. L. Ryan

No. of
Copies

Pacific Northwest Laboratory
(contd)

R. J. Serne
J. W. Shade
D. H. Siemens
D. J. Silviera
R. G. Strickert
J. L. Swanson
H. Tenny
M. T. Thomas
R. P. Turcotte
H. H. Van Tuyl
J. W. Wald
W. E. Weber
R. A. Walter
R. Wang (40)
J. H. Westsik, Jr.
L. D. Williams
G. E. Zima
Technical Information (5)
Publishing Coordination EI (2)
Water and Land Resource
Library (10)